DIVERSITY AND EQUALIZATION IN DIGITAL CELLULAR RADIO

MARTIN V. CLARK

A thesis presented for the degree of Doctor of Philosophy
in Electrical and Electronic Engineering at the
University of Canterbury, Christchurch, New Zealand.

May 1992

ABSTRACT

This thesis analyses and quantifies the performance of a range of important diversity combining receivers operating in a digital cellular radio environment with linear modulation, frequency-selective Rayleigh multipath fading, and co-channel interference (CCI). The following three types of diversity receiver are treated: (i) the *maximum likelihood receiver* (the best-possible receiver); (ii) *optimum linear receivers*; and (iii) *memoryless linear combining receivers* with and without *post-combiner equalization.*

The frequency-selective multipath fading channels are statistically characterized by a *delay spectrum* with an associated root-mean-square *delay spread.* The co-channel interference on each diversity branch is assumed to be composed of (i) a small number (possibly zero) of dominant interferers; and (ii) a large number of weak interferers, the sum of which is modelled as independent gaussian noise, or *noise-like CCI.*

The potential bit-error-rate (BER) performance of the *maximum likelihood receiver* is analysed in the case of noise-like CCI alone (i.e., no dominant interferers), using the *matched filter bound.* The thesis presents a general, exact, and totally analytical solution of the matched filter bound on BER performance taken over the ensemble of multipath channel responses. The key to the solution is the application of the Karhunen-Loève representation of these channel responses.

The BER performance of an *optimum linear receiver*, optimized according to the minimum mean-square error (MMSE) criterion, is estimated using (i) a range of BER computation methods, including Metzger's algorithm and Saltzberg's bound; and (ii) random generation of the channel responses, using the efficient Karhunen-Loève method.

Five sub-classes of the *memoryless linear combining receiver*, with and without post-combiner equalization, are studied. They include arrangements of the following combining and equalization schemes: maximal ratio combining, maximal power combining, MMSE combining, MMSE linear equalization, and ideal intersymbol interference (ISI) cancellation. The BER performances of the five receiver sub-classes are estimated using similar techniques to those used for the optimum (MMSE) linear receiver.

For quarternary phase shift keying (QPSK) and all the above receivers, the thesis presents a set of numerical results that show the influence of the diversity order, the number of dominant interferers (set to zero for matched filter bounds), the delay spectrum shape, the delay spread, and the signal-to-interference ratio. This extensive set of data shows the power of diversity and equalization at combating ISI and CCI in frequency-selective fading environments, and important tradeoffs between receiver performance and complexity.

CONTENTS

PREFACE		**vii**
GLOSSARY		**xi**
Chapter 1	**INTRODUCTION**	**1**
	1.1 Digital Cellular Radio	1
	1.2 Diversity and Equalization	2
	1.3 Aim of the Thesis	3
Chapter 2	**DIGITAL CELLULAR SYSTEM MODEL**	**5**
	2.1 Transmission Links	5
	2.1.1 General	5
	2.1.2 Data Sources and Modulations	7
	2.1.3 Multipath Fading Channels	8
	2.1.4 Co-Channel Interference and Noise	9
	2.2 Karhunen-Loève Representations of Link Responses	12
	2.3 Conclusion	13
	Appendix 2A Solving the Eigensystem	14
Chapter 3	**ANALYSIS OF LINEAR SYSTEMS**	**17**
	3.1 The Linear System	17
	3.2 Equivalent Discrete Linear System	20
	3.3 Mean-Square Error	21
	3.4 Bit-Error-Rate	22
	3.5 Performance Over Channel Ensemble	24
	3.6 Obtaining Numerical Results: The General Approach	25
	3.7 Conclusion	27
	Appendix 3A Metzger's Algorithm	27
Chapter 4	**THE MAXIMUM LIKELIHOOD RECEIVER AND MATCHED FILTER PERFORMANCE BOUNDS**	**29**
	4.1 The Maximum Likelihood Receiver	30
	4.1.1 Noise Whitening	30

4.1.2 Formulation 30
4.2 Matched Filter Performance Bounds 32
4.2.1 Analysis 32
4.2.2 Numerical Results 36
4.3 Conclusion 41

Chapter 5 OPTIMUM LINEAR RECEIVERS 43
5.1 Optimum Linear Receiver Structure 44
5.2 Analysis 45
5.3 MMSE Optimization 46
5.4 Numerical Results 47
5.4.1 General 47
5.4.2 Influence of BER Computation Scheme 47
5.4.3 Influence of Diversity Order and Number of Dominant Interferers 48
5.4.4 Influence of Delay Spread 51
5.4.5 Influence of Delay Spectrum Shape 53
5.5 Conclusion 54

Chapter 6 MEMORYLESS LINEAR COMBINING AND POST-COMBINER EQUALIZATION 57
6.1 Stand-Alone Combining 58
6.1.1 System Description 58
6.1.2 Analysis 59
6.1.3 Maximal Ratio Combining 60
6.1.4 MMSE Combining 60
6.2 Post-Combiner Equalization 61
6.2.1 System Description 61
6.2.2 System Without Dominant CCI 62
6.2.3 System With Dominant CCI 64
6.3 Numerical Results 65
6.3.1 General 65
6.3.2 Influence of BER Computation Scheme 67
6.3.3 Stand-Alone Combining 70
6.3.4 Post-Combiner Equalization 75
6.4 Conclusion 79

Chapter 7 CONCLUSION 81
7.1 Discussion of Results 81
7.2 Practical Issues 83
7.3 Suggestions for Future Work 85

REFERENCES 87

PREFACE

This thesis presents a study of diversity and equalization techniques for digital cellular radio. The research work was motivated by a desire to find performance bounds for various radio receivers operating in a digital cellular radio environment with frequency-selective multipath fading and co-channel interference.

In keeping the thesis brief and to the point, the technical literature in this research area is used extensively throughout. Unless special explanation is appropriate, well known theory and results are applied directly, with proofs cited rather than duplicated.

Chapter 1 of the thesis is an introduction to digital cellular radio systems; to the fundamental problems associated with such systems, including multipath fading, intersymbol interference, and co-channel interference; and to the use of diversity and equalization in digital cellular radio receivers to combat these problems. In addition, Chapter 1 outlines the aim of the thesis and summarizes the original contributions of the work.

Chapter 2 describes a model of a digital cellular radio system, assumed throughout the study of all receivers in subsequent chapters, together with assumptions regarding modulation, multipath propagation, co-channel interference, and additive noise. The frequency-selective multipath fading channel responses are expressed in terms of the Karhunen-Loève orthogonal series expansion. This approach provides a very useful tool for analysis and computer simulation, and to the author's knowledge, has not been exploited in the literature.

All receivers analysed in this thesis have a linear structure, and there are many analytical techniques common to each. These techniques are presented in Chapter 3, along with a discussion on the general approach, used in the next three chapters, to obtaining numerical bit-error-rate (BER) performance results. A variety of BER computation schemes is considered. The application of these methods in subsequent chapters is original work and illustrates the usefulness and limitations of simple BER bounds and approximations in interference-limited systems.

Most of the work's original contributions are contained in Chapters 4, 5, and 6. To put the original work presented into context, each of these chapters begins with a review of the relevant technical literature. Each chapter treats a different type of receiver:

- *Chapter 4 — The Maximum Likelihood Receiver.* To analyse the potential performance of this best-possible receiver, the *matched filter bound* is put to use. This approach conveniently reduces the maximum likelihood receiver to one with a simple linear structure. A general and totally analytical solution of BER performance is presented.

- *Chapter 5 — Optimum Linear Receivers.* An equivalent structure of this type of receiver is formed (independent of the optimality criterion) based on the structure of the maximum likelihood receiver formulated in Chapter 4. This novel approach makes minimum mean-square error (MMSE) receiver optimization quite straightforward compared with other published techniques.

- *Chapter 6 — Memoryless Linear Combining Receivers.* In total, *five* sub-classes of this type of receiver, with and without post-combiner equalization, are studied. They include arrangements of the following combining and equalization schemes: maximal ratio combining, maximal power combining, MMSE combining, MMSE linear equalization, and ideal intersymbol interference cancellation. It is shown how simple memoryless combining can not only combat multipath fading and co-channel interference, but can also effect good equalization without the aid of post-combiner processing.

At the end of each of these three chapters, a set of numerical results is presented. These data show the influence of various system and channel parameters on receiver performance. The focus is on dominant co-channel interference and frequency-selective fading channels.

Finally, Chapter 7 summarizes the results, addresses various practical issues, and highlights possible avenues for further work in this rich area of study.

List of Papers

The following papers have been written as a result of the thesis work. I presented the GLOBECOM'90 paper in San Diego, California, USA in December 1990 (I received a COMSOC student award to attend this conference), and my supervisor, Bill Kennedy, presented the GLOBECOM'91 paper in Phoenix, Arizona, USA in December 1991.

Clark, M.V., Greenstein, L.J., Kennedy, W.K. and Shafi, M. (1990), "MMSE diversity combining for wideband digital cellular radio," In *GLOBECOM '90 Conf. Proc.*, IEEE Communications Society, San Diego, California, December, pp. 495–499.

Clark, M.V., Greenstein, L.J., Kennedy, W.K. and Shafi, M. (1991), "Matched filter performance bounds for diversity combining receivers in digital mobile radio," In *GLOBECOM '91 Conf. Proc.*, IEEE Communications Society, Phoenix, Arizona, December, pp. 1125–1129.

Clark, M.V., Greenstein, L.J., Kennedy, W.K. and Shafi, M. (1992), "MMSE diversity combining for wideband digital cellular radio," Scheduled for June issue of *IEEE Trans. Commun.*, Vol. COM-40.

Clark, M.V., Greenstein, L.J., Kennedy, W.K. and Shafi, M. (1992), "Matched filter performance bounds for diversity combining receivers in digital mobile radio," Accepted for publication in *IEEE Trans. Vehicul. Tech.*

Clark, M.V., Greenstein, L.J., Kennedy, W.K. and Shafi, M. (1992), "Optimum linear diversity receivers in digital cellular radio," Submitted for presentation in *GLOBECOM '92.*

Clark, M.V., Greenstein, L.J., Kennedy, W.K. and Shafi, M. (1992), "Optimum linear diversity receivers in digital cellular radio," Submitted for publication in *IEEE Trans. Vehicul. Tech.*

Acknowledgements

I am indebted to my three supervisors, Bill Kennedy (University of Canterbury), Mansoor Shafi (Telecom Corporation of New Zealand Ltd.), and Larry Greenstein (AT&T Bell Laboratories), for their guidance and encouragement throughout the course of my research. Much of the original work in this thesis has evolved from the countless discussions I have had with them. They also

have reviewed and carefully edited many drafts of the thesis and its associated research papers; their numerous suggested revisions have led to improvements in all the manuscripts. In addition to their unparalleled technical support, my supervisors have shown a great deal of interest in my personal development, provided me with many profitable work-related opportunities, and instilled in me a passion for communications research.

I am grateful to Telecom Corporation of New Zealand Ltd. for providing facilities and personal funding, including the Telecom Scholarship in Digital Mobile Radio, and for sponsorship that enabled my attending GLOBECOM'90 and visiting various telecommunications laboratories in the USA.

There are many staff members and postgraduate students at the University of Canterbury who have in some way contributed to my research work. In particular, I gratefully acknowledge the useful technical advice and support of Hasha Sirisena, Ian Coope, Chris Carlisle, Peter Gardenier, Chris Kaiser, Steve Bly, Mike Shurety, and Dave Van Leeuwen.

Finally, I wish to thank my family and close friends, especially Guy and Jude, for their devoted support, understanding, and encouragement.

GLOSSARY

Mathematical Notation

		Typical Usage
$\triangleq$	defined as	p. 6
$\equiv$	equivalent to	(2.13)
$\approx$	approximately equal to	p. 23
$\rightarrow$	approaches	p. 30
$\Rightarrow$	implies that	(4.1)
$\Leftrightarrow$	if and only if	p. 31
:	such that	(4.11)
$\odot$	convolution	(2.2)
$\forall$	for all	p. 13
i, j	general indices (integers)	(2.28)
$\jmath$	imaginary unit, $\sqrt{-1}$	(2.3)
Re $[x]$	real part of x	(3.17)
Im $[x]$	imaginary part of x	(3.17)
$\lvert x \rvert$	magnitude of x	(3.6)
phase$[x]$	modulo-2π phase of x	(6.2)
x^*	complex conjugate of x	(2.4)
$\mathcal{F}[h(x)]$	Fourier transform of $h(x)$	(2.3)
$\{x_i\}$	set or sequence with elements indexed by i	p. 5
min	minimum element of a set	(4.1)
max	maximum element of a set	(4.1)
$\mathbf{A}$	matrix or vector	(2.23)
$[\mathbf{A}]_i$	ith entry of vector $\mathbf{A}$	p. 14
$[\mathbf{A}]_{i,j}$	entry of matrix $\mathbf{A}$ in the ith row and jth column	(2.28)
$\mathbf{A}^H$	Hermitian transpose of $\mathbf{A}$	(2.22)
$\mathbf{A}^{-1}$	inverse of square matrix $\mathbf{A}$	(5.15)
$\mathbf{A}^{\frac{1}{2}}$	square root of square matrix $\mathbf{A}$	(2.23)
$\lvert \mathbf{A} \rvert$	length of vector $\mathbf{A}$	(4.9)
$\mathbf{0}$	matrix or vector of zeros	(5.13)
diag$[x_1\ x_2\ \ldots\ x_N]$	diagonal matrix with $x_1, x_2, \ldots, x_N$ on main diagonal	(5.11)
Prob $[X]$	probability of event X	p. 24

$E[x]$	expected value of random variable x	(2.4)
$[a, b]$	real interval, $a \leq x \leq b$	p. 26
$[a, b)$	real interval, $a \leq x < b$	p. 7
$\delta(x)$	Dirac delta function	(2.4)
$\delta_{i,j}$	Kronecker delta ($\delta_{i,i} = 1$; $\delta_{i,j} = 0, i \neq j$)	(2.15)
$\partial^i / \partial x^i$	ith partial derivative with respect to x	(5.13)
$\text{sinc}(x)$	sinc function, $\sin(\pi x)/(\pi x)$	(2.29)
$\text{erfc}(x)$	complementary error function, $\frac{2}{\sqrt{\pi}} \int_x^\infty \exp(-y^2)\, dy$	(3.22)

Abbreviations

		Typical Usage
BER	bit-error-rate	p. 22
BPSK	binary phase shift keying	p. 7
CCI	co-channel interference	p. 1
cm	centimetres	p. 5
dB	decibels	p. 2
ISI	intersymbol interference	p. 2
kbit/s	kilobits per second	p. 9
kHz	kilohertz	p. 2
km/h	kilometres per hour	p. 25
m	metres	p. 3
MHz	megahertz	p. 3
MMSE	minimum mean-square error	p. 43
MSE	mean-square error	p. 21
μs	microseconds	p. 9
pdf	probability density function	p. 23
QPSK	quaternary phase shift keying	p. 7
QAM	quadrature amplitude modulation	p. 7
rms	root-mean-square	p. 8
TDL	tapped delay line	p. 83
TDMA	time-division multiple access	p. 27

Symbols

(The following list excludes symbols that are used within only the section in which they are defined.)

System Dimensions and Indices		Definition
M	diversity order	p. 2

N_s	number of co-channel sources	p. 3
N_d	number of dominant co-channel signals	p .9
N_w	number of weak co-channel signals	p .9
$N \equiv N_d - 1$	number of dominant CCI signals	p. 9
m	diversity branch index	p. 5
n	co-channel source index	p. 5
T	symbol period	p. 5
W	bandwidth	p. 7
$B \equiv WT$	excess bandwidth factor	p. 7
$L_a \equiv L$	number of in-phase modulation levels	p. 7, p. 23
L_b	number of quadrature modulation levels	p. 7

Impulse Responses and Frequency Responses

$c_T(t)$; $C_T(f)$	transmit filter	p. 5, p. 7
$c_R(t)$; $C_R(f)$	receive filter	p. 6, p. 7
$g_n(t)$; $G_n(f)$	system response	p. 19
$\tilde{g}_n(t)$; $\tilde{G}_n(f)$	sampled system response	(3.1), (3.4)
$h_{m,n}(t)$; $H_{m,n}(f)$	multipath channel	p. 6
$p_{m,n}(t)$; $P_{m,n}(f)$	matched filter	(4.15), (4.16)
$p_c(t)$; $P_c(f)$	matched filter of combined system	p. 62, (6.23)
$q_{m,n}(t)$; $Q_{m,n}(f)$	link response	(2.2), (2.3)
$q_{cn}(t)$; $Q_{cn}(f)$	equivalent link response of combined system	p. 61, (6.16)
$\mathbf{Q}_n(f)$	link response vector	(2.23)
$\tilde{\mathbf{Q}}_n(f)$	sampled link response vector	(6.5)
$u_m(t)$	continuous-time filter cascade	p. 19
$\tilde{v}_n(t)$; $\tilde{V}_n^*(f)$	transversal filter	p. 44, p. 45
$\tilde{v}_c(t)$; $\tilde{V}_c^*(f)$	transversal filter of combined system	p. 63

Signals and Power Spectra

$r_{m,n}(t)$	received signal from nth source	p. 6
$r_m(t)$	total received signal	p. 10
$r_c(t)$	combined signal	p. 61
$s_m(t)$	noiseless received signal	p. 10
$s_c(t)$	noiseless combined signal	p. 61
$\theta_n(t)$	phase roll	p. 6
$\mathcal{N}(f)$	unfiltered noise in each branch	p. 10
$\eta_m(t)$; $\mathcal{N}_R(f)$	filtered noise	p. 10, (2.8)
$\eta_L(t)$; $\mathcal{N}_L(f)$	noise at sampler input	p. 19
$\tilde{\eta}_L(t)$; $\tilde{\mathcal{N}}_L(f)$	sampled noise	(3.7), (3.8)
$\eta_c(t)$; $\mathcal{N}_c(f)$	combined noise	p. 61, (6.17)

Sequences

$\{a_{n,k}\}$	in-phase data symbols	p. 7

$\{\hat{a}_{n,k}\}$	estimate of in-phase data	p. 22
$\{b_{n,k}\}$	quadrature data symbols	p. 7
$\{\hat{b}_{n,k}\}$	estimate of quadrature data	p. 22
$\{g_{n,k}\}$	discrete impulse response	p. 20, (3.5)
$\{x_{n,k}\}$	complex data symbols	p. 7
$\{\tilde{x}_{n,k}\}$	linear estimate of data	p. 17
$\{\hat{x}_{n,k}\}$	estimate of data	p. 10
$\{z_{n,k}\}$	output of matched filter bank	(4.14)
$\{\theta_{n,k} \equiv \theta_n(kT)\}$	phase roll	p. 6
$\{\eta_k\}$	noise at sampler output	p. 20
$\{\rho_{n,k}\}$	interference coefficients	(3.15)

Others

BER_o	BER threshold	p. 25
$\langle\text{BER}\rangle$	average BER	p. 24
$\{c_{m,n,i}\}$	gaussian variables	p. 12
$\mathbf{c}_n$	gaussian vector	(2.19)
DWR	dominant-interference-to-weak-interference ratio	(2.10)
$d \equiv \tau_0/T$	normalized delay spread	p. 9
f_n	carrier frequency	p. 5
f_r	local oscillator frequency	p. 6
J_n	number of eigenvalues	p. 12
K_η^2	noise variance	p. 60
k_s	timing epoch symbol-offset	p. 59, (6.2)
$P_h(\tau)$	delay spectrum	(2.4)
P_{out}	outage probability	p. 24
P_n	average received power	(2.7)
P_s	combined power of desired signal	(6.18)
$p_\varepsilon(x)$	interference pdf	p. 23
$\mathbf{q}_0$	desired-component vector	(6.6)
$R_H(\alpha)$	frequency autocorrelation function (α is frequency separation)	(2.6)
SIR	signal-to-interference ratio	(2.9)
SIR_w	signal-to-weak-interference ratio	p. 11
S_n	signal gain	p. 6, (2.12)
t_n	timing phase	p. 5, p. 7
t_s	timing epoch	p. 19
t_d	timing epoch at matched filter output	p. 32
w_m^*	branch-weight	p. 58
$\mathbf{w}$	branch-weight vector	(6.4)
Δ_n	carrier frequency offset	p. 6
$\mathcal{N}_w$	weak-interference constant	p. 10, (2.11)
$\mathcal{N}_r$	noise scaling factor	p. 30

$\alpha \equiv B - 1$	rolloff factor	p. 58
ε	residual interference	(3.16)
ϵ	MSE	(3.11)
$\phi_{n,i}(\beta)$	eigenfunction	p. 12
$\boldsymbol{\phi}_n(\beta), \boldsymbol{\phi}(\beta)$	vector of eigenfunctions	(2.21), p. 13
$\lambda_{n,i}, \lambda_i$	eigenvalues	p. 12, p. 34
$\boldsymbol{\Lambda}_n, \boldsymbol{\Lambda}$	vectors of eigenvalues	(2.20), p. 13
μ_i	algebraic multiplicity of eigenvalue	p. 34
$\sigma_a^2, \sigma_b^2, \sigma_x^2$	modulation parameters	p. 7
τ_0	delay spread	(2.5)

Chapter 1
INTRODUCTION

The conventional telephone is burdened with a wire. Users of such communication apparatus are thus tied to fixed locations; they are unable to move about freely. Because of the great desire by people to be free of this tether, wireless or portable communication is a natural and inevitable evolvement in telephony. The remarkable growth in the cordless and cellular telephone industries over the last decade clearly illustrates this eagerness to communicate on the move [Cox, 1989; Goodman, 1991].

Unfortunately, existing cellular radio technology is struggling to meet consumer demand. In particular, first generation cellular systems in the United States, Europe, and Japan are nearing or have reached full capacity. The time has come for a new wave in cellular radio: second generation systems are already operational in Europe, and trials in the United States are under way.

1.1 Digital Cellular Radio

Although there is a host of philosophies on the best future direction of high capacity cellular radio communications, both in and beyond second generation systems, the general opinion is that some form of *digital cellular radio* is the solution [Calhoun, 1988; Balston, 1989; Groves, 1990; Ross, 1991; Goodman, 1991]. Owing to the well known and accepted advantages of digital transmission, especially in its robustness to interference and noise, and to recent advances in low bit-rate speech coding, digital cellular radio promises a significant improvement — in both system capacity and quality of service — over its existing analog counterpart [Calhoun, 1988; Vary, 1988]. There are, however, many challenging problems confronting designers. Most of these problems are grouped into two categories[1]:

- **Limited Bandwidth:** To accommodate many mobile users accessing a limited radio bandwidth in a given service area, it is necessary to reuse radio frequency channels. This multiple user accommodation is achieved through the use of the *cellular* concept [MacDonald, 1979; Cooper and Nettleton, 1983]. *Cells* represent subdivisions of a service area which could be, for example, a city or an entire country. A mobile unit communicates with a base station located within the mobile's cell, the frequency channels for which may be reused by mobiles and base stations in other cells.

  The drawback with frequency reuse is that it introduces *co-channel interference (CCI)*. Because radio signals become weaker as mobiles move away from their base stations and transmission paths may be shadowed by large obstructions, signal-to-CCI ratios can fall to very low values (sometimes less than 10 dB) for typical cell designs and reuse plans

[1] Limited bandwidth (hence frequency reuse and co-channel interference) and multipath propagation (hence fading) are, of course, also inherent in analog cellular systems.

[Schwartz and Yeh, 1982]. The CCI that radio receivers can tolerate thus has a major impact on the capacity of cellular radio systems.

- **Multipath Propagation:** Mobile-to-base transmission (and vice versa) takes place over many paths due to scattering of radio waves by the terrain, buildings, vehicles, and other objects in the environment. The amplitude of the resultant received signal depends on the relative position of the mobile (and the scatterers) with respect to the base station, and on the transmitted frequency [Jakes, 1974, ch. 1]. This *space-selective* and *frequency-selective multipath fading* phenomenon is illustrated in Figure 1.1, where the darkest areas represent a very deep signal fade (more than 30 dB below mean signal level), and the lightest areas represent a very strong received signal (more than 10 dB above mean signal level).

  The bandwidth of the radio signals in a digital cellular system generally depends on the multiple access scheme employed (e.g., time-division or frequency-division) [Calhoun, 1988, ch. 11]. The received signal power of a *narrowband* signal (say, a bandwidth less than 50 kHz) could vary by tens of decibels as the mobile moves just a few centimetres[2] through the multipath environment. A deep fade may result in a complete loss of signal in interference and noise. On the other hand, a *wideband* signal (say, a bandwidth greater than 200 kHz) is less likely to fade to the same extent (only some of its spectral components are likely to fade), but suffers from frequency-selective distortion or, equivalently, *time dispersion*. For digital transmission at high symbol rates, this distortion manifests itself as *intersymbol interference (ISI)* [Chuang, 1987; Calhoun, 1988, ch. 12].

1.2 Diversity and Equalization

Diversity is a well known technique to combat multipath fading [Schwartz *et al.*, 1966, ch. 10; Jakes, 1974, ch. 5]. The principle of diversity is to transmit the radio signal over two or more independent multipath channels, with the hope that at least one of the received signals will not be faded significantly[3]. For example, in an M-fold diversity system, the same signal could be transmitted (i) at M different times (assuming mobile motion or a dynamic multipath environment); (ii) to or from M spatially separated antennas; or (iii) on M different carrier frequencies. These three typical diversity schemes are called *time diversity*, *space diversity*, and *frequency diversity*, respectively. Both time and space diversity exploit the space-selective nature of the multipath channel, whereas frequency diversity exploits its frequency-selective nature. Because bandwidth is a precious resource in digital cellular radio, and both time and frequency diversity lower spectral efficiency, space diversity is likely to be the most favoured of the three schemes[4].

Transmitting a wideband radio signal over a multipath channel (as mentioned in Section 1.1) offers a diversity-like effect referred to as "*intrinsic frequency diversity*." To counter the associated frequency-selective distortion (and therefore ISI), *equalization* techniques can be employed in the receiver [Qureshi, 1985; Proakis, 1991]. In conventional linear equalization, for example, the received signal is passed to an adaptive filter that attempts to flatten out the channel frequency response[5] while avoiding noise enhancement.

---

[2] The spatial correlation depends on the carrier frequency.

[3] The receiver could either choose the least faded signal (*selection* diversity) or combine the received signals in some optimal way (*combining* diversity).

[4] Space diversity also has an advantage over time diversity in static multipath environments.

[5] Usually the *Nyquist equivalent* frequency response [Lucky *et al.*, 1968].

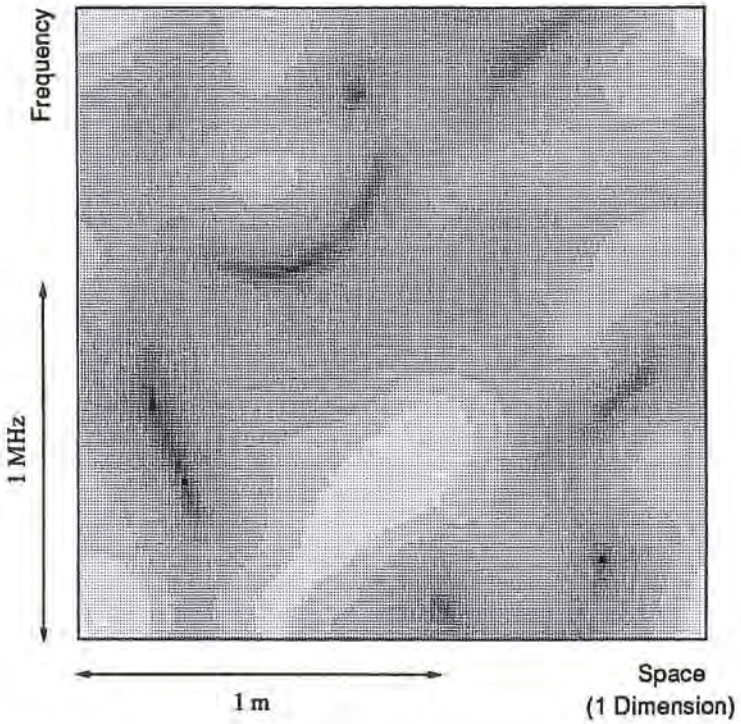

Figure 1.1 Multipath fading: received signal amplitude (logarithmic amplitude represented by lightness; range $\approx$ 40 dB) as a function of mobile position (in one spatial dimension) and frequency. (Generated by computer, assuming 900 MHz carrier, Rayleigh fading, and gaussian spatial and frequency correlation functions with typical urban area statistics.)

There is an additional and not so well known advantage in using space diversity in digital cellular radio. The signal received on each diversity branch from a given mobile (either desired or CCI) is simply a different version of the same transmitted signal. It is possible to exploit this fact, using quite simple diversity combining techniques, to combat interference (ISI and CCI).

In summary, diversity and equalization techniques can be used in digital cellular radio to combat multipath fading, intersymbol interference, and co-channel interference.

1.3 Aim of the Thesis

This thesis presents a study of the communication system illustrated in Figure 1.2, where N_s co-channel sources transmit digital radio signals over multipath fading channels to an M-branch space diversity receiver[6]. The role of the diversity receiver is to somehow process the M received signals to estimate the digital information transmitted from one of more of the N_s co-channel sources.

The broad aim of the work is to determine the potential performance of three important types of diversity receiver: the *maximum likelihood receiver* (the best-possible receiver), *optimum*

[6]The thesis studies mobile-to-base transmission with M-branch space diversity at the base. However, there is no reason why the study does not apply to any M-branch diversity scheme and, assuming the multipath channel statistics are the same for both the forward and reverse links, to the base-to-mobile link. (In practice, this channel reciprocity can be exploited to avoid multiple antennas at the mobile, by using adaptive retransmission or "Ping-Pong" transmission [Henry and Glance, 1981].)

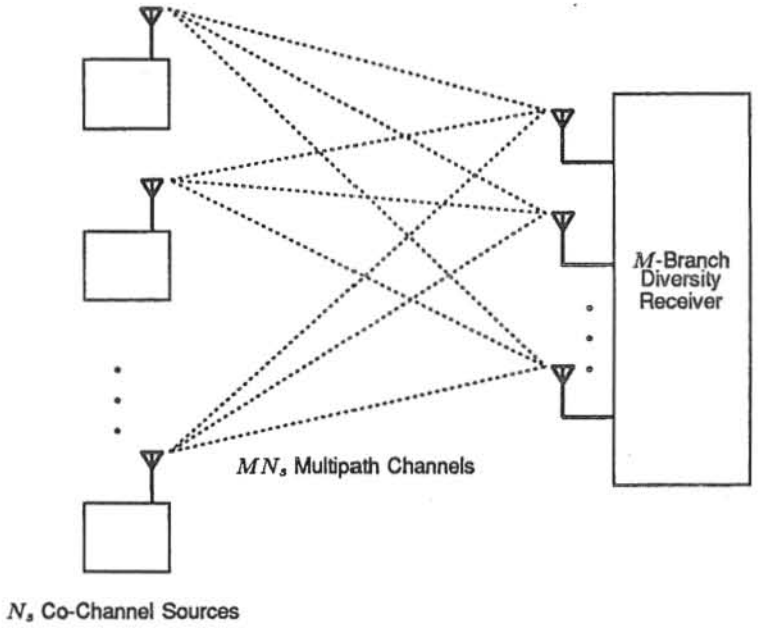

Figure 1.2 Digital cellular radio communication system with N_s co-channel sources and an M-branch diversity receiver.

linear receivers, and *memoryless linear combining receivers* (with and without *post-combiner equalization*). The thesis presents a comprehensive and general treatment of frequency-selective fading and CCI for the three receiver classes, and numerical results that show important tradeoffs between performance and complexity. The original work includes the following key contributions:

- Totally analytical solution for the *matched filter bound* on maximum likelihood receiver performance;
- Novel way to present and analyse the optimum linear receiver, and an in-depth study showing the power of M-branch receiver processing at combating dominant CCI in frequency-selective fading environments;
- A study of *five* important sub-classes of memoryless combining receivers, and results that show how simple memoryless combining can not only combat fading and CCI, but also offer a good equalization capability without the aid of post-combiner processing;
- In-depth study of *bit-error-rate (BER)* computation methods, illustrating the uses and limits of the *mean-square error (MSE)* as a performance measure and optimization criterion;
- Use of the Karhunen-Loève method to achieve very efficient simulation programs.

Ultimately, the performance bounds presented in this thesis are of major importance to engineers needing to know the extent to which the use of diversity and equalization can increase the capacity of digital cellular radio systems.

Chapter 2

DIGITAL CELLULAR SYSTEM MODEL

This chapter develops a model of the digital cellular radio system illustrated in Figure 1.2. It is assumed that the N_s co-channel sources all employ an identical linear digital modulation scheme, each with the same data rate and signal bandwidth. Also, in simplifying system analysis and in pursuit of performance bounds, ideal microscopic space diversity [Cox, 1987] is assumed for the M-branch receiver. That is, the receiving antennas are assumed to be spaced sufficiently close together such that the average received power (taken over the multipath fading) from a given co-channel source is the same on every diversity branch, but spaced sufficiently far apart to ensure independent multipath fading on each branch[1]. Typically, the antenna spacing should be about half a wavelength ($\approx$ 15 cm for a 900 MHz carrier). The noise on each branch is assumed to be independent and gaussian, but with the same power spectral density.

Section 2.1 describes (i) the data transmission link between a given co-channel source and each diversity branch, i.e., the modulation, the fixed transmit and receive filters, and the multipath channel model; and (ii) the co-channel interference and gaussian noise models. Section 2.2 shows how a link frequency response is represented by the Karhunen-Loève orthogonal series expansion, which proves to be a very useful tool for analysis and simulation in later chapters. Both sections introduce notation and list assumptions relating to the analyses and numerical results in the remainder of the thesis.

2.1 Transmission Links

2.1.1 General

Figure 2.1 illustrates the model of the data transmission link between the nth co-channel source and the mth diversity branch, where

- $\{x_{n,k}\}$ is the sequence of data symbols, transmitted at *symbol rate* $1/T$, from the nth source;
- t_n is the timing phase of the data sequence from the nth source;
- $c_T(t)$ is the baseband impulse response of the transmit filter;
- f_n is the carrier frequency[2] of the nth source;
- $\check{h}_{m,n}(t)$ is the *bandpass impulse response* of the multipath channel between the nth source and the mth diversity branch, where the argument t represents *excess* delay [Cox, 1975];

[1] In practice, there will be some branch-to-branch correlation of the multipath fading. This correlation would presumably degrade receiver performance.

[2] The carrier phase of the nth source is omitted in the link model. An arbitrary (but fixed) phase will not affect the link statistics (see Section 2.1.3).

- S_n is a signal gain factor that includes the effects of equipment gains and attenuations, path loss, and slow shadow fading [Calhoun, 1988, ch. 8], for the nth source;
- f_r is the local oscillator frequency of the diversity receiver;
- $c_R(t)$ is the baseband impulse response of the *fixed* receive filter[3]; and
- $r_{m,n}(t)$ is the received (and filtered) baseband signal on the mth diversity branch, from the nth source.

The symbol rate $1/T$ and the transmit filter response $c_T(t)$ are assumed to be the same for every co-channel source; the local oscillator frequency f_r, the receive filter response $c_R(t)$, the timing phases $\{t_n\}$, and the signal gains $\{S_n\}$ are assumed to be the same for every diversity branch. Using standard techniques [Haykin, 1983, ch. 1; Lee and Messerschmitt, 1988, pp. 399–402], it is

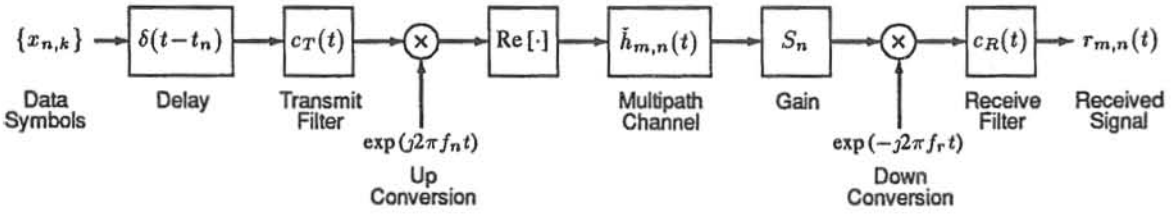

Figure 2.1 Data transmission link between the nth source and the mth diversity branch, including modulator, demodulator, fixed transmit/receive filtering, and multipath channel.

straightforward to show that the *complex baseband equivalent link* is as illustrated in Figure 2.2, where

- $\theta_n(t) \triangleq \exp(\jmath 2\pi \Delta_n t)$ is the *phase-roll* of the nth source's transmitted data signal, where $\Delta_n \triangleq f_n - f_r$ is the difference between the carrier frequency of the nth source and the receiver's local oscillator frequency;
- $\{x_{n,k}\,\theta_{n,k}\}$ is the sequence of phase-rolled data symbols from the nth source, where $\theta_{n,k} \triangleq \theta_n(kT)$;
- $c_T(t - t_n)\,\theta_n(t)$ is the impulse response of the transmit filter, time-shifted by t_n seconds and frequency-shifted by Δ_n hertz;
- $h_{m,n}(t)$ is the *complex baseband equivalent impulse response* of the multipath channel between the nth source and the mth diversity branch, i.e., such that $\check{h}_{m,n}(t) = \mathrm{Re}\,[2\,h_{m,n}(t)\,\exp(\jmath 2\pi f_n t)]$.

The received signal on the mth diversity branch from the nth source is

$$r_{m,n}(t) = S_n \sum_k x_{n,k}\,\theta_{n,k}\,q_{m,n}(t - kT) \tag{2.1}$$

where

$$q_{m,n}(t) = [c_T(t - t_n)\,\theta_n(t)] \odot h_{m,n}(t) \odot c_R(t) \tag{2.2}$$

[3]For optimum receiver design, $c_R(t)$ will depend on the transmit filter response $c_T(t)$ and other factors.

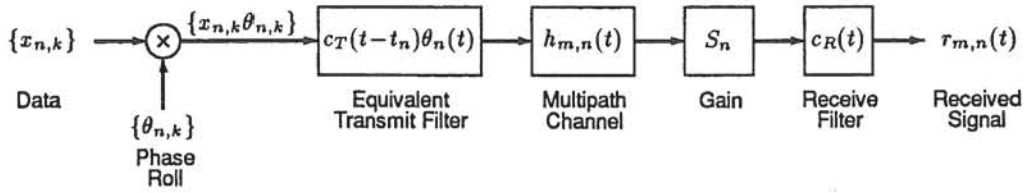

Figure 2.2 Complex baseband equivalent link between the nth source and the mth diversity branch.

is referred to as the *link impulse response* (it excludes the signal gain factor S_n) between the nth phase-rolled source and the mth diversity branch. The corresponding *link frequency response* is

$$Q_{m,n}(f) = \mathcal{F}\left[q_{m,n}(t)\right] = C_n(f)\, H_{m,n}(f) \exp\left(-j2\pi(f+\Delta_n)t_n\right) \tag{2.3}$$

where $C_n(f) \triangleq C_T(f+\Delta_n)\, C_R(f)$; and $C_T(f)$, $C_R(f)$, and $H_{m,n}(f)$ are the Fourier transforms of $c_T(t)$, $c_R(t)$, and $h_{m,n}(t)$, respectively. In this thesis, all analysis is quite general with respect to the carrier difference set $\{\Delta_n\}$ and to the shape of the transmit filter response $C_T(f)$. The only assumption is that the transmit filter has a two-sided bandwidth $W{=}B/T$, where B is the *excess bandwidth factor* (typically, $1 \leq B \leq 2$). That is, $C_T(f) = 0, |f| > W/2$, and $C_n(f){=}0, |f+\Delta_n| > W/2$.

The numerical results, however, are restricted to the case in which all carrier frequencies $\{f_n\}$ are equal, and in which the receiver performs ideal coherent demodulation, i.e., we have $\{\Delta_n{=}0, \forall n\}$.

2.1.2 Data Sources and Modulations

Each of the N_s co-channel sources is assumed to generate a sequence of complex data symbols $\{x_{n,k} = a_{n,k} + jb_{n,k}\}$, where $x_{n,0}$ is referred to as the *current symbol* from the nth source ($x_{n,-k}$ and $x_{n,k}$, $k>0$, are past and future values, respectively). Infinite-length data sequences $\{x_{n,k}\}$ are assumed, so it is arbitrary which symbol from a given source is defined as the current symbol. In this case, the timing phases $\{t_n\}$ are simply regarded as uniformly distributed over $[-T/2, T/2)$.

Although it is easily possible to extend most analysis in this thesis to any linear modulation scheme, the study is restricted, for simplicity, to rectangular signal constellations. Thus, the $a_{n,k}$'s come from the set $\{\pm1, \pm3, \ldots, \pm(L_a{-}1)\}$, where L_a is the number of possible levels in $\{a_{n,k}\}$; and the $b_{n,k}$'s come from the set $\{\pm1, \pm3, \ldots, \pm(L_b{-}1)\}$, where L_b is the number of possible levels in $\{b_{n,k}\}$. Each symbol $x_{n,k}$ corresponds to $N_b = \log_2(L_a L_b)$ *bits* which are assumed to be Gray encoded [Lee and Messerschmitt, 1988, p. 193] onto the rectangular signal constellation. (The *bit rate* of each source is $1/T_b = N_b/T$.)

The data symbols are assumed to be random and uncorrelated. From [Lucky *et al.*, 1968], we have $E\left[|a_{n,k}|^2\right] = \sigma_a^2 = (L_a^2 - 1)/3$, and $E\left[|b_{n,k}|^2\right] = \sigma_b^2 = (L_b^2 - 1)/3$, where the expectation is taken over all possible data sequences. Hence, we get $E\left[|x_{n,k}|^2\right] = \sigma_x^2$, where $\sigma_x^2 = \sigma_a^2 + \sigma_b^2$. Note that the phase-rolled symbols $\{x_{n,k}\,\theta_{n,k}\}$ are also uncorrelated, with $E\left[|x_{n,k}\,\theta_{n,k}|^2\right] = \sigma_x^2$.

Table 2.1 shows the modulation parameters for three typical linear modulation schemes: binary phase shift keying (BPSK), quarternary phase shift keying (QPSK), and 16-level quadrature amplitude modulation (16-QAM).

Modulation	L_a	L_b	σ_a^2	σ_b^2	σ_x^2	N_b
BPSK	2	1	1	0	1	1
QPSK	2	2	1	1	2	2
16-QAM	4	4	5	5	10	4

Table 2.1 Modulation parameters.

2.1.3 Multipath Fading Channels

The shape of $h_{m,n}(t)$ varies as the nth mobile moves through the multipath environment (or as the scatterers in that environment move). To analyse the system and to obtain performance bounds, it is assumed that the receiver can perfectly track these channel dynamics[4]. In this context, $h_{m,n}(t)$ can be viewed as a sample function taken from an *ensemble* of static channel responses, where the ensemble represents an infinite set of such functions taken from the time evolution of the multipath channel.

The ensemble of multipath channel impulse responses is characterized in the following way [Glance and Greenstein, 1983; Proakis, 1989, ch. 7]: The function $h_{m,n}(t)$ is from an independent nonstationary zero-mean complex gaussian (Rayleigh magnitude) random process with the autocorrelation function[5]

$$E[h^*_{m,n}(\tau)\, h_{m,n}(\tau + x)] = P_h(\tau)\, \delta(x) \tag{2.4}$$

where $P_h(\tau)$ is the *delay power spectrum*[6] — or simply the *delay spectrum* — which is assumed to be the same for each source and each branch. The impulse responses in the set $\{h_{m,n}(t)\}$ are scaled so that the area under $P_h(\tau)$ is unity (the gain factor set $\{S_n\}$ takes into account this scaling). The multipath channel's *root-mean-square (rms) delay spread* (or simply the *delay spread*) is

$$\tau_0 = \left[\int_{-\infty}^{\infty} (\tau - \overline{\tau})^2 P_h(\tau)\, d\tau\right]^{\frac{1}{2}} \tag{2.5}$$

where $\overline{\tau} = \int_{-\infty}^{\infty} \tau\, P_h(\tau)\, d\tau$ is the *mean delay*.

The number of independent Rayleigh fading paths and their relative average powers are specified by the delay spectrum. For example, a double-spike delay spectrum corresponds to two paths, and a theoretically continuous delay spectrum corresponds to an infinite number of paths with an infinitesimal delay between consecutive paths[7].

The channel frequency response between the nth source and the mth diversity branch is $H_{m,n}(f) = \mathcal{F}[h_{m,n}(\tau)]$. The function $H_{m,n}(f)$ is from an independent stationary zero-mean complex gaussian random process with the autocorrelation function

$$E[H^*_{m,n}(f)\, H_{m,n}(f + \alpha)] = R_H(\alpha) \tag{2.6}$$

[4] In this study, the data rates are assumed to be large compared with the fading rates, making accurate channel tracking feasible. That is, if accurate tracking requires that at least N_t symbols (typically tens of symbols) be received over an essentially static channel, it is assumed that $N_t T \ll T_c$, where T_c is the multipath channel's *coherence time*, or equivalently, that $W/N_t \gg W_d$, where W_d is the channel's *Doppler spread* [Proakis, 1989, ch. 7]. If this slow-fading channel assumption did not hold, we would require a second-order statistical channel model that incorporated the *Doppler spectrum* as well as the delay power spectrum.

[5] Strictly speaking, two autocorrelation functions are required to characterize a complex random process [Bello, 1964]. However, for all complex random processes in this thesis, it is assumed that the real and imaginary components have the same autocorrelation function and a zero cross-correlation.

[6] Also referred to as the *average power delay profile* or the *multipath intensity profile*.

[7] The *continuous* delay spectrum is a useful approximation to one that characterizes a channel with a large number of paths spaced at most τ_s seconds apart, provided that the signal bandwidth W is much smaller than $1/\tau_s$.

where $R_H(\alpha)$, the *frequency autocorrelation function*, is assumed to be the same for each source and each branch, and is related to the delay spectrum through the Fourier transform $R_H(\alpha) = \mathcal{F}[P_h(\tau)]$.

In Chapters 4, 5, and 6, numerical results are obtained for a representative range of delay spectra whose expressions are given in Table 2.2 with their associated frequency autocorrelation functions. This range is considered for the following reasons: (i) the Exponential spectrum approximates continuous spectra that have been measured in urban environments [Cox, 1975]; (ii) the Gaussian spectrum (also treated in [Glance and Greenstein, 1983] and elsewhere) represents the class of *two*-sided continuous spectra; and (iii) the Double-Spike spectrum (also treated in [Balaban and Salz, 1991; Glance and Greenstein, 1983; Mazo, 1991] and elsewhere) represents spectra typical in mountainous regions and overwater paths, and tends to yield worst-case results for a given rms delay spread, τ_0.

Delay Spectrum	$P_h(\tau)$	$R_H(\alpha)$
Exponential	$\frac{1}{\tau_0}\exp[-\tau/\tau_0],\ \tau \geq 0$	$\frac{1}{1+j2\pi\alpha\tau_0}$
Gaussian	$\frac{1}{\sqrt{2\pi}\tau_0}\exp[-\frac{1}{2}(\tau/\tau_0)^2]$	$\exp[-2(\pi\alpha\tau_0)^2]$
Double-Spike	$\frac{1}{2}[\delta(\tau)+\delta(\tau-2\tau_0)]$	$\frac{1}{2}[1+\exp(-j4\pi\alpha\tau_0)]$

Table 2.2 Delay spectra and frequency autocorrelation functions.

The *time dispersion* and *frequency selectivity* of a multipath fading channel is specified by the normalized delay spread parameter $d \equiv \tau_0/T$ (d=0 for *frequency-flat* fading or, simply, *flat* fading). Thus, a given value of d represents various combinations of channel delay spread and data transmission rate. For example, d=1 may represent QPSK transmission at 250 kbit/s in a typical hilly area with a delay spread of 8 μs, or at 500 kbit/s in an urban area with a delay spread of 4 μs. From the discussion in Chapter 1, it is clear that, in general, increasing d has the advantage of providing a greater intrinsic frequency diversity, but the disadvantage of increasing the level of potential ISI.

2.1.4 Co-Channel Interference and Noise

Using standard techniques [Lucky *et al.*, 1968], it is easily shown that the average received power from the nth source — on each diversity branch, *before* fixed receive filtering — is

$$P_n = \frac{S_n^2\,\sigma_x^2}{T}\int_{-W/2}^{W/2} |C_T(f)|^2\,df \tag{2.7}$$

where the average is taken over the data and multipath channel ensemble (alternatively, P_n is for an unfaded channel set $\{H_{m,n}(f)=1, \forall m\}$ and averaged over the data only). To simplify system analysis, the N_s co-channel signals that are received are divided into two groups:

1. N_d *dominant* co-channel signals (indexed by $n = 0, 1, \ldots, N$) for which $\{P_n\}$, or equivalently $\{S_n\}$, are relatively large; and

2. N_w *weak* co-channel signals (indexed by $n = N+1, N+2, \ldots, N_s - 1$) for which $\{P_n\}$ are relatively small.

(Note that $N_s = N_d + N_w$ and $N = N_d - 1$.) Furthermore, it is assumed that (i) the receiver estimates the data associated with only the N_d dominant co-channel signals, or a subset of them; (ii) the number of weak co-channel signals is much greater than the number of diversity branches, i.e., $N_w \gg M$; (iii) each weak co-channel signal has approximately the same average power; and (iv) the carrier frequency of each weak co-channel signal is equal to the local oscillator frequency. As a result of these assumptions (and based on the Central Limit Theorem and other standard techniques [Papoulis, 1965]), we can regard the *sum* of N_w weak unfiltered co-channel signals received on each diversity branch as an independent stationary zero-mean complex gaussian random process, with the power spectrum (or power spectral density) $\mathcal{N}_w |C_T(f)|^2, |f| \leq W/2$, where $\mathcal{N}_w = \sum_{n>N} S_n^2 \sigma_x^2 / T$. Thus, the combination of N_w weak co-channel signals on each branch is referred to as *noise-like CCI*, and is lumped with all other additive gaussian noise sources (e.g., thermal noise).

It is assumed that the unfiltered gaussian noise on each diversity branch — which includes noise-like CCI — has arbitrary power spectrum $\mathcal{N}(f)$. The *filtered* noise on the mth diversity branch is denoted by $\eta_m(t)$, and has the power spectrum

$$\mathcal{N}_R(f) = \mathcal{N}(f) |C_R(f)|^2 \tag{2.8}$$

All analysis in this thesis is quite general with respect to the unfiltered noise power spectrum $\mathcal{N}(f)$, requiring only that it have no zero within the band of any dominant co-channel signal (always the case in practice). In the numerical results, however, it is assumed that the noise in each branch is composed *entirely* of noise-like CCI, so we get $\eta_m(t) = \sum_{n>N} r_{m,n}(t)$ and $\mathcal{N}(f) = \mathcal{N}_w |C_T(f)|^2, |f| \leq W/2$. Whenever appropriate, this special case is highlighted in the general analysis.

The complex baseband equivalent model of the digital cellular system, in light of the above assumptions, is illustrated in Figure 2.3, where

- $s_m(t) = \sum_{n=0}^{N} r_{m,n}(t)$ is the sum of *dominant* co-channel signals on the mth diversity branch;
- $r_m(t) = s_m(t) + \eta_m(t)$ is the total received signal (dominant co-channel signals, weak co-channel signals, and other gaussian noise sources) on the mth diversity branch; and
- $\{\hat{x}_{n,k}\}$ is the receiver's estimate of the data sequence from the nth source, $\{x_{n,k}\}$ (associated with the nth *dominant* co-channel signal).

(Recall from Section 2.1.1 that the fixed receive filter $c_R(t)$ is included in the link responses, rather than in the diversity receiver.)

When analysing the diversity receiver, it is sufficient to evaluate its performance only in estimating data from a *single* arbitrary source. For this purpose, the sequence $\{x_{0,k}\}$ is regarded as the *desired source*, and the data sequences $\{x_{1,k}\}, \{x_{2,k}\}, \ldots, \{x_{N,k}\}$ as *dominant CCI* sources. For parameterizing the numerical results, two average power ratios are defined:

1. The ratio of average desired signal power to average CCI power (or, simply, the signal-to-interference ratio)

$$\text{SIR} \triangleq \frac{P_0}{\sum_{n \neq 0} P_n} = \frac{S_0^2}{\sum_{n=1}^{N} S_n^2 + \sum_{n>N} S_n^2} \tag{2.9}$$

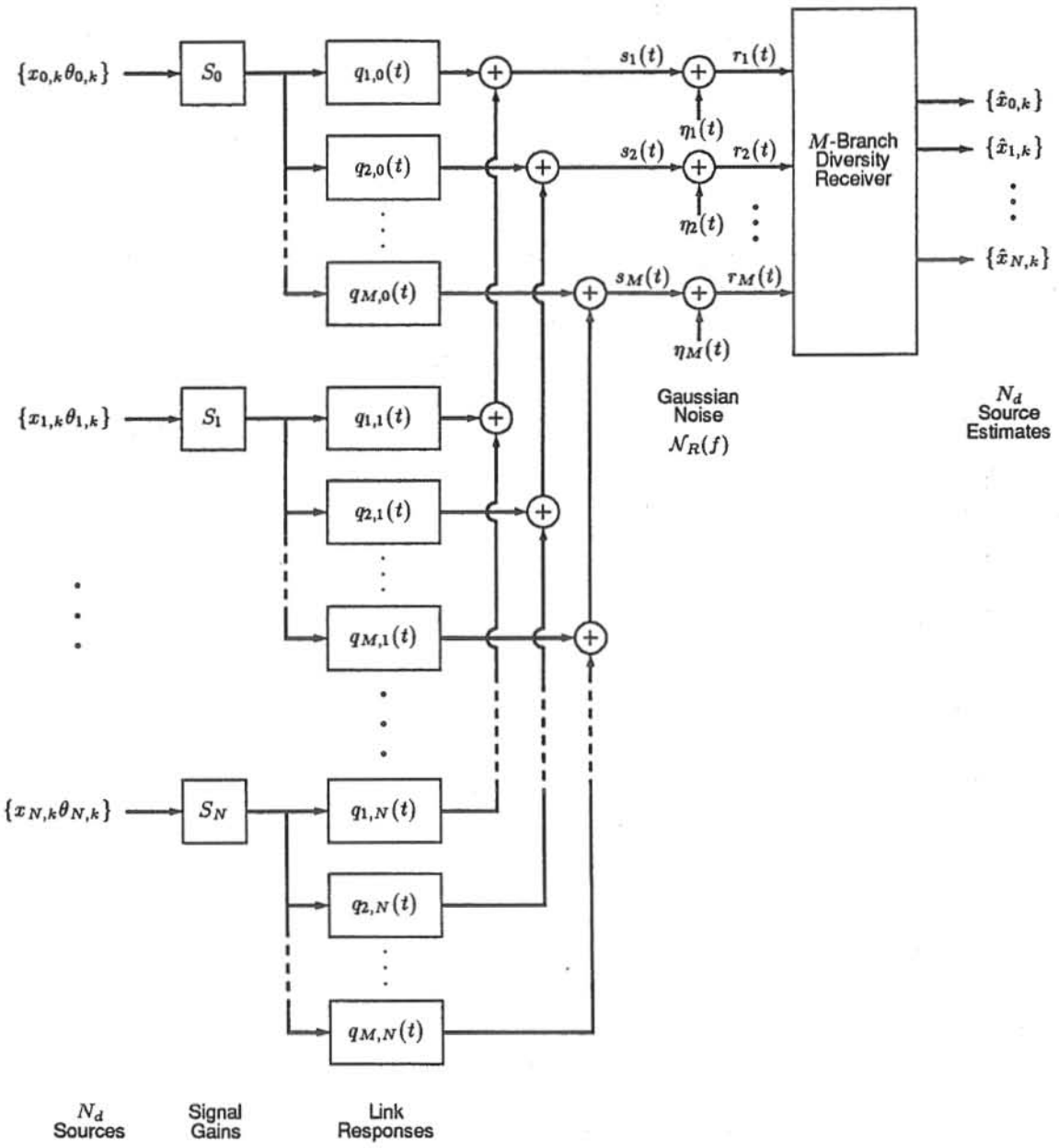

Figure 2.3 Complex baseband equivalent model of the digital cellular radio system.

2. The ratio of average dominant CCI power to average noise-like CCI power (or, simply, the dominant-interference-to-weak-interference ratio)

$$\text{DWR} \triangleq \frac{\sum_{n=1}^{N} P_n}{\sum_{n>N} P_n} = \frac{\sum_{n=1}^{N} S_n^2}{\sum_{n>N} S_n^2} \tag{2.10}$$

Note that we have the useful relationship

$$\mathcal{N}_w = S_0^2 \sigma_x^2 / (T \, \text{SIR}_w) \tag{2.11}$$

where $\text{SIR}_w \triangleq \text{SIR}(\text{DWR} + 1)$ is the ratio of average desired signal power to average noise-like CCI power. For simplicity in the numerical results, moreover, all the dominant interferers are taken to have the same average power. In this case, the dominant interferer gains are given by

$$S_n = S_0[N\text{SIR}((1/\text{DWR}) + 1)]^{-\frac{1}{2}}, \quad n = 1, 2, \ldots, N \tag{2.12}$$

The level of CCI (dominant and noise-like) is specified by the SIR parameter. In a typical cellular environment, this parameter will vary slowly in the range 0 to 40 dB, due to time-varying propagation distances and shadow fading [Calhoun, 1988].

2.2 Karhunen-Loève Representations of Link Responses

The following method is very useful for (i) randomly generating link frequency responses in order to compute numerical results (used in Chapters 5 and 6); and (ii) deriving an analytical solution for the matched filter bound (Chapter 4).

Because there is a linear relationship between the link responses and the multipath channel responses, it follows that $q_{m,n}(t)$ and $Q_{m,n}(f)$ are also complex gaussian random processes, each with their own ensemble. The link frequency response between the nth co-channel source and the mth diversity branch can be written as

$$Q_{m,n}(f) = Z_{m,n}(\beta) \exp(-j2\pi B\beta t_n/T), \quad \beta \equiv (f + \Delta_n)/W \tag{2.13}$$

where $Z_{m,n}(\beta) \triangleq C_n(f)\, H_{m,n}(f)$, $|\beta \equiv (f + \Delta_n)/W| \leq \frac{1}{2}$. Using the Karhunen-Loève orthogonal expansion [Davenport and Root, 1958], we have

$$Z_{m,n}(\beta) = \sum_{i=1}^{J_n} \sqrt{\lambda_{n,i}}\, c_{m,n,i}\, \phi_{n,i}(\beta), \tag{2.14}$$

where $\{\lambda_{n,i}\}$ is a set of J_n eigenvalues; $\{c_{m,n,i}\}$ is a set of independent zero-mean complex gaussian random variables with $E\left[|c_{m,n,i}|^2\right] = 1$, and $\{\phi_{n,i}(\beta)\}$ is a set of orthonormal eigenfunctions, i.e., such that

$$\int_{-1/2}^{1/2} \phi^*_{n,i_1}(\beta)\, \phi_{n,i_2}(\beta)\, d\beta = \delta_{i_1,i_2} \tag{2.15}$$

The eigenvalues and eigenfunctions satisfy the integral equation

$$\int_{-1/2}^{1/2} R_{Zn}(\beta_1, \beta_2)\, \phi_{n,i}(\beta_2)\, d\beta_2 = \lambda_{n,i}\, \phi_{n,i}(\beta_1), \quad |\beta_1| \leq \frac{1}{2} \tag{2.16}$$

where

$$R_{Zn}(\beta_1, \beta_2) = E[Z^*_{m,n}(\beta_1)\, Z_{m,n}(\beta_2)] = C^*_n(f_1)\, C_n(f_2)\, R_H(f_2 - f_1),$$
$$|\beta_1 \equiv (f_1 + \Delta_n)/W| \leq \frac{1}{2}, \quad |\beta_2 \equiv (f_2 + \Delta_n)/W| \leq \frac{1}{2} \tag{2.17}$$

The eigensystem in (2.16) is solved using standard methods (see Appendix).

Alternatively, the orthogonal expansion can be written in matrix form,

$$\mathbf{Z}_n(\beta) \triangleq \begin{bmatrix} Z_{1,n}(\beta) \\ Z_{2,n}(\beta) \\ \vdots \\ Z_{M,n}(\beta) \end{bmatrix} = \mathbf{c}_n\, \mathbf{\Lambda}_n^{\frac{1}{2}}\, \boldsymbol{\phi}_n(\beta), \quad |\beta| \leq \frac{1}{2} \tag{2.18}$$

where

$$\mathbf{c}_n = \begin{bmatrix} c_{1,n,1} & c_{1,n,2} & \cdots & c_{1,n,J_n} \\ c_{2,n,1} & c_{2,n,2} & \cdots & c_{2,n,J_n} \\ \vdots & \vdots & \ddots & \vdots \\ c_{M,n,1} & c_{M,n,2} & \cdots & c_{M,n,J_n} \end{bmatrix} \tag{2.19}$$

$$\Lambda_n = \text{diag}[\ \lambda_{n,1} \quad \lambda_{n,2} \quad \ldots \quad \lambda_{n,J_n}\ ] \tag{2.20}$$

and

$$\phi_n(\beta) = \begin{bmatrix} \phi_{n,1}(\beta) \\ \phi_{n,2}(\beta) \\ \vdots \\ \phi_{n,J_n}(\beta) \end{bmatrix} \tag{2.21}$$

For the nth source, the orthonormal property of $\{\phi_{n,i}(\beta)\}$ in (2.15) is equivalent to

$$\int_{-1/2}^{1/2} \phi_n(\beta)\phi_n^H(\beta)\, d\beta = \mathbf{I}_n \tag{2.22}$$

where $\mathbf{I}_n$ is a $J_n \times J_n$ identity matrix. The M link frequency responses for the nth source can be written as

$$\mathbf{Q}_n(f) \triangleq \begin{bmatrix} Q_{1,n}(f) \\ Q_{2,n}(f) \\ \vdots \\ Q_{M,n}(f) \end{bmatrix} = \mathbf{c}_n\, \Lambda_n^{\frac{1}{2}}\, \phi_n(\beta)\, \exp\left(-\jmath 2\pi B\beta t_n/T\right), \quad |\beta \equiv (f+\Delta_n)/W| \leq \frac{1}{2} \tag{2.23}$$

To randomly generate $\{Q_{m,n}(f)\}$ for the nth source, we (i) generate MJ_n independent zero-mean unity-variance complex gaussian random variables in the matrix $\mathbf{c}_n$; (ii) generate the random variables $\{t_n/T\}$ uniformly distributed on $[-\frac{1}{2}, \frac{1}{2})$; and (iii) compute $\{Q_{m,n}(f)\}$ via (2.23). Given the cascade filter response $C_n(f)$, the delay spectrum shape $P_h(\tau)$, and the delay spread τ_0, the matrix $\Lambda_n^{\frac{1}{2}}\phi_n(\beta)$ need be computed only once at the start of the ensemble generation. (In the numerical results we have $\{\Delta_n = 0, \forall n\}$, so $\Lambda_n^{\frac{1}{2}}\phi_n(\beta)$ is the same for every co-channel source.) This approach is very fast and accurate compared with computing the time-sampled functions $\{h_{m,n}(t)\}$ via (2.4) and taking discrete Fourier transforms.

Note: For delay spectra consisting of just a few spikes, the Karhunen-Loéve expansion is not the best method for random generation of $\{Q_{m,n}(f)\}$ (it is, however, useful in computing matched filter bounds — see Chapter 4). A more efficient approach is simply to generate a set of MN_dN_p independent zero-mean complex gaussian random variables $\{h_{m,n,j}\}$ with $E\left[|h_{m,n,j}|^2\right] = \Omega_j$, and compute $Q_{m,n}(f) = C_n(f)\exp(-\jmath 2\pi f t_n)\sum_{j=1}^{N_p} h_{m,n,j}\exp\left(-\jmath 2\pi f\tau_j\right), \forall m, n$ (see Appendix for definitions of N_p, $\{\Omega_j\}$, and $\{\tau_j\}$).

2.3 Conclusion

This chapter has developed a quite general digital cellular system model that includes frequency-selective multipath fading, co-channel interference, and diversity reception. The model is used, together with its associated terminology and notation, in the remainder of the thesis.

At this stage, details on the operation of the diversity receiver are unspecified. The next chapter, however, discusses the operation and analyses the performance of an important class of receivers: *linear diversity receivers*.

Appendix 2A Solving the Eigensystem

Depending on the nature of $R_{Zn}(\beta_1, \beta_2)$ in (2.17), it may be possible to solve for $\{\lambda_{n,i}\}$ in (2.16) using analytical techniques [Davenport and Root, 1958]. In this Appendix, however, methods for computing the eigenvalues $\{\lambda_{n,i}\}$ for general $R_{Zn}(\beta_1, \beta_2)$ are outlined.

Finite-Spike Delay Spectra

For a finite number of propagation paths, we have

$$P_h(\tau) = \sum_{j=1}^{N_p} \Omega_j \, \delta(\tau - \tau_j); \quad \text{and} \quad R_H(\alpha) = \sum_{j=1}^{N_p} \Omega_j \, \exp\left(-\jmath 2\pi \alpha \tau_j\right) \tag{2.24}$$

where $\{\Omega_j\}$ and $\{\tau_j\}$ are sets of N_p mean-square path magnitudes and N_p path delays, respectively. Substituting (2.17), with the $R_H(\alpha)$ shown in (2.24), into (2.16), we get

$$\begin{aligned} &C_n^*(f_1) \textstyle\sum_{j=1}^{N_p} \Omega_j \exp\left(\jmath 2\pi f_1 \tau_j\right) \\ &\quad \cdot \textstyle\int_{-1/2}^{1/2} C_n(f_2) \exp\left(-\jmath 2\pi f_2 \tau_j\right) \phi_{n,i}(\beta_2) \, d\beta_2 = \lambda_{n,i} \, \phi_{n,i}(\beta_1), \quad |\beta_1| \le \tfrac{1}{2} \end{aligned} \tag{2.25}$$

Because the integral in (2.25) is independent of β_1 (and therefore f_1), we have

$$\phi_{n,i}(\beta) = C_n^*(f) \sum_{j=1}^{N_p} \psi_{n,i,j} \, \Omega_j \exp\left(\jmath 2\pi f \tau_j\right) \tag{2.26}$$

where $\{\psi_{n,j}\}$ is a set of values yet to be determined. Substituting (2.26) into (2.25), and equating for all β_1, we obtain the system of N_p linear equations

$$\mathbf{S}_n \boldsymbol{\psi}_{n,i} = \lambda_{n,i} \boldsymbol{\psi}_{n,i} \tag{2.27}$$

where

$$[\mathbf{S}_n]_{j,j'} = \Omega_j \int_{-1/2}^{1/2} |C_n(f)|^2 \exp\left(-\jmath 2\pi f(\tau_j - \tau_{j'})\right) d\beta \tag{2.28}$$

and $[\boldsymbol{\psi}_{n,i}]_j = \psi_{n,i,j}$. Note that in the special case where $\Delta_n = 0$ and $C_n(f)$ is unity across the signal band, we get

$$[\mathbf{S}_n]_{j,j'} = \Omega_j \, \mathrm{sinc}(W(\tau_j - \tau_{j'})) \tag{2.29}$$

More specifically, for the double-spike delay spectrum given in Table 2.2, the eigenvalues are $\lambda_{n,1} = \frac{1}{2}(1 + \mathrm{sinc}(2Bd))$ and $\lambda_{n,2} = \frac{1}{2}(1 - \mathrm{sinc}(2Bd))$. For general finite-spike delay spectra, the eigensystem in (2.27) can be solved and normalized (according to (2.15)) using standard numerical methods [Press *et al.*, 1986; Moler, 1990].

Continuous Delay Spectra

Using Simpson's method of numerical integration, the integral equation in (2.16) can be expressed as the system of J_n linear equations

$$\mathbf{R}_n \mathbf{D}_n \boldsymbol{\phi}_{n,i} = \lambda_{n,i} \boldsymbol{\phi}_{n,i} \tag{2.30}$$

where

$$[\mathbf{R}_n]_{j,j'} = R_{Zn}(\beta_j, \beta_{j'}) \tag{2.31}$$

$$[\mathbf{D}_n]_{j,j'} = \begin{cases} \Delta_\beta/3, & j = j' = 1 \text{ or } j = j' = J_n \\ 4\Delta_\beta/3, & j = j' = 2, 4, \ldots, J_n - 1 \\ 2\Delta_\beta/3, & j = j' = 3, 5, \ldots, J_n - 2 \\ 0, & j \neq j' \end{cases} \tag{2.32}$$

$[\phi_{n,i}]_j = \phi_{n,i}(\beta_j)$; $\Delta_\beta = 1/(J_n - 1)$; $\beta_j = -1/2 + (j-1)\Delta_\beta$; and J_n is an odd integer (e.g., in the numerical results: $J_n = 25, 37$, and 49 for $d = 0.5, 1$, and 2, respectively). The eigensystem in (2.30) is solved and normalized (according to (2.15)) using standard numerical methods [Press *et al.*, 1986; Moler, 1990].

Chapter 3

ANALYSIS OF LINEAR SYSTEMS

As mentioned in Chapter 1, three types of diversity receiver are studied in this thesis: the maximum likelihood receiver (Chapter 4), optimum linear receivers (Chapter 5), and memoryless linear combining receivers (Chapter 6). The structures of the receivers studied out of these three classes are either linear or, for the purposes of analysis, reduced to being linear (for example, in computing the matched filter bound on maximum likelihood receiver performance). Consequently, the entire digital cellular system (shown in Figure 2.3) is linear for all diversity receivers analysed and, furthermore, there are many analytical techniques common to each receiver. This chapter presents a general analysis of the linear digital cellular system.

Section 3.1 describes the general linear receiver and introduces the linear system to be analysed. The key to simplifying system analysis is the formulation of the *equivalent discrete linear system*, given in Section 3.2. Using this discrete system, it is straightforward to compute performance measures such as the mean-square error (Section 3.3) and the bit-error-rate (Section 3.4). Sections 3.5 and 3.6 describe the approach to obtaining numerical results in Chapters 4, 5, and 6, and techniques underlying their computation.

3.1 The Linear System

The general linear receiver for the digital cellular system consists of up to N_d linear *sub-receivers*, one associated with each of the co-channel sources (of dominant co-channel signals). Its continuous-time form is illustrated in Figure 3.1, where

- $u_{m,n}(t)$ is the (continuous-time) impulse response of the linear filter (or filter cascade) in the mth diversity branch of the nth sub-receiver;
- t_{sn} is the *timing epoch* of the nth sub-receiver;
- $1/\tilde{S}_n$ is the *gain control factor* of the nth sub-receiver, where $\tilde{S}_n$ is the receiver's estimate of S_n;
- $\{\tilde{\theta}^*_{n,k} = \exp(-j2\pi\tilde{\Delta}_n kT)\}$ is the *inverse phase-roll* sequence of the nth sub-receiver, where $\tilde{\Delta}_n$ is the receiver's estimate of Δ_n;
- $\{\tilde{x}_{n,k}\}$ is the receiver's *linear estimate* of the data sequence from the nth source, $\{x_{n,k}\}$.

The responses $\{u_{m,n}(t)\}$ will depend on the structure of the linear receiver (e.g., finite or infinite length impulse responses) and its criterion of optimality. The timing epochs, gain control factors, and inverse phase roll sequences will depend on the timing recovery, gain control, and carrier recovery schemes employed, respectively.

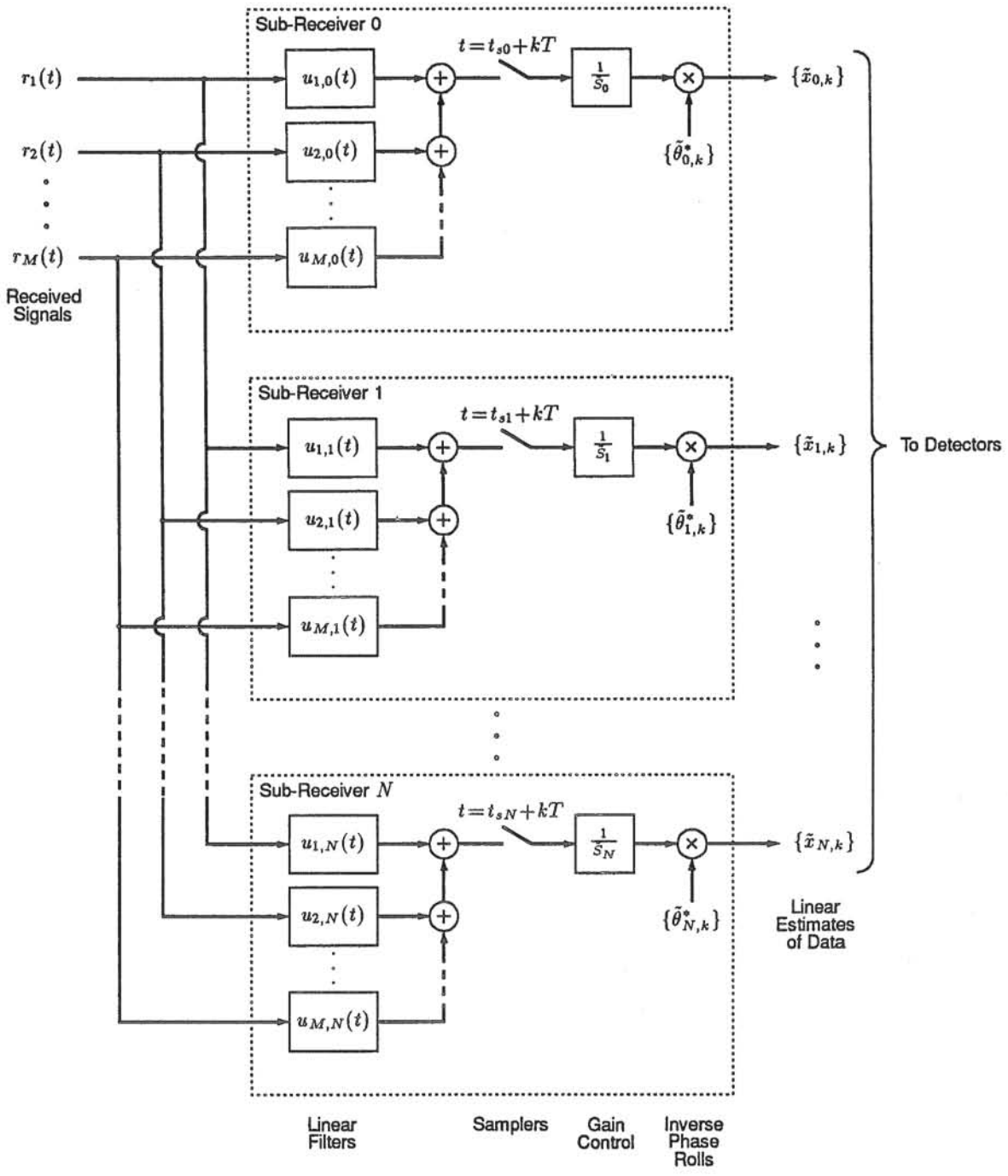

Figure 3.1 General form of the linear receiver.

The symbol estimate $\hat{x}_{n,k}$ (see Section 2.1.4) is formed by choosing, from the signal constellation, the symbol that is closest (smallest Euclidean distance) to the linear estimate $\tilde{x}_{n,k}$. Thus, $\hat{x}_{n,k}$ is formed by simply using a pair of threshold detectors at the output of the nth sub-receiver (see Section 3.4).

For the linear receivers analysed in this thesis, we focus on estimation of the data sequence from the *desired* source, $\{x_{0,k}\}$ (i.e., the 0th sub-receiver). Furthermore, for analytical simplicity, ideal gain control and ideal carrier recovery are assumed, i.e., $\tilde{S}_0 = S_0$ and $f_r = f_0 \Rightarrow \tilde{\Delta}_0 = \Delta_0 = 0$. Thus, the form of the sub-receiver for the desired source is as shown in Figure 3.2, where

$u_m(t) \equiv u_{m,0}(t)$ and $t_s \equiv t_{s0}$. In point of fact, a practical linear receiver implementation would probably have samplers in each diversity branch followed by finite-tap *transversal* filters (tapped delay lines). The received signals may also be sampled at a rate higher than $1/T$ (fractionally-spaced filter taps[1]), and possibly with a different timing epoch (i.e., a different timing recovery loop) in each branch. Furthermore, the filter responses may be split, with processing in each branch as well as a common filter at the combiner output. Nevertheless, every implementation can be viewed as equivalent to the general form shown in Figure 3.2.

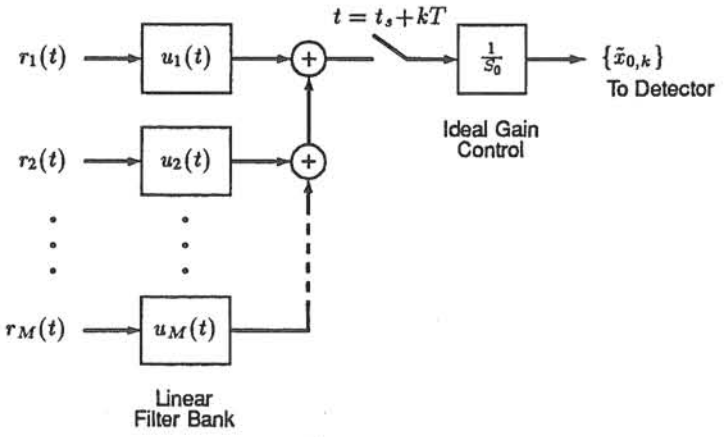

Figure 3.2 General form of the linear sub-receiver for the desired source, with ideal gain control and ideal carrier recovery.

The linear digital cellular system to be analysed is illustrated in Figure 3.3, where $g_n(t) = \sum_m q_{m,n}(t) \odot u_m(t)$ is the impulse response (excluding the gain factor S_n) between the nth phase-rolled co-channel source and the output of the linear filter bank (input to the sampler) in the receiver, and $\eta_L(t) = \sum_m \eta_m(t) \odot u_m(t)$ is the gaussian noise at that output. The Fourier transform of $g_n(t)$ is denoted by $G_n(f)$, and the power spectrum of $\eta_L(t)$ by $\mathcal{N}_L(f)$.

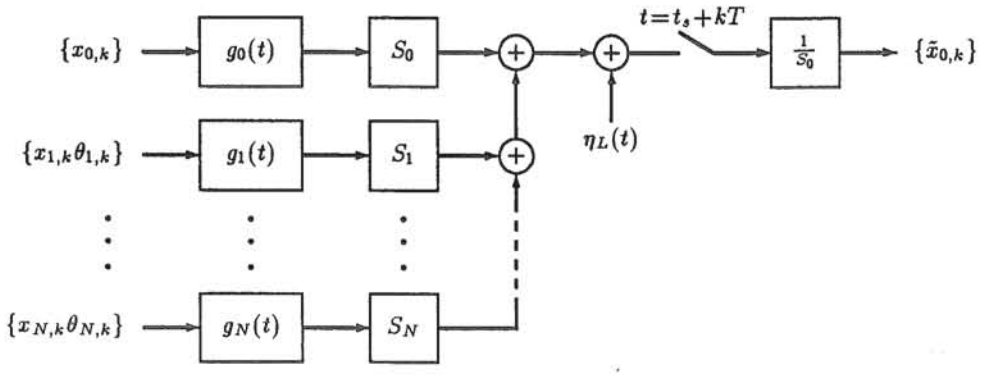

Figure 3.3 The linear digital cellular system.

[1]The optimum linear filter responses can be synthesized with fractionally-spaced tapped delay lines [Qureshi, 1985].

3.2 Equivalent Discrete Linear System

Because linear receiver detection is done on a symbol-by-symbol basis, it is convenient to formulate a discrete-time equivalent of the digital cellular system shown in Figure 3.3. For the linear receivers analysed in this thesis, the equivalent discrete linear system is utilized and the following definitions and relationships used freely.

The *sampled impulse response* between the nth phase-rolled co-channel source and the sampler output is $S_n\,\tilde{g}_n(t)$, where

$$\tilde{g}_n(t) = \sum_k g_{n,k}\,\delta(t - t_s - kT) \tag{3.1}$$

and $g_{n,k} \equiv g_n(t_s + kT)$. The Fourier transform of $\tilde{g}_n(t)$ is

$$\tilde{G}_n(f) = \sum_k g_{n,k} \exp\left(-\jmath 2\pi f(t_s + kT)\right) \tag{3.2}$$

Alternatively, we have the product form

$$\tilde{g}_n(t) = g_n(t) \sum_k \delta(t - t_s - kT) \tag{3.3}$$

so the Fourier transform of $\tilde{g}_n(t)$ is also given by the convolution of $G_n(f)$ with the well known Fourier transform of the Dirac comb function [Haykin, 1983, ch. 1], which results in the *periodic frequency response*[2]

$$\tilde{G}_n(f) = \frac{1}{T} \sum_i G_n(f - i/T) \exp\left(-\jmath 2\pi i t_s/T\right) \tag{3.4}$$

The sample values $\{g_{n,k}\}$ are expressed by the inverse Fourier transform of $G_n(f)$, or in terms of $\tilde{G}_n(f)$ by noting that (3.2) forms a Fourier series [Haykin, 1983, ch. 1]. That is,

$$g_{n,k} = \int_{-\infty}^{\infty} G_n(f) \exp\left(\jmath 2\pi f(t_s + kT)\right) df = T \int_{-1/2T}^{1/2T} \tilde{G}_n(f) \exp\left(\jmath 2\pi f(t_s + kT)\right) df \tag{3.5}$$

Using Parseval's Power Theorem [Haykin, 1983, ch. 1], we have the useful relationship

$$\sum_k |g_{n,k}|^2 = T \int_{-1/2T}^{1/2T} |\tilde{G}_n(f)|^2\, df \tag{3.6}$$

The *sampled noise* is

$$\tilde{\eta}_L(t) = \sum_k \eta_k\,\delta(t - t_s - kT) \tag{3.7}$$

where $\eta_k \equiv \eta_L(t_s + kT)$. Using the fact that $\eta_L(t)$ is a band-limited stationary process (so its Fourier transform is nonstationary with an impulsive autocorrelation function [Bello, 1964]), it is readily verified that the power spectrum of $\tilde{\eta}_L(t)$ is

$$\tilde{\mathcal{N}}_L(f) = \frac{1}{T^2} \sum_i \mathcal{N}_L(f - i/T) \tag{3.8}$$

which is referred to as the *periodic noise power spectrum* at the sampler output. The mean-square value of the gaussian noise samples $\{\eta_k\}$ is given by [Haykin, 1983, ch. 5]

$$E\left[|\eta_k|^2\right] = \int_{-\infty}^{\infty} \mathcal{N}_L(f)\, df = T^2 \int_{-1/2T}^{1/2T} \tilde{\mathcal{N}}_L(f)\, df \tag{3.9}$$

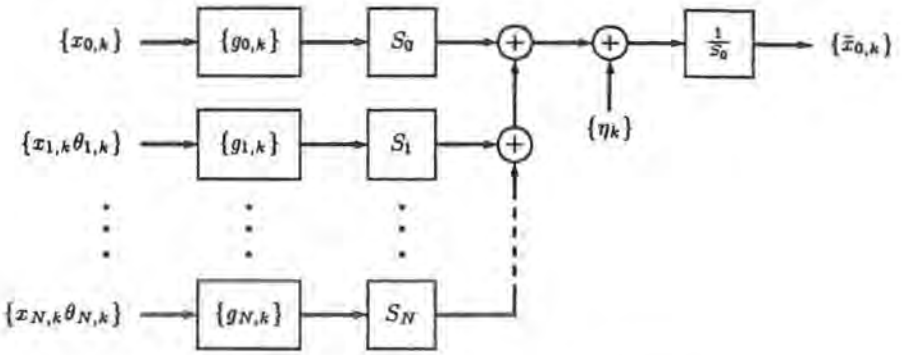

Figure 3.4 Equivalent discrete linear system.

Thus, the equivalent discrete linear system, illustrated in Figure 3.4, is conveniently characterized by $\{g_{n,k}\}$ and $E\left[|\eta_k|^2\right]$, or by $\{\tilde{G}_n(f)\}$ and $\tilde{N}_L(f)$. The linear estimate of the current symbol from the desired source is[3]

$$\tilde{x}_{0,0} = x_{0,0} + \underbrace{\sum_k x_{0,k}\,(g_{0,-k} - \delta_{0,k})}_{\text{ISI}} + \underbrace{\sum_{n=1}^{N} \frac{S_n}{S_0} \sum_k x_{n,k}\,\theta_{n,k}\,g_{n,-k}}_{\text{CCI}} + \underbrace{\frac{1}{S_0}\eta_0}_{\text{Noise}} \tag{3.10}$$

The goal of linear receiver design is to optimize the filter responses $\{u_m(t)\}$ to minimize the ISI, CCI, and noise components shown in (3.10), given some filter constraints (e.g., finite tap implementation) and some criterion of optimality (e.g., minimum symbol error rate).

3.3 Mean-Square Error

The *mean-square error* (MSE) is a useful statistical performance metric that measures the average square error in the linear estimate $\tilde{x}_{0,k}$, taken over all possible data sequences $\{x_{n,k}\}$ (assuming that the channel responses $\{q_{m,n}(t)\}$ are static, and the receiver responses $\{u_m(t)\}$ are optimized in some way). The *minimum MSE (MMSE)* is a useful optimization criterion, because it is easy to implement a receiver that gets close to the MMSE solution, and minimizing the MSE tends towards minimizing the bit-error-rate (see Section 3.4). Linear receivers in Chapters 5 and 6 are optimized to minimize the MSE.

The MSE is given by

$$\epsilon = E\left[|\tilde{x}_{0,0} - x_{0,0}|^2\right] \equiv \epsilon_{\text{ISI}} + \epsilon_{\text{CCI}} + \epsilon_{\text{Noise}} \tag{3.11}$$

where

$$\begin{aligned} \epsilon_{\text{ISI}} &= \sigma_x^2 \sum_k |g_{0,k} - \delta_{0,k}|^2 \\ &= \sigma_x^2 T \int_{-1/2T}^{1/2T} |\tilde{G}_0(f) - \exp(-j2\pi f t_s)|^2\, df \end{aligned} \tag{3.12}$$

[2]The Nyquist-bandlimited $T\tilde{G}_n(f)$ is often referred to as the *Nyquist equivalent* frequency response [Lucky *et al.*, 1968].

[3]For simplifying analyses in subsequent chapters, the ISI component shown in (3.10) includes the error in $g_{0,0}$ (ideally, $g_{0,0}$ should be unity). The equation could be rewritten as $\tilde{x}_{0,0} = g_{0,0}\,x_{0,0} + \sum_{k\neq 0} x_{0,k}\,g_{0,-k} + \text{CCI} + \text{Noise}$, where the second term is the actual ISI.

$$\begin{aligned}\epsilon_{\text{CCI}} &= \sigma_x^2 \sum_{n=1}^{N} \left(\frac{S_n}{S_0}\right)^2 \sum_k |g_{n,k}|^2 \\ &= \sigma_x^2 \sum_{n=1}^{N} \left(\frac{S_n}{S_0}\right)^2 T \int_{-1/2T}^{1/2T} |\tilde{G}_n(f)|^2 \, df\end{aligned} \tag{3.13}$$

and

$$\begin{aligned}\epsilon_{\text{Noise}} &= \frac{1}{S_0^2} E[|\eta_0|^2] \\ &= \frac{1}{S_0^2} \int_{-\infty}^{\infty} \mathcal{N}_L(f) \, df = \frac{T^2}{S_0^2} \int_{-1/2T}^{1/2T} \tilde{\mathcal{N}}_L(f) \, df\end{aligned} \tag{3.14}$$

where expectation is taken over all possible transmitted data sequences $\{x_{n,k}\}$. Thus, the MSE is conveniently expressed in terms of $\{\tilde{G}_n(f)\}$ and $\tilde{\mathcal{N}}_L(f)$.

3.4 Bit-Error-Rate

The ideal memoryless detector for the desired source has the form shown in Figure 3.5, where $\hat{a}_{0,k} = \text{Re}\,[\hat{x}_{0,k}]$ and $\hat{b}_{0,k} = \text{Im}\,[\hat{x}_{0,k}]$. In order to compute the probability of a bit error,

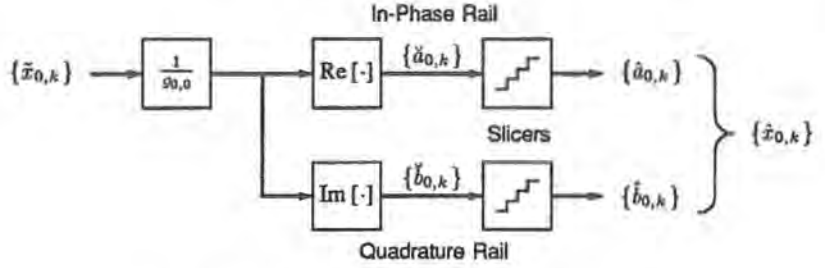

Figure 3.5 Memoryless detector for 0th sub-receiver.

or the *bit-error-rate*[4] (BER), it is sufficient to compute the probability that the detection of $\breve{a}_{0,0} = \text{Re}\,[\tilde{x}_{0,0}/g_{0,0}]$ causes a bit error. Thus, defining

$$\rho_{n,k} \triangleq \begin{cases} g_{0,-k}/g_{0,0}, & n = 0,\ k \neq 0 \\ (S_n/S_0)\,\theta_{n,k}\,g_{n,-k}/g_{0,0} & n = 1, 2, \ldots, N,\ \forall k \\ 0 & n = 0,\ k = 0 \end{cases} \tag{3.15}$$

we have $\breve{a}_{0,0} = a_{0,0} + \varepsilon + \eta$, where

$$\varepsilon = \text{Re}\left[\sum_{n,k} x_{n,k}\rho_{n,k}\right] \tag{3.16}$$

is (again, assuming that the channel responses are static and the receiver is optimized in some way) a zero-mean peak-limited interference sample (ISI+dominant CCI), and η is a zero-mean

[4] Strictly speaking, the *bit-error-rate* is a sample estimate of the *bit-error-probability*. In this thesis, the two statistics are synonymous.

gaussian noise sample. The interference sample ε has a symmetrical probability density function (pdf) denoted by $p_\varepsilon(x)$, a maximum (peak) value

$$\varepsilon_p = (L_a - 1)\sum_{n,k} |\text{Re}\,[\rho_{n,k}]\,| + (L_b - 1)\sum_{n,k} |\text{Im}\,[\rho_{n,k}]\,| \tag{3.17}$$

and a variance

$$\sigma_\varepsilon^2 = \sigma_a^2 \sum_{n,k} (\text{Re}\,[\rho_{n,k}])^2 + \sigma_b^2 \sum_{n,k} (\text{Im}\,[\rho_{n,k}])^2 \tag{3.18}$$

The gaussian noise sample η has the variance

$$\sigma_\eta^2 = \frac{\frac{1}{2}E\left[|\eta_0|^2\right]}{S_0^2\,|g_{0,0}|^2} \tag{3.19}$$

For computation of numerical results, the summations over k in (3.16), (3.17) and (3.18) are limited to $|k| \le k_{\max}$, where $k_{\max}$ relates to the frequency resolution used for each $\tilde{G}_n(f)$. Note also, if $L_a = L_b$ (square signal constellation, or QAM), we get

$$\sigma_\varepsilon^2 = \frac{1}{2}\sigma_x^2 \sum_{n,k} |\rho_{n,k}|^2 = \frac{1}{2}\sigma_x^2 T \left[\frac{1}{|g_{0,0}|^2}\left(\sum_{n=0}^{N}\left(\frac{S_n}{S_0}\right)^2 \int_{-1/2T}^{1/2T} |\tilde{G}_n(f)|^2\,df\right) - 1\right] \tag{3.20}$$

The bit-error-rate[5] is given by

$$\text{BER} = \frac{L-1}{L}\int_0^{\varepsilon_p} p_\varepsilon(x)\,\Xi[x, \sigma_\eta]\,dx \tag{3.21}$$

where $L \equiv L_a$ and

$$\Xi[x, \sigma] \triangleq \text{erfc}[(1-x)/\sqrt{2\sigma^2}] + \text{erfc}[(1+x)/\sqrt{2\sigma^2}] \tag{3.22}$$

If there were no ISI or dominant CCI, we would have

$$\text{BER} = \frac{L-1}{L}\text{erfc}\left[1/\sqrt{2\sigma_\eta^2}\right] \tag{3.23}$$

For a large number of elements in $\{\rho_{n,k}\}$, it is a very intensive computational task exactly to compute $p_\varepsilon(x)$ and, in turn, BER. We resort to one of four approximations/bounds, listed in descending order of computational accuracy and complexity:

- **Metzger's Algorithm:** [Metzger, 1987] $p_\varepsilon(x)$ is approximated by a set of N_ε weighted Dirac delta pulses, i.e.,

$$p_\varepsilon(x) \approx \sum_{i=1}^{N_\epsilon} p_{\varepsilon i}\,\delta(|x| - (i + \tfrac{1}{2})\varepsilon_p/N_\varepsilon) \tag{3.24}$$

  where $\{p_{\varepsilon i}\}$ is computed using Metzger's algorithm (see Appendix). The bit-error-rate is approximated by

$$\text{BER} \approx \frac{L-1}{L}\sum_{i=1}^{N_\epsilon} p_{\varepsilon i}\,\Xi\left[(i+\tfrac{1}{2})\varepsilon_p/N_\varepsilon, \sigma_\eta\right] \tag{3.25}$$

  Metzger's algorithm is more accurate for higher N_ε (but higher accuracy naturally involves more computation). For the results in this thesis, $N_\varepsilon = 100$ is used. After many tests, it was confirmed that this value generally yields a BER in error by no more than 1% from the BER computed via (3.21) with exhaustive computation of $p_\varepsilon(x)$, i.e., computing every possible equal-probability value of ε from (3.16).

[5] If L is greater than 2, the bit-error-rate is slightly higher than the one shown in (3.21). However, for small BER (less than 10^{-1}), (3.21) represents a very tight lower bound on the true bit-error-rate.

- **Peak-Limited Gaussian Approximation:** $p_\varepsilon(x)$ is approximated by a peak-limited gaussian pdf, i.e.,

$$p_\varepsilon(x) \approx \begin{cases} K_\varepsilon \exp\left[-\frac{1}{2}(x/\sigma_\varepsilon)^2\right], & |x| \le \varepsilon_p \\ 0, & |x| > \varepsilon_p \end{cases} \tag{3.26}$$

where $K_\varepsilon = [\sqrt{2\pi}\sigma_\varepsilon(1 - \text{erfc}[\varepsilon_p/\sqrt{2\sigma_\varepsilon^2}])]^{-1}$ ensures that the area under $p_\varepsilon(x)$ is unity. (Note that the variance of this crude approximation to $p_\varepsilon(x)$ is not generally equal to σ_ε^2.) The bit-error-rate is approximated by

$$\text{BER} \approx \frac{L-1}{L} K_\varepsilon \int_0^{\varepsilon_p} \exp[-\tfrac{1}{2}(x/\sigma_\varepsilon)^2]\, \Xi[x, \sigma_\eta]\, dx \tag{3.27}$$

Because residual interference (after receiver processing) often consists of several small components, it is reasonable to approximate the interference pdf, $p_\varepsilon(x)$, by a gaussian pdf (see next item). Unfortunately, this approximation sometimes leads to significant inaccuracies because, unlike a gaussian pdf, the actual interference pdf is peak-limited; it does not have tails that run to infinity. These tails play a critical part in the BER computation, so the peak-limited approximation to $p_\varepsilon(x)$, which simply truncates the tails at the peak interference value, often leads to relatively accurate results.

- **Gaussian Approximation:** $p_\varepsilon(x)$ is approximated by a gaussian pdf (letting $\varepsilon_p \to \infty$). Thus, the bit-error-rate is approximated by

$$\text{BER} \approx \frac{L-1}{L} \text{erfc}\left[1/\sqrt{2(\sigma_\varepsilon^2 + \sigma_\eta^2)}\right] \tag{3.28}$$

By comparing the BER computed using this expression with that of Metzger's algorithm, we can identify for which receiver types and under what conditions it is valid to regard the interference as gaussian.

- **Saltzberg's Bound:** We use only the simplest form of this upper bound [Saltzberg, 1968], in which

$$\text{BER} \le \frac{L-1}{L} \exp\left[-1/[2(\sigma_\varepsilon^2 + \sigma_\eta^2)]\right] \tag{3.29}$$

Like the gaussian approximation, this simple form of Saltzberg's bound tends to be tightest for gauss-like interference. It is included as a candidate for BER computation because it is very easy to compute and is used widely in the literature [Foschini and Salz, 1983; Wong and Greenstein, 1984; Balaban and Salz, 1991].

3.5 Performance Over Channel Ensemble

The linear receiver can be optimized, in some way, assuming knowledge of L_a, L_b, M, N, T, $\{S_n\}$, $\{q_{m,n}(t)\}$, and $\mathcal{N}_R(f)$. The BER can then be evaluated using one or more of the methods outlined in Section 3.4. But the channel responses $\{q_{m,n}(t)\}$ are random processes characterized by the channel ensemble described in Section 2.1.3, so BER is a random variable. (The channel ensemble is, in turn, characterized by $\{C_n(f)\}$, $P_h(\tau)$ and d.) Two BER statistics, taken over the channel ensemble, are defined:

- **Outage Probability:** $P_{\text{out}} \triangleq \text{Prob}\,[\text{BER} > \text{BER}_o]$.
- **Average BER:** $\langle \text{BER} \rangle \triangleq E\,[\text{BER}]$.

where BER_o is a specified performance threshold. If the outage probability is plotted against BER_o, we obtain the *BER distribution.*

The outage probability is most relevant to slow moving (or stationary) vehicles or pedestrians, whereas the average BER is the significant performance measure for rapidly moving vehicles. Alternatively, the two BER statistics can be used together in the following way. For a vehicle moving at a typical speed (say, 50 km/h), $\langle \text{BER} \rangle$ represents the proportion of transmitted bits that are incorrectly detected over, say, a few seconds (the number of seconds being inversely proportional to the vehicle speed). The outage probability with $\text{BER}_o = \langle \text{BER} \rangle$ provides a measure of how "bursty" the bit errors are: if P_{out} is close to 0.5 (which is the maximum possible value if $\text{BER}_o = \langle \text{BER} \rangle$), the bit errors are likely to be spread out evenly over the few seconds; if P_{out} is close to $2\langle \text{BER} \rangle$ (which is the minimum possible value if $\text{BER}_o = \langle \text{BER} \rangle$), the bit errors are likely to occur in short bursts over the few seconds. Knowledge of this "burstiness" is important in the design of error-correcting codes.

Ideally, one strives to compute the BER statistics analytically, as it generally leads to additional insight and avoids the need for time consuming Monte Carlo simulations of the channel responses $\{q_{m,n}(t)\}$. However, it is also the most difficult approach, and sometimes it is not feasible to evaluate the performance of complex receivers in this way. Thus, for most results, we resort to Monte Carlo simulations with a sufficient number of trials to yield confident estimates of P_{out} and $\langle \text{BER} \rangle$ (usually thousands of trials). The channel responses are randomly generated using the efficient scheme described in Section 2.2.

3.6 Obtaining Numerical Results: The General Approach

The numerical results in Chapters 4, 5, and 6 show the statistical bit-error-rate performance of various diversity receivers operating in an environment with multipath fading and co-channel interference. The following list is a summary of the assumptions that are invoked to simplify the results, to treat worst-case CCI scenarios, and to obtain performance bounds:

- Identical modulation, data rate, and bandwidth for all co-channel sources;
- Independent Rayleigh fading of each co-channel signal in each diversity branch, with common delay spectrum; same average power received on each branch from a given co-channel source;
- Identical carrier frequencies for all co-channel sources, and coherent demodulation, i.e., $\{\Delta_n = 0\}$;
- Ideal gain control and channel tracking (quasi-static channel responses);
- Co-channel interference is composed of N dominant equal-average-power signals, and a great many weak equal-average-power signals (the sum of weak CCI signals on each diversity branch is thus taken to be gaussian and independent — other gaussian noise sources are taken to be negligible).

The digital cellular radio system thus has the following parameters:

- Number of modulation levels, L_a and L_b;
- Transmit and receive filter responses, $C_T(f)$ and $C_R(f)$;

- Excess bandwidth factor, B;
- Diversity order, M;
- Number of dominant CCI sources, N;
- Delay spectrum shape, $P_h(\tau)$ (or frequency autocorrelation function, $R_H(\alpha)$);
- Normalized delay spread, d;
- Signal-to-CCI ratio, SIR;
- Dominant-CCI-to-weak-CCI ratio, DWR.

(Note that DWR is a redundant parameter if N=0.) To keep the number of results manageable, and to focus on the important parameters, the following are assumed in *all results*:

- QPSK ($L_a \equiv L = 2$ and $L_b = 2$);
- 50% excess bandwidth ($B = 1.5$);
- Weak CCI power 1% of dominant CCI power (DWR = 20 dB).

Results for other modulations (such as BPSK or 16-QAM) at SIR=SIR_0 (where SIR_0 is specified) are approximately the same as those for QPSK at SIR=$2\text{SIR}_0/\sigma_x^2$. (Note also that different modulations should, in general, be compared at the same $\tau_0/T_b = N_b d$.)

The fixed transmit and receive filter responses depend on the receiver studied, and are discussed and specified in Chapters 4, 5, and 6. The parameters that are varied in the numerical results take on the following range of values:

- $M = 1, 2, 3$, or 4;
- $N = 0, 1, 2$, or 3;
- $P_h(\tau)$ = exponential, gaussian, or double-spike;
- $d = [0, \infty]$;
- SIR = $[-20, 30]$ dB.

Each section presenting numerical results begins with a summary of the method used in computing the performance of the receiver being considered. The remainder of each of these sections is devoted to the presentation of graphs that show the influence of the above five parameters on the outage probability (plotted against BER_o or SIR) and the average BER (plotted against SIR). For the BER distributions, SIR is set to either 10 dB, representing a severe level of CCI, or 20 dB, representing a typical level of CCI (in today's cellular systems). Also, a bit-error-rate of 0.1% is regarded as an acceptable performance for the plots of outage probability against SIR (i.e., $\text{BER}_o=10^{-3}$) or in the quantitative comparison in the plots of average BER against SIR (i.e., SIR values are compared at $\langle\text{BER}\rangle=10^{-3}$). Depending on error-correction coding schemes, the acceptable BER in real systems may be even higher (e.g., 1–5% before coding) than the stringent performance requirement specified here. Nevertheless, the trends and relative ranking amongst the different receivers should be similar for different degrees of optimism in specifying the acceptable performance criterion.

Finally, the emphasis in the results is on *significant* time dispersion, i.e., rms delay spreads that are not small with reference to the digital symbol period (values of d in the range 0.5–2). (Results for flat fading, or d=0, are also given as a reference to show the relative benefits and pitfalls of dispersive channels.) An obvious application of the results is to cellular time-division multiple access (TDMA) links that use relatively high bit rates (for example, in the Pan-European GSM system[6] [Balston, 1989]).

3.7 Conclusion

This chapter has discussed and analysed a general linear diversity receiver operating in the digital cellular system described in Chapter 2, and outlined an approach to obtaining numerical results for such a receiver. The techniques developed here are used in the following three chapters.

Appendix 3A Metzger's Algorithm

The following is a summary of Metzger's algorithm [Metzger, 1987] for computing the set of coefficients $\{p_{\varepsilon i}\}$ (described in Section 3.4) given L_a, L_b, $\{\rho_{n,k}, n = 0,1,\ldots,N; \forall k : |k| \leq k_{\max}\}$, and N_ε:

1. Form the set $\{\rho_l,\ l = 1,2,\ldots,N_\rho\}$ that contains all non-zero elements in the sets $\{2^i \mathrm{Re}\,[\rho_{n,k}]\ ,\ i = 0,1,\ldots,\log_2(L_a) - 1; \forall n,k\}$ and $\{2^i \mathrm{Im}\,[\rho_{n,k}]\ ,\ i = 0,1,\ldots,\log_2(L_b) - 1; \forall n,k\}$, and whose elements are sorted in descending order: $\rho_1 \geq \rho_2 \geq \cdots \geq \rho_{N_\rho} > 0$, where $N_\rho \leq (N+1)(2k_{\max}+1)\log_2(L_aL_b)$

2. Compute $p_j = \sum_{l=j}^{N_\rho} \rho_l$ and $\kappa_j = p_j/N_\varepsilon$ for $j = 1,2,\ldots,N_\rho$ $(\rho_1 \equiv \varepsilon_p, \kappa_1 = \varepsilon_p/N_\varepsilon)$

3. Set $h_i = 1, \quad i = 1,2,\ldots,N_\varepsilon$

4. Compute the following for $j = N_\rho, N_\rho - 1,\ldots,2$:

   - $h(x) = \begin{cases} h_i, & (i-1)\kappa_j \leq |x| < i\kappa_j, \quad i = 1,2,\ldots,N_\varepsilon \\ 0, & |x| > p_j \end{cases}$
   - $\hat{h}_i = \int_{(i-1)\kappa_{j-1}}^{i\kappa_{j-1}} h(x)\,dx, \quad i = 1,2,\ldots,N_\varepsilon$
   - $h_i = \hat{h}_{i+l} + \hat{h}_{\mathrm{abs}(i-l)}, \quad i = 1,2,\ldots,N_\varepsilon,$

     where l = integer part of $(\rho_{j-1}/\kappa_{j-1} + \frac{1}{2})$; $\mathrm{abs}(l) = \begin{cases} l, & l \geq 1 \\ -l+1, & l < 1 \end{cases}$

5. Compute $p_{\varepsilon i} = \dfrac{h_i}{2\kappa_1 \sum_{l=1}^{N_\varepsilon} h_l}, \quad i = 1,2,\ldots,N_\varepsilon$

[6]The GSM system uses gaussian minimum shift keying (GMSK). The trends in the results of this thesis should be similar for QPSK and GMSK.

Chapter 4

THE MAXIMUM LIKELIHOOD RECEIVER AND MATCHED FILTER PERFORMANCE BOUNDS

The *maximum likelihood receiver* is the best possible receiver: it minimizes the probability of incorrectly detecting the information transmitted [Wozencraft and Jacobs, 1965]. For receivers without diversity (M=1), the structure of the maximum likelihood receiver, for detecting a sequence of data symbols from *a single source* (N_s=1) in the presence of ISI and gaussian noise, is well known [Forney, 1972; Proakis, 1989, pp. 548–554]. It consists of a matched filter followed by a T-spaced sampler and a maximum likelihood sequence estimator (which can be implemented using the Viterbi algorithm [Forney, 1973]). Van Etten [1976] formulates the maximum likelihood receiver for multiple-source linear diversity systems. The resultant structure is a bank of matched filters (one filter corresponding to each source for each diversity branch), the outputs associated with each source being summed over all diversity branches, followed by a bank of T-spaced samplers (one sampler corresponding to each source), and a vector form of the maximum likelihood sequence estimator. In this chapter, the maximum likelihood receiver is formulated (Section 4.1), using a quite different approach to that of Van Etten, for the digital cellular system described in Chapter 2.

It is difficult to analyse the performance of a maximum likelihood receiver (even for static channel conditions) because of its complexity. Nevertheless, a very useful bound on maximum likelihood performance — called the *matched filter bound* [Lucky *et al.*, 1968] — is obtained by simply assuming that the data symbol $x_{0,0}$ (i.e., the current symbol from the desired source) is transmitted in *isolation*: there is no ISI or dominant CCI, only additive noise. Clearly, the probability of detecting this symbol incorrectly must be at least as small as that of detecting any symbol in a *sequence* incorrectly, when ISI and CCI are present[1]. Furthermore, the matched filter bound is easy to compute for static channel conditions (a simple linear system analysis), and has been found to be quite tight for maximum likelihood receivers operating in a variety of systems: an M-branch maximum likelihood receiver has been shown to be capable of almost completely eliminating all ISI and up to $M-1$ dominant CCI signals [Forney, 1972; Van Etten, 1976].

Many authors have computed matched filter bounds for various channels, usually as a benchmark for realizable equalizers [Wong and Greenstein, 1984; Valenzuela, 1989; Balaban and Salz, 1991]. They have, however, almost always resorted to Monte Carlo simulation when computing BER performance over an ensemble of channels. An exception is Mazo [1991], who analytically derived the matched filter bound in the single-branch case (M=1) with two-path Rayleigh fading channels and additive white gaussian noise. Section 4.2.1 presents a totally analytical solution for the matched filter bound, which extends the treatment of Mazo to M-branch receivers, and to the general multipath channel model and arbitrary noise power spectrum described in Chapter 2. The key to the analysis is the application of the Karhunen-Loève expansion

[1]This implicitly assumes that there is no correlation in the data sequences.

of the channel frequency responses (see Section 2.1.3).

In addition to the general matched filter bound analysis, a set of numerical results is presented in Section 4.2.2 for the representative range of delay power spectra shown in Table 2.2, and for the noise-like CCI power spectrum (see Section 2.1.4). The results provide important performance bounds for realizable receivers in the digital cellular system, and quantify the best possible benefits of space diversity and intrinsic frequency diversity.

4.1 The Maximum Likelihood Receiver

4.1.1 Noise Whitening

The maximum likelihood formulation in Section 4.1.2 requires that the filtered gaussian noise sources $\{\eta_m(t)\}$, discussed in Section 2.1.4, have a flat power spectrum (i.e., *white* noise). This is simply achieved by making the fixed receive filter a *noise whitening* filter[2], i.e., such that

$$C_R(f) = \sqrt{\frac{\mathcal{N}_r}{\mathcal{N}(f)}} \Longrightarrow \mathcal{N}_R(f) = \mathcal{N}_r, \quad -W/2 + \min\{\Delta_n\} \le f \le W/2 + \max\{\Delta_n\} \quad (4.1)$$

where $\mathcal{N}_r$ is an arbitrary constant and $\{\Delta_n\}$ are the carrier differences of the *dominant* co-channel signals. It is assumed that the fixed receive filter has a realizable inverse, so that the filtering operation is information lossless [Wozencraft and Jacobs, 1965, pp. 485–492]. In this case, the minimum attainable probability of error is not affected by $c_R(t)$.

Sections presenting numerical results treat the case in which (i) $\{\Delta_n = 0, \forall n\}$; and (ii) the noise in each branch is composed entirely of noise-like CCI. Recalling that $\mathcal{N}(f) = \mathcal{N}_w |C_T(f)|^2$ for noise-like CCI, and setting $\mathcal{N}_r = \mathcal{N}_w$ in (4.1), we thus get $C_R(f) = 1/C_T(f) \Rightarrow \mathcal{N}_R(f) = \mathcal{N}_w, |f| \le W/2$, and $C_n(f) = 1, \forall n, |f| \le W/2$, regardless of the *shape* of the transmit filter response.

4.1.2 Formulation

From Chapter 2, the received signal on the mth diversity branch is $r_m(t) = s_m(t) + \eta_m(t)$, where

$$s_m(t) = \sum_{n=0}^{N} S_n \sum_k x_{n,k}\, \theta_{n,k}\, q_{m,n}(t - kT) \quad (4.2)$$

The maximum likelihood receiver forms the estimates $\{\hat{x}_{n,k}\}$ from the received signals $\{r_m(t)\}$, maximizing the probability of detecting the correct message, i.e., maximizing Prob $[\{\hat{x}_{n,k}\} = \{x_{n,k}\}]$. The receiver is formulated as follows.

First, suppose the N_d=N+1 sources each generate a sequence of K_s symbols (i.e., $K_s \to \infty$ for infinite-length data sequences). The set of all symbols from *all* sources, i.e., $\{x_{n,k}, n = 0, 1, 2, \ldots, N; \forall k\}$, is referred to as the *message*, and out of the $P = (L_a L_b)^{N_d K_s}$ equally-likely messages, the pth message is denoted by $\{x_{n,k,p}\}$, and the corresponding mth noiseless received signal by $s_{m,p}(t)$.

Each $s_m(t)$ can be represented as an orthonormal expansion

$$s_m(t) = \sum_{j=1}^{N_\psi} s_{m,j} \psi_j(t) \quad (4.3)$$

[2]The noise whitening filter is merely an analytical aid. The maximum likelihood receiver could, in fact, be realized with an arbitrary (but information lossless) fixed filter $c_R(t)$, or without one at all.

where N_ψ is greater than or equal to the *dimensionality* of each $s_m(t)$ for all P possible messages; $\{\psi_j(t)\}$ is an arbitrary orthonormal base; and the coefficients of the expansion are given by

$$s_{m,j} = \int_{-\infty}^{\infty} s_m(t)\psi_j(t)\,dt \tag{4.4}$$

Defining

$$r_{m,j} \triangleq \int_{-\infty}^{\infty} r_m(t)\psi_j(t)\,dt \tag{4.5}$$

and

$$\eta_{m,j} \triangleq \int_{-\infty}^{\infty} \eta_m(t)\psi_j(t)\,dt \tag{4.6}$$

we have

$$\mathbf{r} = \mathbf{s} + \boldsymbol{\eta} \tag{4.7}$$

where

$$\mathbf{r} = \begin{bmatrix} r_{1,1} \\ r_{1,2} \\ \vdots \\ r_{1,N_\psi} \\ r_{2,1} \\ r_{2,2} \\ \vdots \\ r_{2,N_\psi} \\ \vdots \\ r_{M,1} \\ r_{M,2} \\ \vdots \\ r_{M,N_\psi} \end{bmatrix}; \quad \mathbf{s} = \begin{bmatrix} s_{1,1} \\ s_{1,2} \\ \vdots \\ s_{1,N_\psi} \\ s_{2,1} \\ s_{2,2} \\ \vdots \\ s_{2,N_\psi} \\ \vdots \\ s_{M,1} \\ s_{M,2} \\ \vdots \\ s_{M,N_\psi} \end{bmatrix}; \quad \text{and} \quad \boldsymbol{\eta} = \begin{bmatrix} \eta_{1,1} \\ \eta_{1,2} \\ \vdots \\ \eta_{1,N_\psi} \\ \eta_{2,1} \\ \eta_{2,2} \\ \vdots \\ \eta_{2,N_\psi} \\ \vdots \\ \eta_{M,1} \\ \eta_{M,2} \\ \vdots \\ \eta_{M,N_\psi} \end{bmatrix} \tag{4.8}$$

It can be shown [Wozencraft and Jacobs, 1965, ch. 4] that, because $\{\psi_j(t)\}$ is an orthonormal set,

1. $\mathbf{r}$ is *sufficient* (information lossless) to determine which of the P messages was most likely transmitted; and
2. The noise samples in $\boldsymbol{\eta}$ are *statistically independent* zero-mean complex gaussian random variables with $E[|\eta_{m,j}|^2] = \mathcal{N}_r$.

If the pth message is transmitted, then $s_m(t) = s_{m,p}(t) \Leftrightarrow s_{m,j} = s_{m,j,p} \Leftrightarrow \mathbf{s} = \mathbf{s}_p$. Assuming the above properties of $\boldsymbol{\eta}$, it is well known that the maximum likelihood receiver decides that message $\hat{p}$ was transmitted if the square *Euclidean distance*

$$|\mathbf{r} - \mathbf{s}_i|^2 = |\mathbf{r}|^2 - 2\mathrm{Re}\left[\mathbf{s}_i^H \mathbf{r}\right] + |\mathbf{s}_i|^2, \quad i = 1, 2, \ldots, P \tag{4.9}$$

is minimum for $i = \hat{p}$. The $|\mathbf{r}|^2$ term is independent of i, so we can form the decision statistics

$$d_i = \mathrm{Re}\left[\mathbf{s}_i^H \mathbf{r}\right] + \xi_i = \mathrm{Re}\left[\sum_{m=1}^{M}\sum_{j=1}^{N_\psi} r_{m,j} s_{m,j,i}^*\right] + \xi_i, \quad i = 1, 2, \ldots, P \tag{4.10}$$

where $\xi_i = -|\mathbf{s}_i|^2/2$ is a bias term independent of the received signals. The receiver decides that message $\hat{p}$ was transmitted if $d_{\hat{p}}$ is maximum out of the set $\{d_i\}$. Therefore, the estimates of the N_d transmitted data sequences are

$$\{\hat{x}_{n,k}\} = \{x_{n,k,\hat{p}}\} : d_{\hat{p}} > d_i, \forall i \tag{4.11}$$

We now consider how the decision statistics are formed from the received signals $\{r_m(t)\}$. Substituting (4.5) into (4.10), we obtain

$$d_i = \text{Re}\left[\sum_{m=1}^{M} \int_{-\infty}^{\infty} r_m(t) s_{m,i}^*(t)\, dt\right] + \xi_i, \quad i = 1,2,\ldots,P \tag{4.12}$$

Thus, each decision statistic d_i could be formed by (i) passing each of the received signals $r_m(t)$ through a matched filter with impulse response $s_{m,i}^*(t_d - t)$ (where t_d is a delay chosen to make the responses causal[3]); (ii) adding the M matched filter outputs together; (iii) sampling the real part of the result at time t=t_d; and (iv) adding the bias term ξ_i.

The implementation described above requires a total of MP matched filters (where $MP \to \infty$ for infinite-length data sequences). Nevertheless, by substituting (4.2), with $s_m(t) = s_{m,p}(t) \Leftrightarrow x_{n,k} = x_{n,k,p}$, into (4.12), we get

$$d_i = \text{Re}\left[\sum_{n=0}^{N} S_n \sum_{k} x_{n,k,i}^*\, \theta_{n,k}^*\, z_{n,k}\right] + \xi_i, \quad i = 1,2,\ldots,P \tag{4.13}$$

where

$$z_{n,k} = \sum_{m=1}^{M} \int_{-\infty}^{\infty} r_m(t)\, q_{m,n}^*(t - kT)\, dt \tag{4.14}$$

From (4.13), it is clear that $\{z_{n,k}\}$ is a sufficient set of statistics for the estimation of $\{x_{n,k}\}$, and based on (4.14), each $z_{n,k}$ can be obtained simply by (i) passing each of the received signals $r_m(t)$ through a matched filter with impulse response

$$p_{m,n}(t) = q_{m,n}^*(t_d - t) \tag{4.15}$$

and frequency response

$$P_{m,n}(f) = Q_{m,n}^*(f) \exp(-j2\pi f t_d); \tag{4.16}$$

(ii) adding the M matched filter outputs together; and (iii) sampling the result at time $t = t_d + kT$. Thus, this implementation requires only MN_d matched filters to form the statistics $\{z_{n,k}\}$, as illustrated in Figure 4.1. The data source estimates $\{\hat{x}_{n,k}\}$ can then be formed from these statistics using the sequence estimation[4] rules described by (4.11) and (4.13).

4.2 Matched Filter Performance Bounds

4.2.1 Analysis

For an isolated data symbol $x_{0,0}$, the maximum likelihood receiver discussed in Section 4.1 reduces to a particularly simple form, i.e., one consisting of (i) a matched filter structure for estimating

[3]This is really a practical consideration that makes the receiver realizable. Theoretically, performance is independent of the choice of t_d.

[4]The difficulty with this sequence estimation approach is that the receiver complexity grows exponentially as $K_s \to \infty$. A more realistic approach would be to use the Viterbi Algorithm [Forney, 1972; Forney, 1973; Magee and Proakis, 1973; Ungerboeck, 1974; Van Etten, 1975; D'Avella *et al.*, 1989].

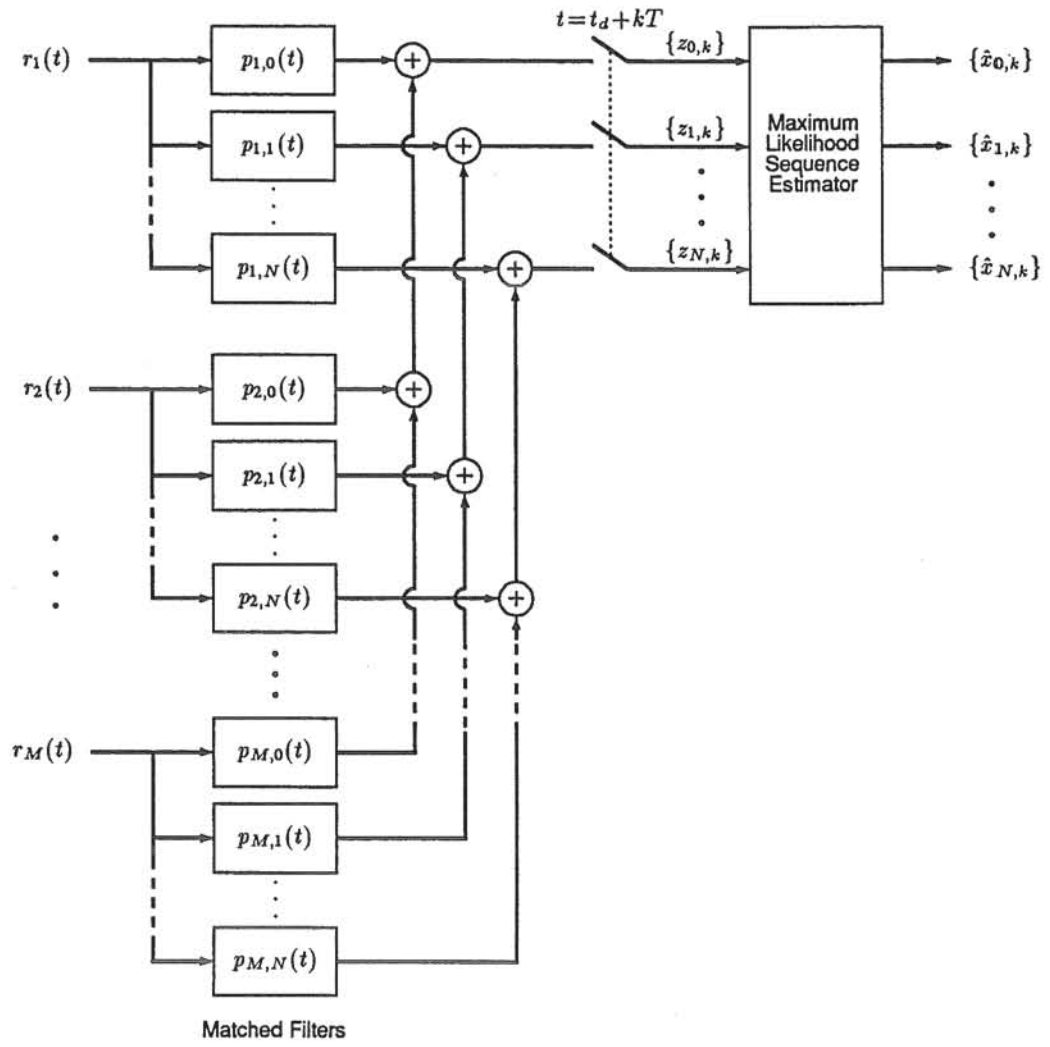

Figure 4.1 The maximum likelihood receiver.

a single source; (ii) a single sample at the output of the matched filter structure; and (iii) a memoryless threshold detector. The system is illustrated in Figure 4.2 (where $\tilde{x}_{0,0}$ is the linear symbol estimate to be processed by the threshold detector), with ideal gain control and ideal carrier recovery assumed. Because the receiver structure is linear, its BER performance can be evaluated using techniques outlined in Chapter 3 (with $u_m(t) = p_{m,0}(t_d - t)$, $t_s = t_d$, and ignoring the effects of ISI and dominant CCI).

From Section 3.2, we have $\tilde{x}_{0,0} = g_{0,0}\, x_{0,0} + \eta_0/S_0$, where

$$g_{0,0} = \int_{-W/2}^{W/2} \sum_{m=1}^{M} Q_{m,0}(f)\, P_{m,0}(f) \exp(j2\pi f t_d)\, df$$

$$= \sum_{m=1}^{M} \int_{-W/2}^{W/2} |Q_{m,0}(f)|^2\, df \tag{4.17}$$

and

$$E[|\eta_0|^2] = \sum_{m=1}^{M} \int_{-W/2}^{W/2} \mathcal{N}_R(f) |P_{m,0}(f)|^2\, df = \mathcal{N}_r\, g_{0,0} \tag{4.18}$$

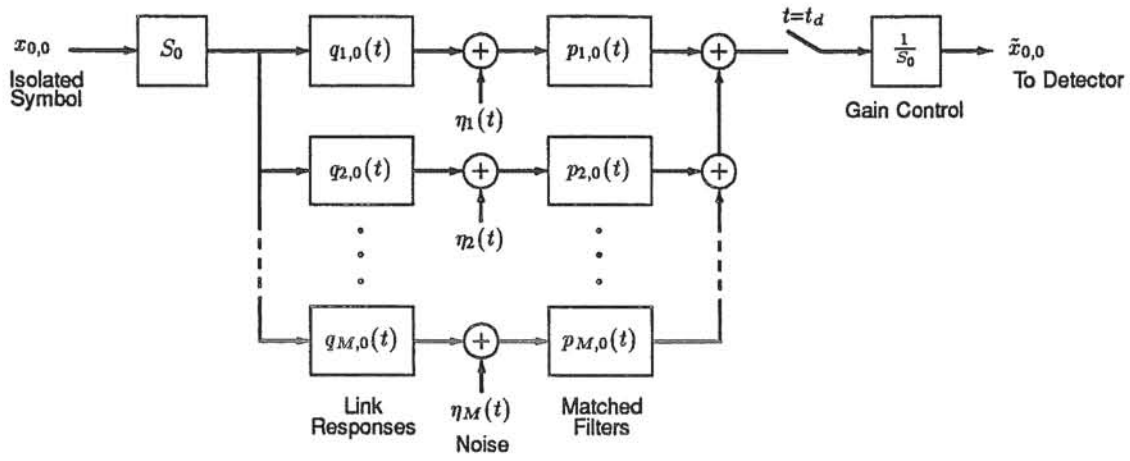

Figure 4.2 Maximum likelihood receiver for an isolated data pulse — system for computing the matched filter performance bound.

From Section 3.4, the bit-error-rate is therefore

$$\text{BER} = \frac{L-1}{L}\,\text{erfc}\left[\sqrt{\frac{S_0^2\, g_{0,0}}{\mathcal{N}_r}}\right] \tag{4.19}$$

To determine the BER performance over the channel ensemble, we require the probability density function of $g_{0,0}$, taken over the ensemble of $\{Q_{m,0}(f)\}$. From (2.13), we get

$$g_{0,0} = W \sum_{m=1}^{M} \int_{-1/2}^{1/2} |Z_{m,0}(\beta)|^2\, d\beta \tag{4.20}$$

Substituting (2.14) into (4.20) and using the orthonormality of the eigenfunctions, we have

$$g_{0,0} = W \sum_{m=1}^{M} \sum_{i=1}^{J_0} \lambda_{0,i}\, |c_{m,0,i}|^2 \tag{4.21}$$

which can be written as $g_{0,0} \equiv Wz$, where

$$z = \sum_{m=1}^{M} \sum_{i=1}^{N_\lambda} \lambda_i \sum_{j=1}^{\mu_i} |c_{m,0,i,j}|^2 \tag{4.22}$$

$\{\lambda_i\}$ is a set of N_λ *distinct* eigenvalues associated with the desired source, λ_i having algebraic multiplicity μ_i (i.e., the distinct eigenvalues have new indices, with $\sum_{i=1}^{N_\lambda} \mu_i = J_0$); and $\{c_{m,0,i,j}\}$ are the same gaussian random variables as those shown in (4.21), but with new indexing. Rearranging the order of summation in (4.22), we get

$$z = \sum_{i=1}^{N_\lambda} \gamma_i \tag{4.23}$$

where $\gamma_i = \lambda_i \sum_m \sum_j |c_{m,0,i,j}|^2$ is an independent gamma random variable of order $M\mu_i$. Therefore, the characteristic function of the distribution of z is [Papoulis, 1965]

$$\Gamma_z(\xi) = \prod_{i=1}^{N_\lambda} (1 - j2\pi\xi\lambda_i)^{-M\mu_i} = \begin{cases} (1 - j2\pi\xi\lambda)^{-M\mu}, & N_\lambda = 1 \\ \displaystyle\sum_{i=1}^{N_\lambda} \sum_{j=1}^{M\mu_i} A_{i,j}\, (1 - j2\pi\xi\lambda_i)^{-j}, & N_\lambda \geq 2 \end{cases} \tag{4.24}$$

where for $N_\lambda = 1$, $\mu \equiv \mu_1$ and $\lambda \equiv \lambda_1$; and for $N_\lambda \geq 2$, the coefficients of the partial fraction expansion are evaluated from [Nagrath and Gopal, 1982]

$$A_{i,M\mu_i-l} = \frac{1}{(-\lambda_i)^l\, l!}\left[\frac{\partial^l}{\partial s^l}\left\{\prod_{\substack{p=1\\p\neq i}}^{N_\lambda}(1-\lambda_p s)^{-M\mu_p}\right\}\right]_{s=1/\lambda_i} \tag{4.25}$$

Taking the Fourier transform of (4.24), we obtain the probability density function of z,

$$p(z) = \mathcal{F}[\Gamma_z(\xi)] = \begin{cases} \dfrac{\lambda^{-M\mu}}{(M\mu-1)!} z^{M\mu-1} e^{-z/\lambda}, & N_\lambda = 1 \\ \displaystyle\sum_{i=1}^{N_\lambda}\sum_{j=1}^{M\mu_i} \frac{A_{i,j}}{\lambda_i^j (j-1)!} z^{j-1} e^{-z/\lambda_i}, & N_\lambda \geq 2 \end{cases} \tag{4.26}$$

From (4.19), the bit-error-rate is

$$\text{BER} = q(z) = \frac{L-1}{L}\text{erfc}\left[\sqrt{\mathcal{E}z}\right] \tag{4.27}$$

where $\mathcal{E} \triangleq S_0^2 W/\mathcal{N}_r$ (for noise-like CCI, $\mathcal{N}_r = \mathcal{N}_w \Rightarrow \mathcal{E} = B\,\text{SIR}/\sigma_x^2$).

The outage probability, taken over the ensemble of $\{Q_{m,0}(f)\}$, is

$$\begin{aligned} P_{\text{out}} &= \text{Prob}\,[\text{BER} \geq \text{BER}_o] = \int_0^{z_o} p(z)\,dz \\ &= \begin{cases} 1 - e^{-z_o/\lambda}\displaystyle\sum_{l=0}^{M\mu-1}\frac{(z_o/\lambda)^l}{l!}, & N_\lambda = 1 \\ \displaystyle\sum_{i=1}^{N_\lambda}\sum_{j=1}^{M\mu_i} A_{i,j}\left(1 - e^{-z_o/\lambda_i}\sum_{l=0}^{j-1}\frac{(z_o/\lambda_i)^l}{l!}\right), & N_\lambda \geq 2 \end{cases} \end{aligned} \tag{4.28}$$

where $\text{BER}_o = q(z_o)$. The result in (4.28) is obtained using the well-known integral of a gamma density [Jakes, 1974, eq. (5.2-15)].

The average BER is

$$\begin{aligned} \langle\text{BER}\rangle &= \int_0^\infty p(z)\,q(z)\,dz \\ &= \begin{cases} \dfrac{L-1}{L}\left[1 - \displaystyle\sum_{l=0}^{M\mu-1}\zeta_l(\mathcal{E}\lambda)\right], & N_\lambda = 1 \\ \dfrac{L-1}{L}\left[\displaystyle\sum_{i=1}^{N_\lambda}\sum_{j=1}^{M\mu_i} A_{i,j}\left(1 - \sum_{l=0}^{j-1}\zeta_l(\mathcal{E}\lambda_i)\right)\right], & N_\lambda \geq 2 \end{cases} \end{aligned} \tag{4.29}$$

where

$$\zeta_l(x) = \frac{1\cdot 3\cdot 5\cdots(2l-1)}{2\cdot 4\cdot 6\cdots(2l)}\sqrt{\frac{x}{(x+1)^{2l+1}}} \tag{4.30}$$

The result in (4.29) is obtained using integration by parts; the error function derivative [Abramowitz and Stegun, 1972, eq. (7.1.19)]; the integral of $p(z)$ as in (4.28); and a standard definite exponential integral [Abramowitz and Stegun, 1972, eq. (7.4.4)];

The $\langle\text{BER}\rangle$ formula is consistent with results reported by other authors. First, it agrees with Mazo's matched filter bound [Mazo, 1991] for single-branch reception of BPSK (and QPSK)

signals subjected to two-path Rayleigh fading and additive white gaussian noise (in the notation used here, this corresponds to M=1; L=2; $\sum_i \mu_i$=2; and $\mathcal{N}(f)$=2N_0). Second, if M=1, we can view the matched filter as a RAKE filter [Price and Green, 1958; Proakis, 1989] (or a maximal ratio combiner [Brennan, 1959; Proakis, 1989]) with N_λ sets of tap weights, where the ith set of μ_i taps have a common average signal-to-noise ratio $\overline{\gamma}_i$=$\mathcal{E}\lambda_i$. Using this notion, the $\langle$BER$\rangle$ formula agrees with the following standard results for RAKE reception of frequency-selective Rayleigh fading signals: (i) μ-tap RAKE (N_λ=1) with $\overline{\gamma}_1$=$\mathcal{E}\lambda$ [Proakis, 1989, eq. (7.4.15)]; and (ii) N_λ-tap RAKE (μ_i=1, all i) with $\overline{\gamma}_i = \mathcal{E}\lambda_i$ [Proakis, 1989, eq. (7.4.28)].

4.2.2 Numerical Results

4.2.2.1 General

The analysis in Section 4.2.1 gives expressions from which one may compute matched filter performance bounds for a space diversity receiver operating in a digital cellular radio environment. The formulae are quite general with respect to transmit filter spectrum, delay power spectrum, and noise power spectrum. The following sections present numerical results for the range of delay spectra listed in Table 2.2, and for a noise power spectrum that arises from noise-like CCI. Note that because the transmit filter spectrum (i.e., $C_T(f)$) of each interfering signal is assumed to be identical to that of the desired signal, the computed performance depends only on the filter bandwidth W and not on its spectral shape (see Section 4.1.1).

The general approach to obtaining numerical results in this thesis is outlined in Section 3.6. The following is a summary of the method for computing matched filter bounds (both outage probability and average BER):

1. Specify parameters M, $P_h(\tau)$ (or $R_H(\alpha)$), and d;
2. Compute eigenvalues using the method described in Appendix 2A; form set of N_λ distinct eigenvalues $\{\lambda_i\}$ and associated multiplicities $\{\mu_i\}$;
3. Compute partial fraction coefficients $\{A_{i,j}\}$ via (4.25);
4. Compute outage probability P_{out} via (4.28), and average bit-error-rate $\langle$BER$\rangle$ via (4.29), for a specified range of SIR values.

Results in the following sections are computed using the above method, except those for a large Md product (e.g., $Md \geq 4$ for a gaussian delay power spectrum or $Md \geq 6$ for an exponential). In these cases, the coefficients in the set $\{A_{i,j}\}$ are subject to significant roundoff error due to high order polynomials with repeated roots (see (4.25)). To overcome the consequential numerical inaccuracy in the final results, $p(z)$ is computed via the fast-Fourier transform of the product form of $\Gamma_z(\xi)$ in (4.24). The corresponding outage probability and average BER are then evaluated by numerical integration.

The performance results show the influence of diversity order, delay spectrum shape, and delay spread. In Figure 4.3, BER distributions are plotted for a fixed level of CCI, and in Figures 4.4 and 4.5, the outage probability and average BER, respectively, are plotted against the level of CCI. For the purposes of Figure 4.3, SIR is fixed at 10 dB to represent a relatively severe level of CCI. Figure 4.6 explicitly presents the increase in tolerance to CCI achievable by taking advantage of the combination of space diversity and the intrinsic frequency diversity associated with transmission over frequency-selective channels.

4.2.2.2 Outage Probability and Average BER

Figures 4.3 to 4.5 show the influence of diversity order, delay spectrum shape, and delay spread on the BER distribution (P_{out} plotted against BER_o), outage probability (plotted against SIR), and average BER (plotted against SIR), respectively. When comparing two BER distributions that cross, we regard the one with the smaller BER variance (steeper gradient at the crossover point) as representing the better performance of the two, because it has a lower probability of a high BER (after the crossover).

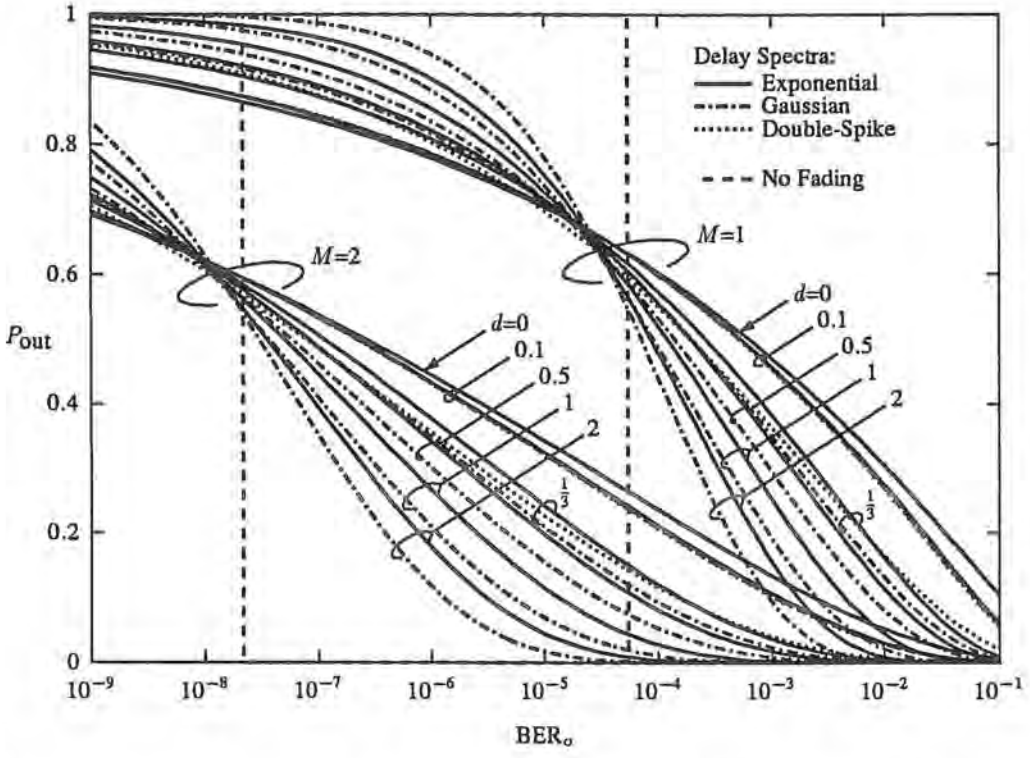

Figure 4.3 Matched filter performance bounds. BER distribution (SIR=10 dB): Influence of diversity order, delay spectrum shape, and delay spread. Results for QPSK and B=1.5.

For the two continuous delay spectra, the results show that performance is slightly better for a gaussian delay spectrum, and is improved as the delay spread is increased. The improved performance with increasing d is due to the intrinsic frequency diversity introduced by the frequency-selective nature of the channel. The asymptotic limit on this performance (as $d \to \infty$) is the same as the performance for a set of *unfaded* frequency-flat channels ($H_m(f)$=1, all m). This fact is because each $H_m(f)$ is ergodic ($R_H(\alpha) \to 0$ as $\alpha\tau_0 \to \infty$), so in the limiting case, the BER becomes deterministic (i.e., the same for any $\{H_m(f)\}$ from the ensemble). These BER values are labelled "No Fading" in Figures 4.3 to 4.5.

For channels consisting of a few independently fading paths (two for the double-spike channel), the performance reaches a limit as the delay spread is increased. This limit occurs when $W=1/\tau_s$, where τ_s is the delay between paths (with B=1.5, this corresponds to $d=\frac{1}{3}$ for a double-spike channel). At this point, the receiver can resolve the paths, so there is no further improvement for increasing delay spread. In other words, the matched filter combiner becomes equivalent to the optimum (maximal ratio) diversity combining of the individual paths [Mazo, 1991].

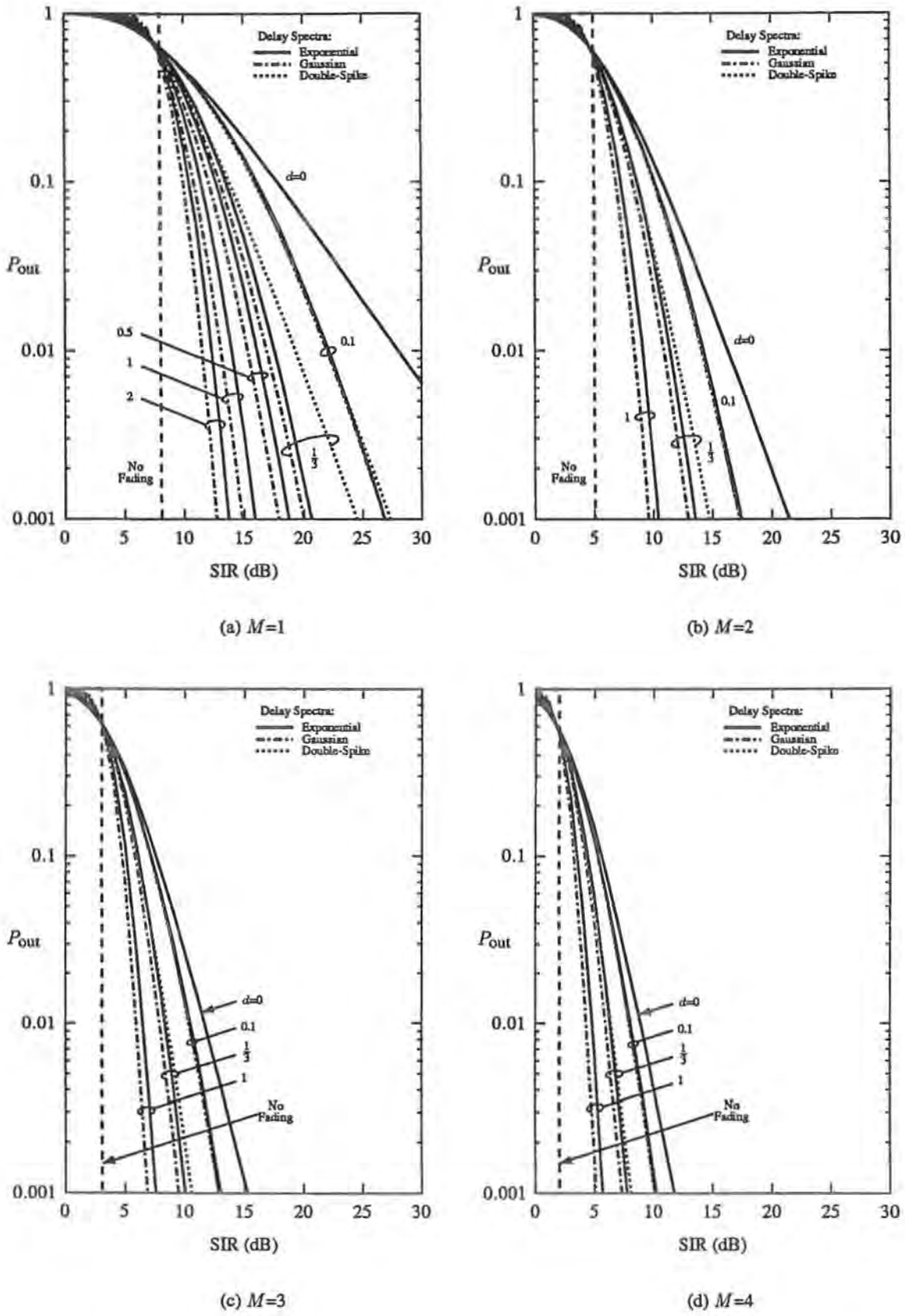

Figure 4.4 Matched filter performance bounds. Outage probability ($BER_o=10^{-3}$): Influence of diversity order, delay spectrum shape, and delay spread. Results for QPSK and B=1.5.

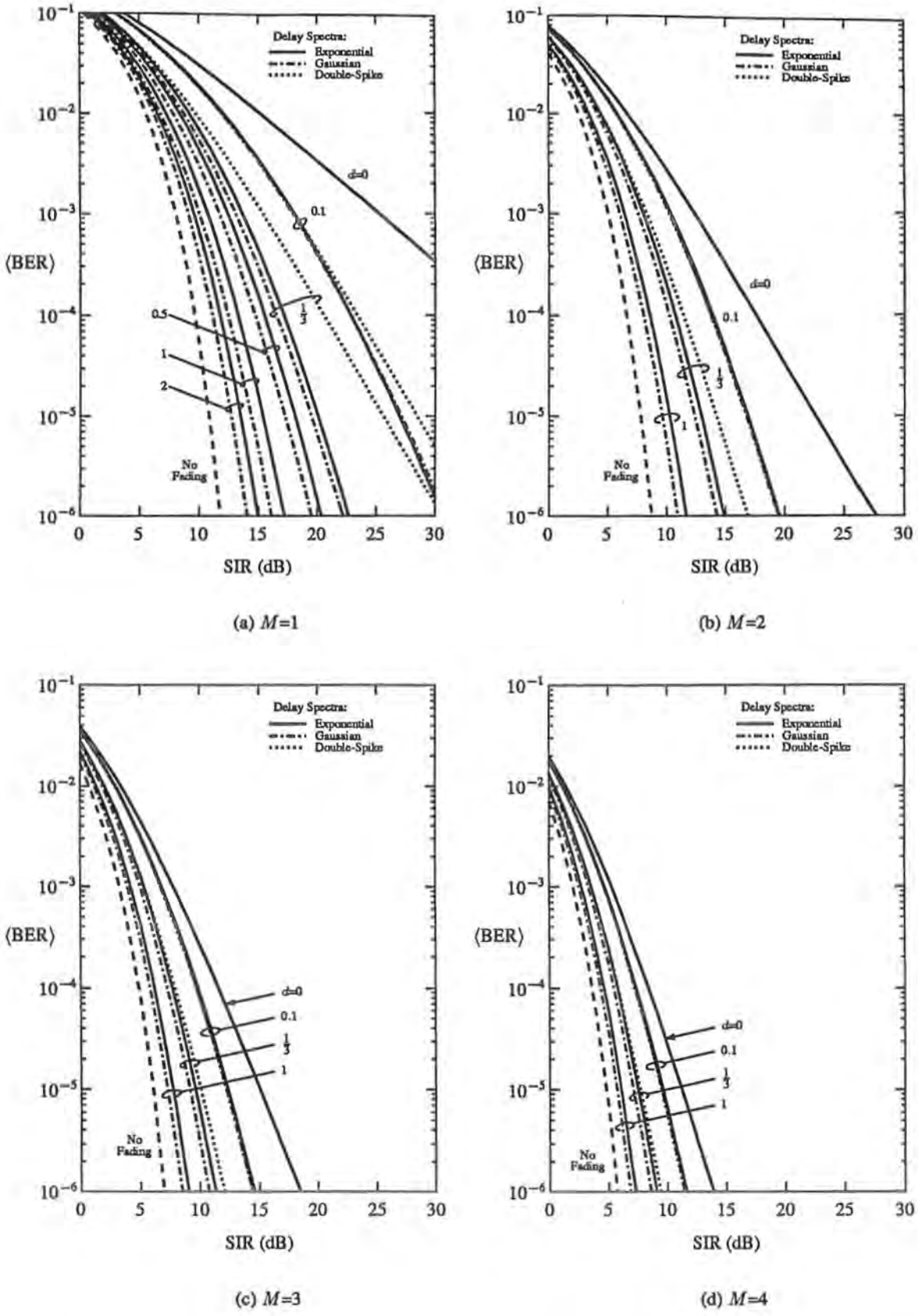

Figure 4.5 Matched filter performance bounds. Average BER: Influence of diversity order, delay spectrum shape, and delay spread. Results for QPSK and B=1.5.

4.2.2.3 Diversity Gain

As indicated previously, improved performance for fading channels may be achieved by space diversity or intrinsic frequency diversity. For an average BER of 10^{-3}, Figure 4.6 summarizes these performance gains by plotting the *diversity gain* (improvement in tolerance to CCI) against the delay spread, using as a reference the case of single-branch reception (no space diversity) of flat fading signals (no intrinsic frequency diversity) in which SIR≈25dB at the selected BER (Figure 4.5(a)). The relative level of CCI tolerated with a set of M unfaded channels is also shown in Figure 4.6.

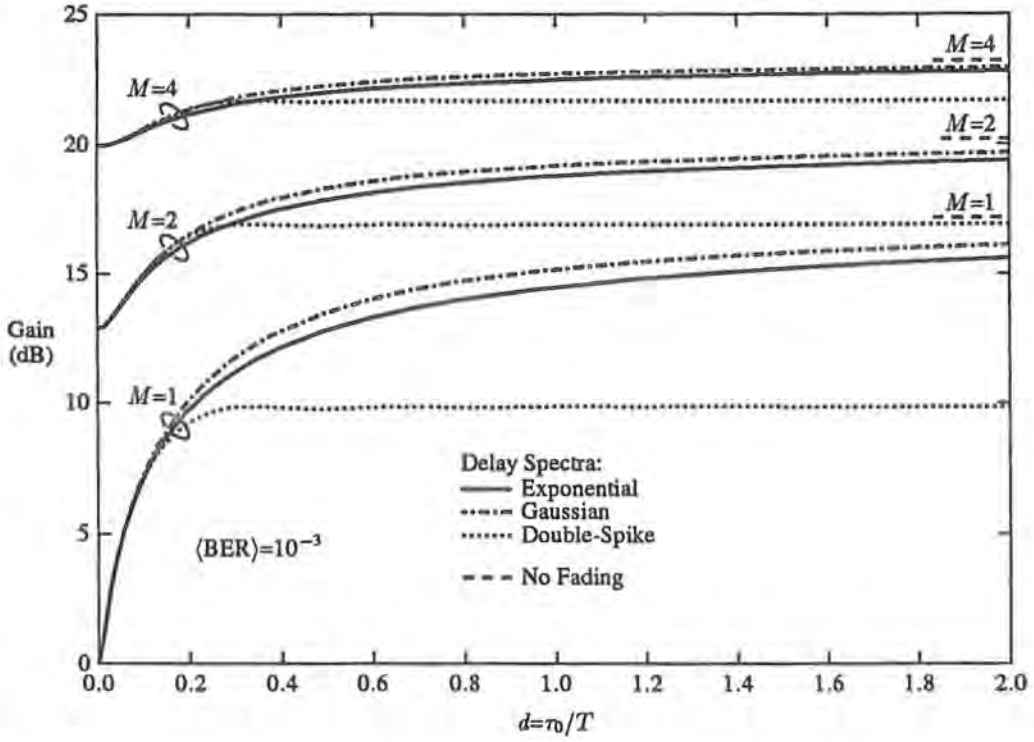

Figure 4.6 Matched filter performance bounds. Diversity gain (⟨BER⟩=10^{-3}). Results for QPSK and B=1.5.

We observe the following: (i) two-branch space diversity and a small frequency selectivity (e.g., d=0.2) provides a better diversity gain than single-branch reception and a large frequency selectivity (e.g., d=2); (ii) intrinsic frequency diversity is significantly more beneficial to a single-branch system than it is to a multiple-branch system; and (iii) only a small frequency selectivity (d=0.5) is required to obtain a high proportion of the possible intrinsic frequency diversity benefit.

We should bear in mind that, in a real system, we need some form of equalization to combat the ISI introduced by frequency-selective fading. An equalizer can not possibly eliminate all ISI without enhancing the noise, so a realistic diversity gain will be somewhat less than the bounds presented here. Fortunately, as noted above, systems with only a small frequency selectivity, in which good equalizers cope well with ISI, are adequate to benefit substantially from intrinsic frequency diversity. However, in terms of both potential performance *and* combating ISI in realistic systems, it is far better to employ space diversity than it is to employ wideband transmission (providing intrinsic frequency diversity) to overcome the problem of multipath fading.

4.3 Conclusion

Using analytical techniques, this chapter has derived matched filter performance bounds for an ideal space diversity receiver operating in a digital cellular radio environment with frequency-selective multipath fading.

In addition, this chapter has presented numerical results illustrating the influence of various system parameters on ideal system performance in a cellular environment with many co-channel interferers. The best possible benefits of space diversity and intrinsic frequency diversity have been quantified for various delay power spectra and a range of rms delay spreads.

In the following chapter, the matched filter bound is compared with the performance of an optimum linear receiver.

Chapter 5

OPTIMUM LINEAR RECEIVERS

It is important to know how well an optimum linear diversity receiver performs in the digital cellular system described in Chapter 2. With enough diversity branches, for instance, it may perform almost as well as the maximum likelihood receiver (Chapter 4), indicating that increased complexity buys only a small potential performance gain.

The structure of the optimum linear receiver for single-source linear systems (N_s=1) without diversity (M=1), has has been formulated for a variety of optimality criteria and is well known [Smith, 1965; George, 1965; Aaron and Tufts, 1966; Lucky *et al.*, 1968]. In all cases, it consists of a matched filter in cascade with a T-spaced transversal filter. Kaye and George [1970], Van Etten [1975], and Salz [1985] extend this formulation to multiple-source linear diversity systems (again, for a variety of criteria), and all find that the optimum linear receiver for estimating the desired source consists of a bank of matched filters (one filter corresponding to each source for each diversity branch), the outputs for each source being summed over all diversity branches, followed by a bank of T-spaced transversal filters (one filter corresponding to each source). The reason for these common structures is pointed out by Forney [1972] and Van Etten [1976], in relation to the matched filter structure of the maximum likelihood receiver (see Section 5.1 for a discussion on this relationship).

Balaban and Salz [1991] have produced performance results for the optimum two-branch linear diversity receiver[1] (for two criteria of optimality: minimum mean-square error or MMSE, and zero-forcing) operating in digital cellular radio systems with two-path Rayleigh fading channels and without dominant CCI. Results also have been obtained for optimum finite-tap diversity receivers (including decision feedback ISI cancellation) operating in a variety of radio systems with and without dominant CCI [Monsen, 1984; Despins *et al.*, 1991; Lo *et al.*, 1990].

This chapter presents results for the optimum linear diversity receiver (MMSE criterion) that extend those of Balaban and Salz to systems with dominant CCI, and to the range of delay spectra given in Table 2.2. The MMSE optimization is performed in a novel and quite simple way, starting with the optimum linear receiver structure described in Section 5.1. (In more complicated approaches [Kaye and George, 1970; Salz, 1985], the structure is a result of the optimization.) In addition, the bit-error-rate is computed using the range of methods described in Chapter 3 (Balaban and Salz used only the loosest form of Saltzberg's bound). We shall see that the performance of the optimum linear receiver is remarkably good in an interference-limited environment.

The optimum linear receiver is analysed in Sections 5.1 and 5.2, and optimized in the MMSE sense in Section 5.3. The set of numerical results is presented in Section 5.4.

[1] Balaban and Salz [1991] also obtained results for decision feedback equalization and matched filter bounds.

5.1 Optimum Linear Receiver Structure

Assume that the diversity receiver (for the desired source) of the digital cellular system described in Chapter 2 has the the general form shown in Figure 3.2. The question is, what are the optimum filter responses $\{u_m(t)\}$ for some given criterion of optimality? This problem is easily solved by observing an interesting corollary of the maximum likelihood formulation given in Section 4.1: because $\{z_{n,k}\}$ is a sufficient set of statistics to estimate $\{x_{n,k}\}$, and the matched filters perform linear operations, the effect of the optimum filter responses $\{u_m(t)\}$ must be equivalent to the optimum linear combination of the members in $\{z_{n,k}\}$, *regardless of the criterion of optimality.* Therefore, the receiver shown in Figure 3.2 with optimum responses $\{u_m(t)\}$ is equivalent to the structure shown in Figure 5.1, where $p_{m,n}(t) = q^*_{m,n}(t_d - t)$ (as in (4.15)); and $\{\tilde{v}_n(t)\}$ are the impulse responses of a set of infinite-length transversal filters, each with delay T between taps. Note also, the fixed receive filter $c_R(t)$ should have a noise whitening response (Section 4.1.1) and the choice of t_d is arbitrary (requiring only that it make the matched filter responses $\{p_{m,n}(t)\}$ causal).

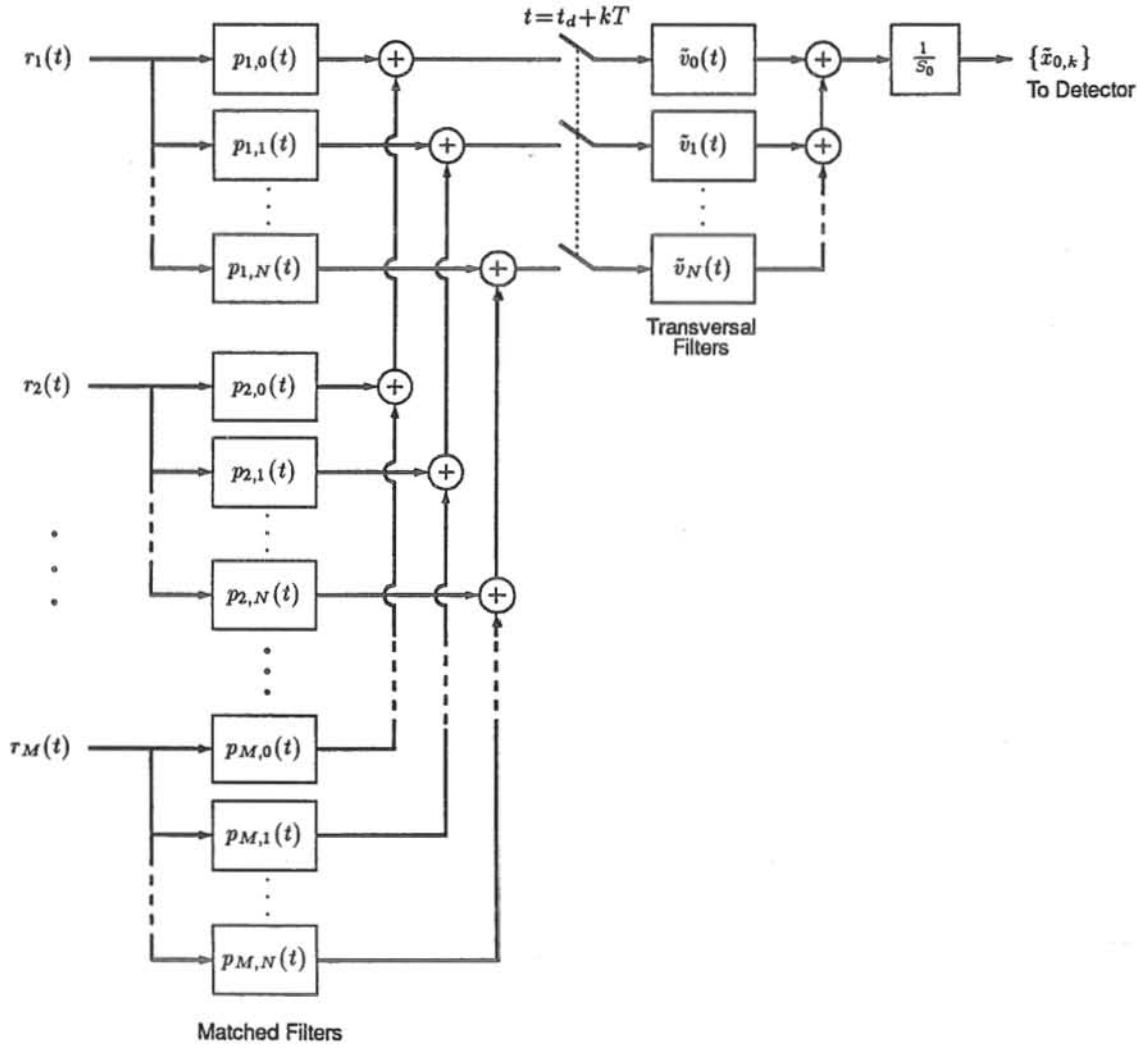

Figure 5.1 Optimum linear receiver (for the desired source).

One of the main reasons for formulating this equivalent structure is that it is much easier to

optimize the discrete-time filters $\{\tilde{v}_n(t)\}$ than it is to optimize the continuous-time filters $\{u_m(t)\}$ (see Section 5.3). In practice, however, the optimum or near-optimum linear receiver (including the cascade of fixed receive filters, matched filters, and transversal filters) would probably be realized with just M transversal filters, one in each diversity branch, that are ideally infinite-length and have fractionally-spaced taps (T-spaced taps would, in general, be information lossy).

5.2 Analysis

The equivalent discrete system (see Section 3.2) for the optimum linear receiver is here formulated, so that system performance can be evaluated. For analytical simplicity, assume that $\{\tilde{v}_n(t)\}$ are non-causal, and let the periodic frequency response of the nth transversal filter be denoted by $\tilde{V}_n^*(f)$ (the complex conjugate being used to aid the following). The equivalent discrete linear system is thus characterized by

$$\tilde{G}_n(f) = \tfrac{1}{T}\textstyle\sum_{n'=0}^{N} \tilde{V}_{n'}^*(f) \sum_m \sum_i Q_{m,n}(f - i/T)\, P_{m,n'}(f - i/T) \cdot \exp\left(-\jmath 2\pi i t_d/T\right), \quad n = 0, 1, 2, \ldots, N \tag{5.1}$$

and

$$\tilde{\mathcal{N}}_L(f) = \frac{\mathcal{N}_r}{T^2} \sum_{n=0}^{N} \sum_{n'=0}^{N} \tilde{V}_n(f)\, \tilde{V}_{n'}^*(f) \sum_m \sum_i P_{m,n}^*(f - i/T)\, P_{m,n'}(f - i/T) \tag{5.2}$$

(Recall that $\mathcal{N}_r = \mathcal{N}_w$ for noise-like CCI.) The frequency response of the matched filter in the mth branch for the nth source is $P_{m,n}(f) = Q_{m,n}^*(f) \exp(-\jmath 2\pi f t_d)$ (as in (4.16)). Substituting this $P_{m,n}(f)$ into (5.1) and (5.2), and rewriting in matrix form, we have

$$[\, \tilde{G}_0(f) \quad \tilde{G}_1(f) \quad \ldots \quad \tilde{G}_N(f)\,] = \mathbf{V}^H(f)\, \mathbf{X}(f) \exp(-\jmath 2\pi f t_d) \tag{5.3}$$

and

$$\tilde{\mathcal{N}}_L(f) = \mathcal{N}_r\, \mathbf{V}^H(f)\, \mathbf{X}(f)\, \mathbf{V}(f) \tag{5.4}$$

where

$$\mathbf{X}(f) \triangleq \sum_i \mathbf{Q}^H(f - i/T)\, \mathbf{Q}(f - i/T) \tag{5.5}$$

$$\mathbf{Q}(f) \triangleq [\, \mathbf{Q}_0(f) \quad \mathbf{Q}_1(f) \quad \ldots \quad \mathbf{Q}_N(f)\,] \tag{5.6}$$

$$\mathbf{V}(f) \triangleq \frac{1}{T} \begin{bmatrix} \tilde{V}_0(f) \\ \tilde{V}_1(f) \\ \vdots \\ \tilde{V}_N(f) \end{bmatrix} \tag{5.7}$$

and $\mathbf{Q}_n(f)$ is defined in Section 2.2.

Given the optimized $\mathbf{V}(f)$ (e.g., that in Section 5.3), $\{\tilde{G}_n(f)\}$ and $\tilde{\mathcal{N}}_L(f)$ can be computed via (5.3) and (5.4). It is then straightforward, using the techniques described in Sections 3.2 and 3.4, to compute the bit-error-rate.

5.3 MMSE Optimization

The mean-square error in (3.11) can be rewritten as

$$\epsilon = \sigma_x^2 T \int_{-1/2T}^{1/2T} D(f)\, df \tag{5.8}$$

where

$$D(f) = \sum_{n=0}^{N} \left(\frac{S_n}{S_0}\right)^2 |\tilde{G}_n(f)|^2 - 2\mathrm{Re}\left[\tilde{G}_0(f)\exp(j2\pi f t_s)\right] + \frac{T}{S_0^2\sigma_x^2}\tilde{\mathcal{N}}_L(f) + 1 \tag{5.9}$$

is the *distortion spectrum* (ideally, it should be zero for all f). Using (5.3) and (5.4) (with $t_s = t_d$), we get

$$D(f) = \mathbf{V}^H(f)\,\mathbf{X}(f)\left[\mathbf{S}^2\,\mathbf{X}^H(f) + \mathcal{N}_0\,\mathbf{I}\right]\,\mathbf{V}(f) - 2\mathrm{Re}\left[\mathbf{V}^H(f)\,\mathbf{X}(f)\,\mathbf{U}\right] + 1 \tag{5.10}$$

where

$$\mathbf{S} \triangleq \frac{1}{S_0}\,\mathrm{diag}\,[\,S_0 \quad S_1 \quad \ldots \quad S_N\,] \tag{5.11}$$

$$\mathbf{U} \triangleq \begin{bmatrix} 1 \\ 0 \\ \vdots \\ 0 \end{bmatrix} \qquad (\text{an } N_d \times 1 \text{ vector}) \tag{5.12}$$

$\mathbf{I}$ is an $N_d \times N_d$ identity matrix, and $\mathcal{N}_0 \triangleq \mathcal{N}_r\,T/(S_0^2\sigma_x^2)$ (for noise-like CCI, $\mathcal{N}_0 = 1/\mathrm{SIR}_w$). We obtain the minimum mean-square error when

$$\frac{\partial\epsilon}{\partial\mathbf{V}(f)} = 0 \quad\Longrightarrow\quad \frac{\partial D(f)}{\partial\mathbf{V}(f)} = 2\mathbf{X}(f)\left[\mathbf{S}^2\,\mathbf{X}^H(f) + \mathcal{N}_0\,\mathbf{I}\right]\mathbf{V}(f) - 2\mathbf{X}(f)\,\mathbf{U} = \mathbf{0} \tag{5.13}$$

where Haykin's definition [Haykin, 1986, pp. 105–107] of differentiation with respect to a complex vector[2] is adopted. Hence, provided $\mathcal{N}_0 > 0$ (well-conditioned system of equations), the MMSE solution for the transversal filter responses is

$$\mathbf{V}(f) = \left[\mathbf{S}^2\,\mathbf{X}^H(f) + \mathcal{N}_0\,\mathbf{I}\right]^{-1}\mathbf{U} \tag{5.14}$$

which is solved (for each $f : |f| \le 1/2T$) using standard numerical methods [Moler, 1990; Press *et al.*, 1986]. The minimum attainable MSE is given by

$$\epsilon_{\min} = \sigma_x^2 T \int_{-1/2T}^{1/2T} \mathcal{N}_0\mathbf{U}^H\left[\mathbf{S}^2\,\mathbf{X}^H(f) + \mathcal{N}_0\,\mathbf{I}\right]^{-1}\mathbf{U}\, df \tag{5.15}$$

Note that for single-source transmission ($N_d = 1 \Rightarrow$ scalars: $\mathbf{X}(f) \equiv X(f), \mathbf{S} = 1, \mathbf{U} = 1$), the optimization reduces to a solution for a single transversal filter,

$$\frac{1}{T}\tilde{V}_0(f) = \frac{1}{X(f) + \mathcal{N}_0} \tag{5.16}$$

and a minimum MSE

$$\epsilon_{\min} = \sigma_x^2 T \int_{-1/2T}^{1/2T} \left(\frac{\mathcal{N}_0}{X(f) + \mathcal{N}_0}\right) df \tag{5.17}$$

which, for a single-branch system (M=1), is consistent with standard results [Qureshi, 1985, Sec. II].

[2] Strictly speaking, differentiation with respect to a complex number is not analytic.

5.4 Numerical Results

5.4.1 General

The analysis and optimization presented in Sections 5.2 and 5.3 constitute a simple method with which one may analyse BER performance of an optimum (MMSE) linear receiver operating in a digital cellular radio environment with static multipath responses. Section 3.5 describes the simulation method for computing BER performance over an ensemble of such multipath channels.

The following sections present numerical performance results that show the influence of the BER computation scheme (Figure 5.2), the diversity order and number of dominant interferers (Figures 5.3 to 5.5), the delay spread (Figures 5.6 to 5.8), and the delay spectrum shape (Figure 5.9). The general approach to obtaining numerical results is, again, outlined in Section 3.6. The following is a summary of the method for computing optimum (MMSE) linear receiver performance results:

1. Specify parameters M, N, $P_h(\tau)$, and d (and number of Monte Carlo trials, N_T).
   Specify range of SIR values.
   Compute S and $\mathcal{N}_0$ for each SIR value (Sections 5.3 and 2.1.4).

2. Compute eigenvalues and eigenfunctions (Appendix 2A).
   Compute the matrix $\Lambda^{\frac{1}{2}}\phi(\beta)$ (Section 2.2).

3. Do the following steps N_T times:

   - Generate $\{\mathbf{c}_n\}$ and $\{t_n/T\}$ (Section 2.2).
   - Compute $\mathbf{Q}(f)$ via (5.6) and (2.23), and $\mathbf{X}(f)$ via (5.5).
   - Do the following steps for each SIR value:
     - Solve $\left[\mathbf{S}^2\,\mathbf{X}^H(f)+\mathcal{N}_0\,\mathbf{I}\right]\mathbf{V}(f)=\mathbf{U}$ over Nyquist band.
     - Compute $\{\tilde{G}_n(f)\}$ and $\tilde{\mathcal{N}}_L(f)$ via (5.3) and (5.4).
     - Compute and store BER (Section 3.4).

4. For each SIR value, compute P_{out} (for specified value or range of BER_o) and $\langle\text{BER}\rangle$ (Section 3.5).

5.4.2 Influence of BER Computation Scheme

Except for these results specifically comparing the various BER approximations (Section 3.4), the results shown in this chapter have been computed using Metzger's algorithm — the most accurate BER computation method of the four schemes described in Section 3.4. In the preliminary results of this work, it was determined that the gaussian approximation to the interference pdf $p_\varepsilon(x)$ (see Section 3.4) yields a reasonably accurate estimate of the optimum linear receiver's performance in all cases (BER well within an order of magnitude of that computed using Metzger's algorithm, for all BER$>10^{-4}$). This gauss-like $p_\varepsilon(x)$ is due to the optimum receiver's ability to suppress any dominant interference components (ISI or CCI). The sum of many small residual interference terms naturally tends to be gaussian distributed.

The gaussian approximation is least accurate in the cases where $M \leq N$ because the M-branch receiver does not have the degrees of freedom to effectively suppress more than $M-1$ dominant co-channel interferers. In the worst case — a single dominant residual interference component — the interference pdf is a double-spike.

Figure 5.2 shows flat fading (d=0) results for (i) a single-branch receiver and one dominant co-channel interferer (M=N=1); and (ii) a two-branch receiver and two dominant co-channel interferers (M=N=2). Out of all simulations performed for the optimum linear receiver, the results in these two cases are the most dramatically influenced by the BER computation scheme. Nevertheless, the gaussian approximation to $p_\varepsilon(x)$ is still reasonable: it results in an error in SIR of no more than 1 or 2 dB for any given outage probability (with BER_o=10^{-3}), and a negligible error in SIR for any given average BER. The simple Saltzberg bound is in error by up to 3 or 4 dB for both performance measures.

5.4.3 Influence of Diversity Order and Number of Dominant Interferers

Figures 5.3 to 5.5 show the influence of diversity order and the number of dominant interferers on the optimum linear receiver's performance, for a frequency-selective fading channel with an exponential delay spectrum and a normalized delay spread d=1. To conveniently quantify relative performance, assume that an acceptable average BER is 10^{-3}. Table 5.1 shows the SIR that can be tolerated to achieve this performance criterion, for various M and N. The figures in brackets show the *dominant CCI gain*, which is defined as the SIR gain ($\langle\text{BER}\rangle$=10^{-3}) with reference to the N=0 case, for a given number of diversity branches. (The relative SIR gains for P_{out}=0.01 are approximately the same as the values shown in Table 5.1.)

		Optimum Linear Receiver			
M	MFB	N=0	N=1	N=2	N=3
1	10.7	15.5	14.7 (0.8)	15.1 (0.4)	–
2	6.4	8.9	−5.9 (14.8)	4.8 (4.1)	–
4	2.7	4.0	−14.5 (18.5)	−12.4 (16.4)	−8.2 (12.2)

Table 5.1 Performance of optimum (MMSE) linear receiver. Tolerable SIR (±0.5 dB) for $\langle\text{BER}\rangle$=10^{-3}: Influence of diversity order and number of dominant interferers. (MFB ≡ Matched Filter Bound; figures in brackets show the dominant CCI gain.) Results for QPSK, B=1.5, $P_h(\tau)$=exponential, d=1, and DWR=20 dB.

For comparison, matched filter bounds (from Section 4.2, the N=0 case) are also shown in Table 5.1. The results show that as diversity order is increased in the purely noise-like CCI case (N=0), the performance of the optimum linear receiver gets closer to the matched filter bound (only 1.3 dB difference in SIR for the M=4 case). This has an important practical implication: with multiple branch receivers, simple linear equalization is very powerful — there is only a small potential advantage in employing more complex receivers (e.g., employing decision feedback equalization or maximum likelihood detection at the combiner output); on the other hand, in the case of no diversity (M=1), there is a significant potential advantage in employing sophisticated equalizers.

The results also show how well an M-branch receiver deals with a few dominant interferers[3] while combating ISI caused by dispersion. The maximum possible dominant CCI gain is equal to the DWR, which is 20 dB in all results. Thus, from Table 5.1, a four-branch receiver can almost completely eliminate a single dominant interferer. Good CCI cancellation is also achieved by a four-branch receiver combating two dominant interferers, or a two-branch receiver combating

[3] In the preliminary results of this thesis work, performances for larger values of N (e.g., N=20) also were computed. As expected, this showed that as $N \to \infty$, performance converges on the N=0 case. In these cases of large N, simulations with many trials were avoided because they ran too slowly on the available computing facilities.

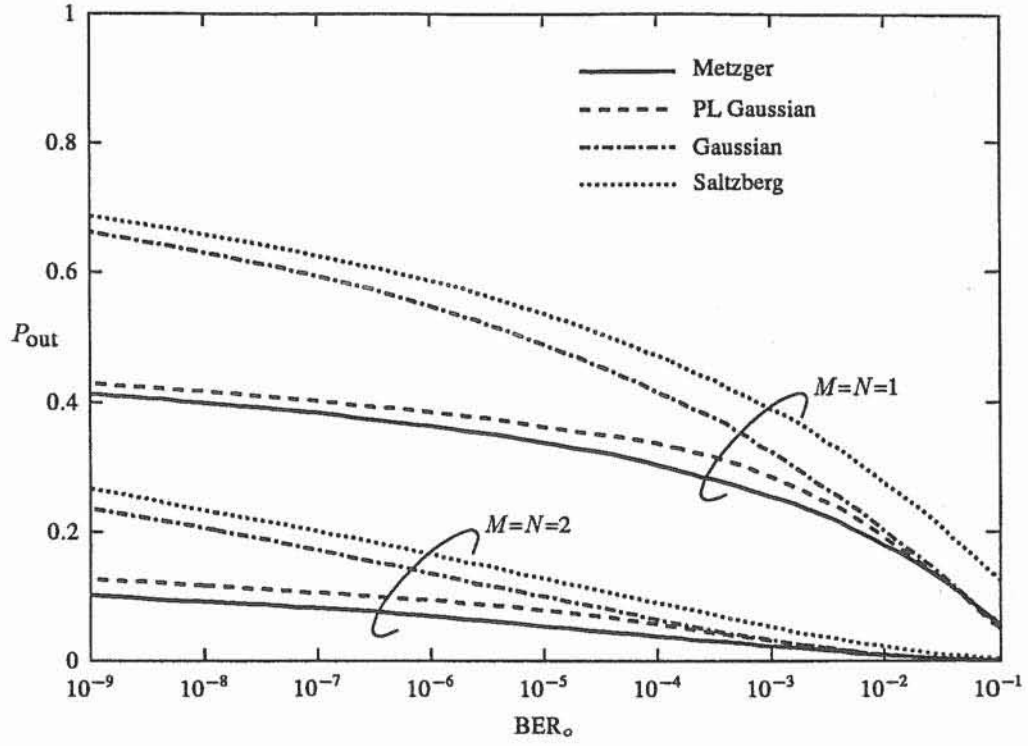

(a) BER distribution (SIR=10 dB).

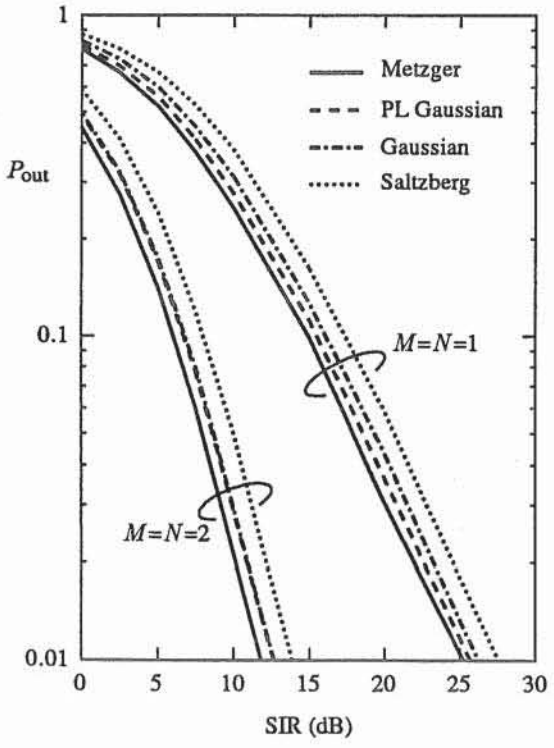

(b) Outage probability ($BER_o=10^{-3}$).

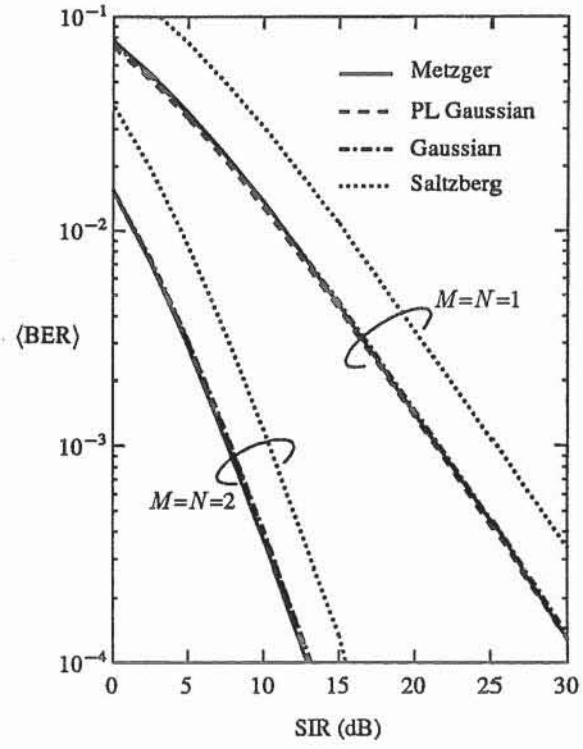

(c) Average BER.

Figure 5.2 Performance of optimum (MMSE) linear receiver. Influence of BER computation method (PL ≡ Peak-Limited). Results for QPSK, B=1.5, d=0, and DWR=20 dB.

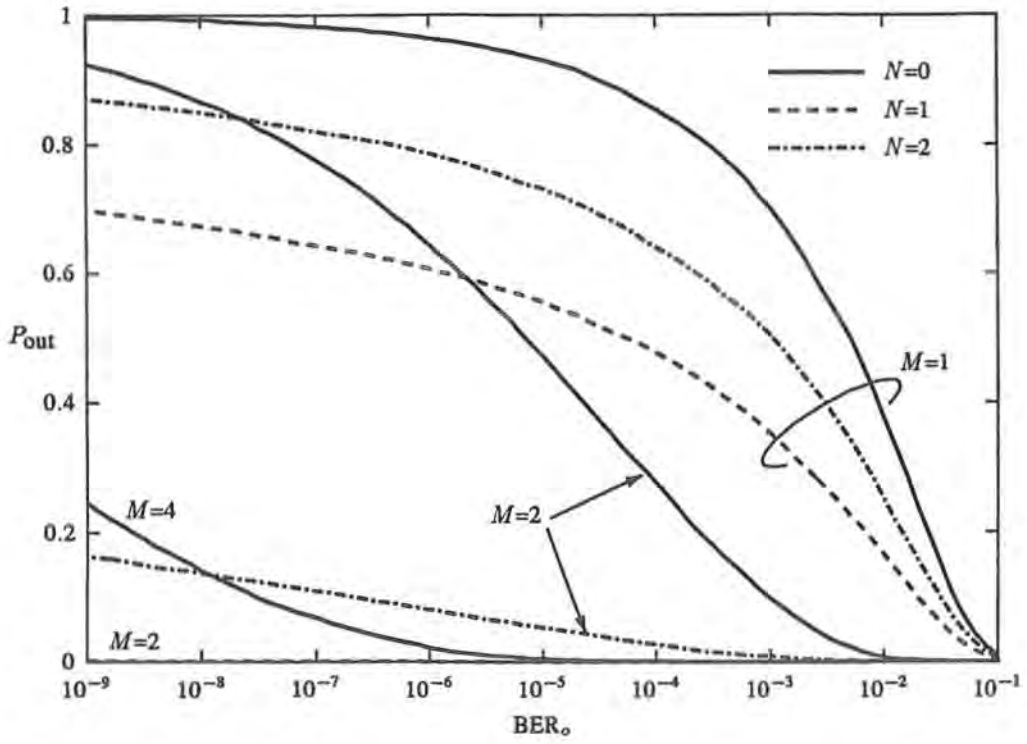

Figure 5.3 Performance of optimum (MMSE) linear receiver. BER distribution (SIR=10 dB): Influence of diversity order and number of dominant interferers. Results for QPSK, B=1.5, $P_h(\tau)$=exponential, d=1, and DWR=20 dB.

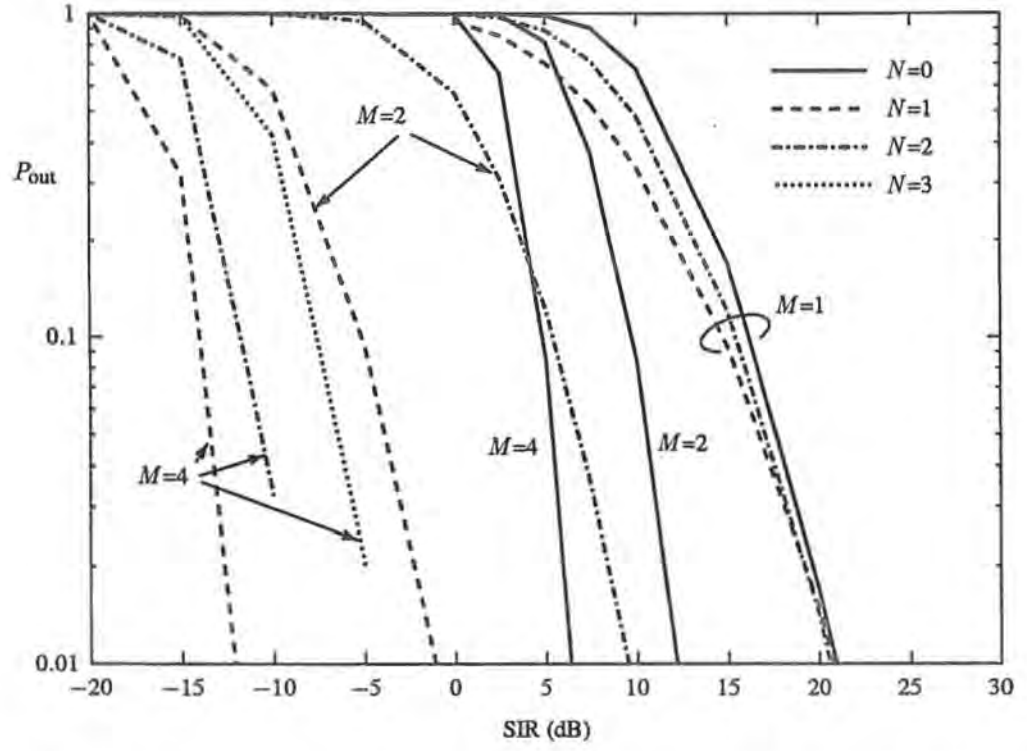

Figure 5.4 Performance of optimum (MMSE) linear receiver. Outage probability (BER_o=10^{-3}): Influence of diversity order and number of dominant interferers. Results for QPSK, B=1.5, $P_h(\tau)$=exponential, d=1, and DWR=20 dB.

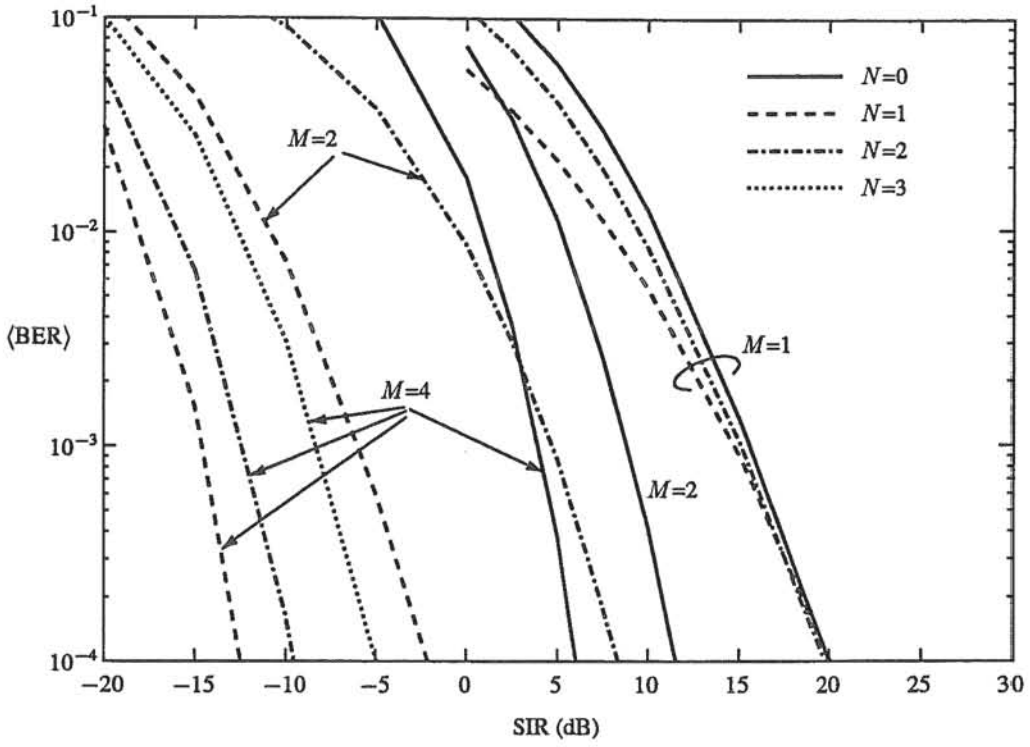

Figure 5.5 Performance of optimum (MMSE) linear receiver. Average BER: Influence of diversity order and number of dominant interferers. Results for QPSK, B=1.5, $P_h(\tau)$=exponential, d=1, and DWR=20 dB.

one. Note also, at higher average BER values (see Figure 5.5), there is a small dominant CCI gain even in single-branch systems.

5.4.4 Influence of Delay Spread

Figures 5.6 to 5.8 show the influence of delay spread (for an exponential delay spectrum) on the optimum linear receiver's performance. As with the matched filter bounds presented in Section 4.2, the performance of the optimum linear receiver improves with increasing delay spread. This improvement is due to the associated benefits of intrinsic frequency diversity. Table 5.2 shows the diversity gains for the optimum linear receiver, assuming the same performance criterion discussed in the previous section. (Matched filter bounds, N=0 case, are shown for comparison.)

	Matched Filter Bound (N=0)			Optimum Linear Receiver			
				N=0			N=1
d	M=1	M=2	M=4	M=1	M=2	M=4	M=2
0	25.3	12.3	5.4	25.6	12.7	5.8	0.0
0.5	12.4 (12.9)	7.4 (4.9)	3.3 (2.1)	17.2 (8.4)	9.7 (3.0)	4.5 (1.3)	−4.4 (4.4)
1	10.7 (14.6)	6.4 (5.9)	2.7 (2.7)	15.6 (10.0)	8.9 (3.8)	4.0 (1.8)	−5.9 (5.9)
2	9.6 (15.7)	6.0 (6.3)	2.5 (2.9)	14.5 (11.1)	8.2 (4.5)	3.7 (2.1)	−7.1 (7.1)

Table 5.2 Performance of optimum (MMSE) linear receiver. Tolerable SIR (±0.5 dB) for ⟨BER⟩=10^{-3}: Influence of delay spread. (Figures in brackets show SIR gain with reference to d=0 case.) Results for QPSK, B=1.5, $P_h(\tau)$=exponential, and DWR=20 dB.

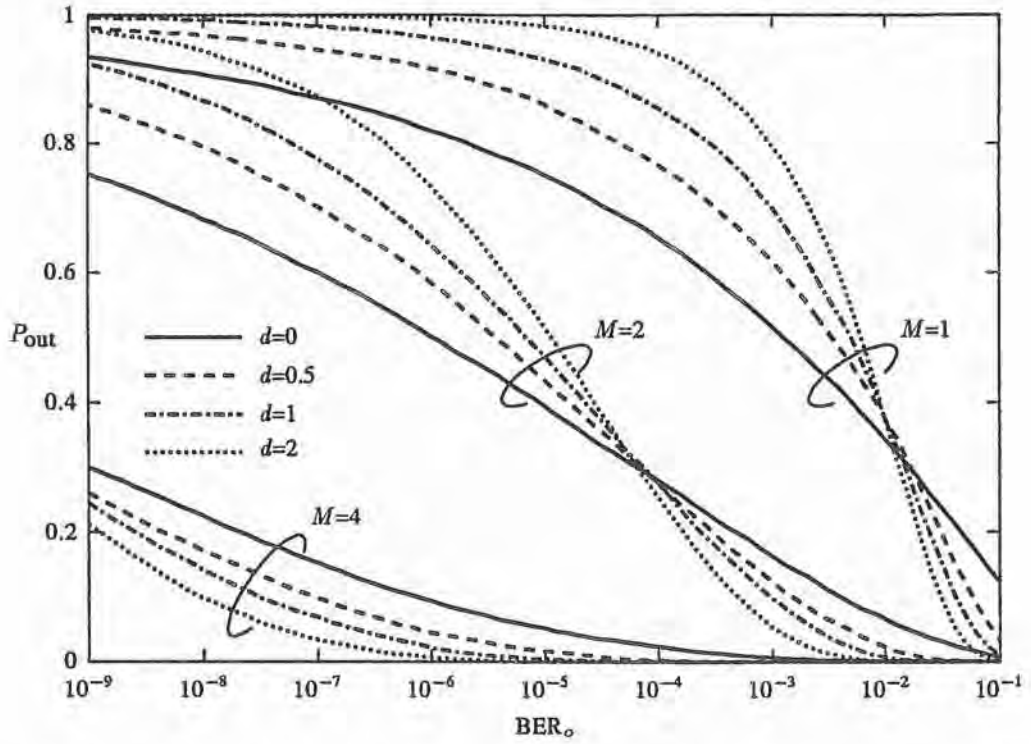

Figure 5.6 Performance of optimum (MMSE) linear receiver. BER distribution (SIR=10 dB): Influence of delay spread. Results for QPSK, B=1.5, N=0, $P_h(\tau)$=exponential, and DWR=20 dB

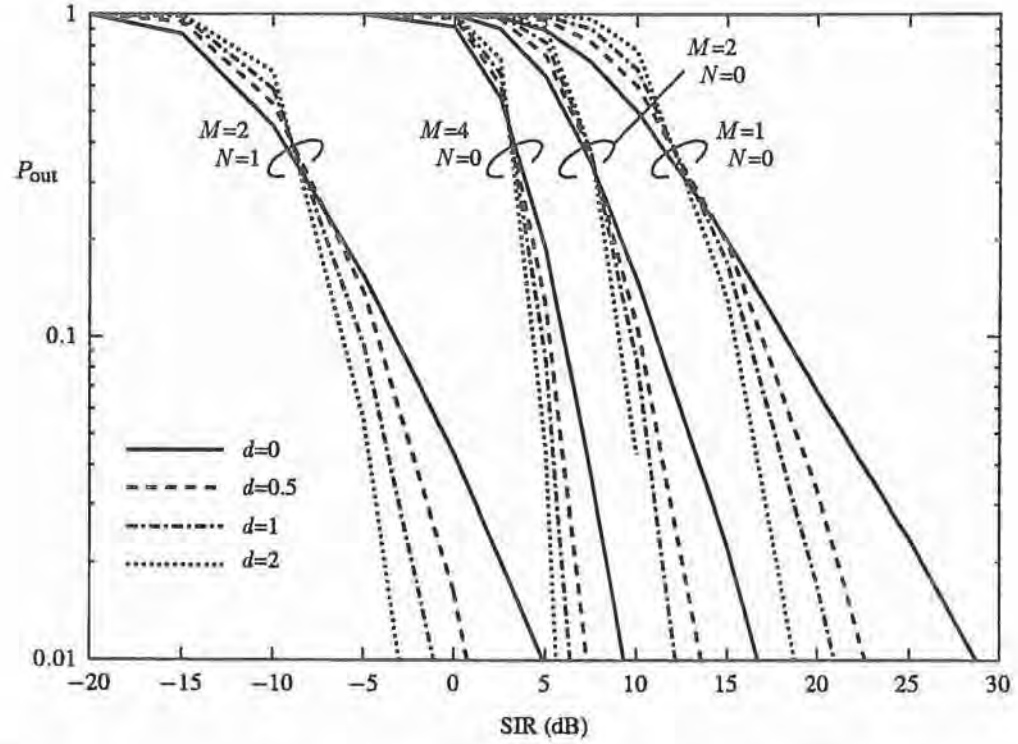

Figure 5.7 Performance of optimum (MMSE) linear receiver. Outage probability ($BER_o=10^{-3}$): Influence of delay spread. Results for QPSK, B=1.5, $P_h(\tau)$=exponential, and DWR=20 dB.

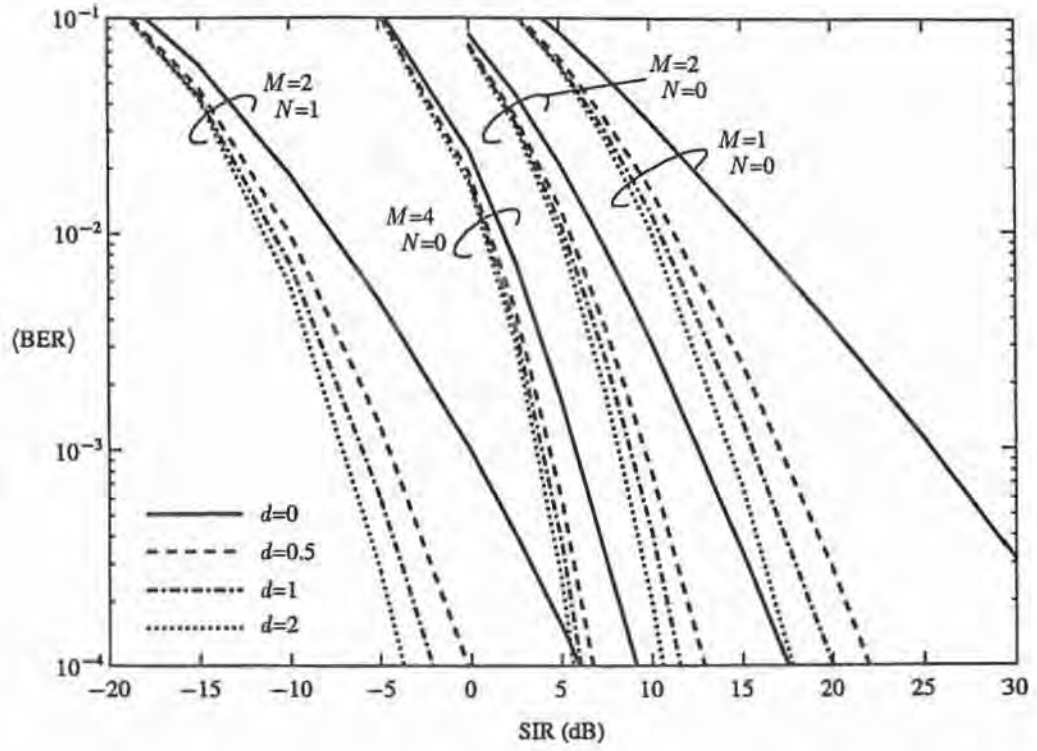

Figure 5.8 Performance of optimum (MMSE) linear receiver. Average BER: Influence of delay spread. Results for QPSK, B=1.5, $P_h(\tau)$=exponential, and DWR=20 dB.

Performance results in the case of flat fading (d=0) and purely noise-like CCI (N=0) are almost as good as the matched filter bound (about 0.4 dB difference at ⟨BER⟩=10^{-3}). They are not exactly the same for the following reason. For additive coloured gaussian noise (as in the noise-like CCI case at hand), one can not generally achieve optimum noise immunity without introducing ISI — the cascade of transmit filter and noise whitening filter does not generally have a Nyquist response. Because ISI is taken to be eliminated in computing the matched filter bound, the optimum linear receiver, which must deal with ISI, can not possibly do as well as the bound[4].

For dispersive channels (d=0.5–2) and noise-like CCI, the single-branch receiver performs within about 5 dB of the matched filter bound, and the two- and four-branch receivers perform within about 1 or 2 dB (again illustrating the power of simple linear processing in space diversity receivers).

In two-branch reception, note also that the gains due to increasing delay spread in the dominant CCI case (N=1) are better, by up to 2.5 dB, than those in the noise-like CCI case. That is, frequency-selective fading offers an additional gain, over flat fading, in the ability of receivers to combat dominant CCI as opposed to noise.

5.4.5 Influence of Delay Spectrum Shape

Figure 5.9 shows the influence of delay spectrum shape on optimum linear receiver performance. As with the matched filter bounds presented in Chapter 4, performance for the gaussian delay spectrum is slightly better than that for the exponential delay spectrum. Also, the performance for

[4]If the noise were white, or if in the noise-like CCI case the transmit filters had a zero excess bandwidth (B=1), the optimum linear receiver's performance would be identical to the matched filter bound in the N=0, d=0 case.

double-spike channels does not improve if d is increased beyond $\frac{1}{3}$ (the performance in the graph is shown for d=0.5).

5.5 Conclusion

This chapter has presented performance results for an optimum (MMSE) linear diversity receiver operating in a digital cellular radio environment with and without dominant co-channel interference.

The results show that by employing space diversity, the performance of the relatively low-complexity optimum linear receiver is very close to that of the high-complexity best-possible (maximum likelihood) receiver with the same number of diversity branches, in combating fading and intersymbol interference. The optimum linear diversity receiver also offers substantial gains in combating dominant CCI as opposed to noise-like CCI.

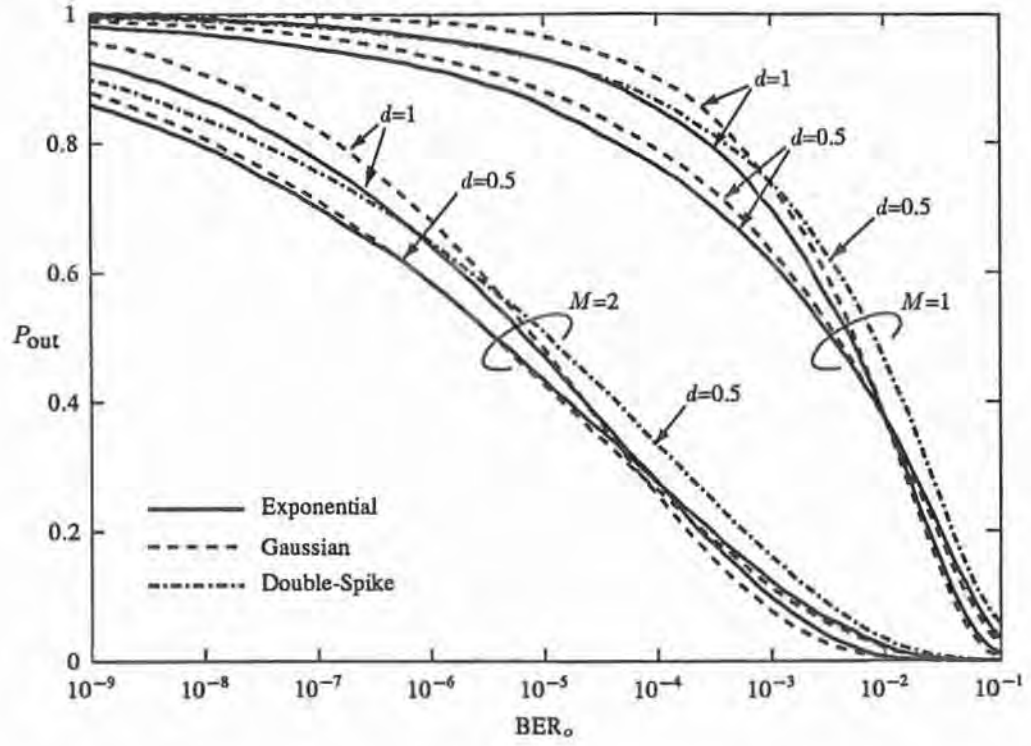

(a) BER distribution (SIR=10 dB).

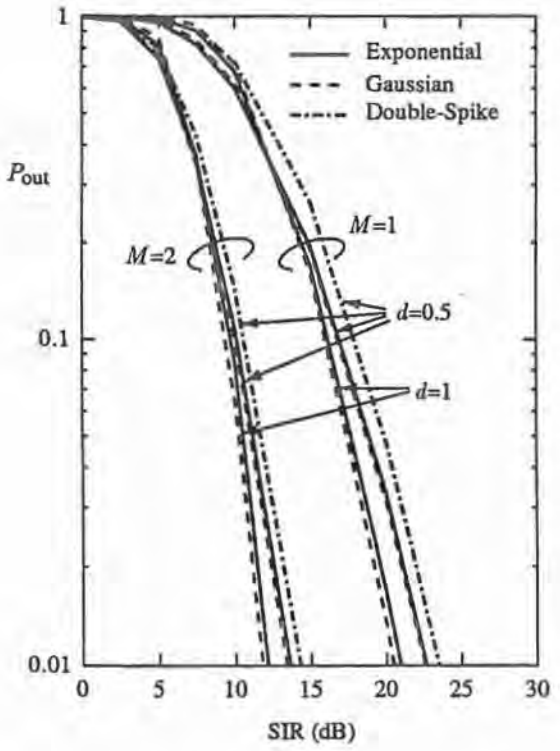

(b) Outage probability ($BER_o=10^{-3}$).

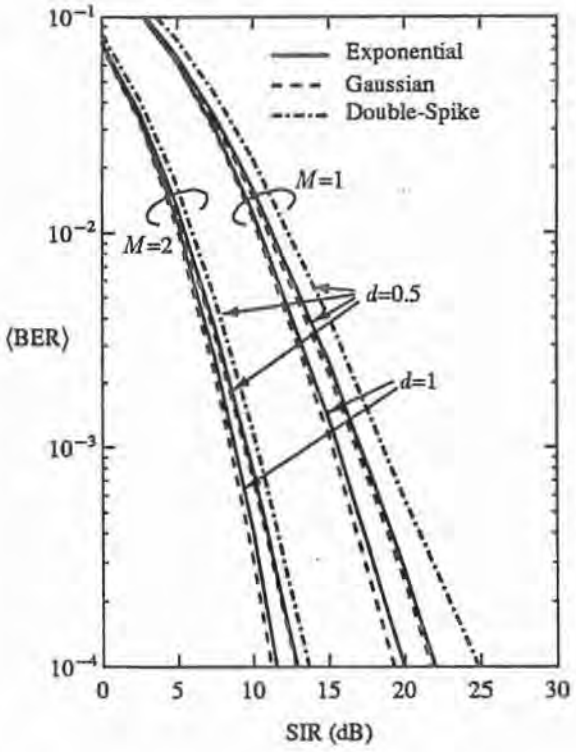

(c) Average BER.

Figure 5.9 Performance of optimum (MMSE) linear receiver. Influence of delay spectrum shape. Results for QPSK, B=1.5, and N=0.

Chapter 6

MEMORYLESS LINEAR COMBINING AND POST-COMBINER EQUALIZATION

In *memoryless linear combining*, the processing in each diversity branch consists of a single complex baseband weight. The main advantage with such a simple combiner structure is that it puts less demand on branch-weight adaptation algorithms than that of a diversity combiner with tapped delay lines in each branch. That is, because the weights must be updated before the channel responses change appreciably, and a greater number of adjustable weights generally requires more computation time, there is a practical limit on the number of weights that can be handled by the adaptive algorithm. A memoryless combiner has the minimum number of weights, M, in an M-branch receiver; it is a receiver implementation that puts the least demand on adaptive algorithms. Furthermore, if a receiver employs *post-combiner equalization* and the tap-weights of the diversity combiner and equalizer are jointly adapted by a single algorithm, it may be better to assign more weights from the available total to the equalizer rather than the combiner (more on this in Chapter 7). The memoryless combiner brings about the most extreme allocation of these weights.

In systems employing narrowband transmission (i.e., systems with flat multipath fading) and not having CCI (i.e., only noise), it is well known that *maximal ratio combining* is optimum [Brennan, 1959; Jakes, 1974, ch. 5]. Provided that the number of diversity branches is large, maximal ratio combining (without post-combiner equalization) can also put up a good defence against frequency-selective fading and CCI [Glance and Greenstein, 1983]. There is, however, a memoryless combining scheme better suited to mitigating these impairments: Bogachev and Kisalev [1980] and Winters [1984] showed that *MMSE combining* is effective in mobile radio environments with flat fading and dominant CCI; Greenstein and Yeh [1985] showed that the same combining scheme with just two diversity branches is effective, even without post-combiner equalization, at combating ISI in point-to-point microwave links (with frequency-selective fading). This chapter presents an original study of stand-alone MMSE combining (i.e., MMSE combining without post-combiner equalization) operating in the digital cellular system described in Chapter 2: a system with frequency-selective fading *and* dominant CCI.

In addition to stand-alone memoryless combining, this chapter studies memoryless combining with post-combiner equalization. Such equalization allows the combiner to devote most of its effort to combating multipath fading and dominant CCI, leaving ISI to the equalizer. In implementing the receiver, the combiner and equalizer would be either separately or jointly optimized, the latter of which is better and of more interest.

This chapter considers the following two receivers with post-combiner equalization: (i) jointly optimized combiner and *ideal* equalizer (i.e., optimum filtering and ideal ISI cancellation); and (ii) jointly optimized combiner and infinite-length *linear* equalizer. Unfortunately, it is unclear how to perform analytically either of these two joint optimizations, except in one case: in the first receiver

operating in an environment *without* dominant CCI, *maximal power combining* [Greenstein and Yeh, 1985] is optimum, and the receiver's performance is specified by the *post-combiner matched filter bound* (see Sections 6.2.2.1 and 6.2.2.2). In other cases, however, there are useful lower bounds on the BER performance. In the second receiver operating in an environment without dominant CCI, for instance, it is expected that maximal power combining is *near-optimum* (see Section 6.2.2.3): the optimum receiver's BER performance is thus lower bounded by analysing maximal power combining with MMSE post-combiner equalization. And the dominant CCI gains (performance gain with reference to the N=0 case, as defined in Section 5.4.3) of the first receiver can be lower bounded via analysis of a sub-optimum receiver with MMSE combining, fixed filtering, and ideal ISI cancellation (see Section 6.2.3). Finally, the dominant CCI gains of the second receiver are expected to be approximately the same as those of the first receiver (see Section 6.2.3).

In summary, this chapter studies the following five memoryless combining receivers:

I. Maximal ratio combining (without post-combiner equalization, but with fixed filtering).

II. MMSE combining (without post-combiner equalization, but with fixed filtering).

III. Maximal power combining with ideal post-combiner equalization (post-combiner matched filter bound).

IV. Maximal power combining with optimum (MMSE) linear post-combiner equalization.

V. MMSE combining with fixed filtering and ideal post-combiner ISI cancellation.

Receivers I and II (stand-alone combiners) are described and analysed in Section 6.1, and receivers III, IV, and V (combiners with post-combiner equalization) in Section 6.2. Receivers I, II, and V are treated in cases *with or without* dominant CCI, but as discussed above, receivers III and IV are treated in only cases *without* dominant CCI. Section 6.3 presents numerical results for all five memoryless combining receivers.

6.1 Stand-Alone Combining

6.1.1 System Description

The structure of the diversity receiver with stand-alone memoryless combining is shown in Figure 6.1, where $\{w_m^*\}$ is a set of branch-weights (the conjugates being used to simplify the following analyses). Because there is no filtering after the combiner, the fixed transmit and receive filters, and the timing epoch t_s, need to be specified. In the numerical results, the following pulse shaping and timing recovery are assumed:

- **Pulse Shaping:** Root cosine rolloff shaping is assumed for the transmit and receive filters [Wong and Greenstein, 1984], i.e., $C_T(f) = T\sqrt{C(f)}$ and $C_R(f) = \sqrt{C(f)}$ where

$$C(f) = \begin{cases} 1, & |f| < (1-\alpha)/(2T) \\ \frac{1}{2}\left[1 + \cos(\frac{\pi}{\alpha}(|fT| - (1-\alpha)/2))\right], & (1-\alpha)/(2T) \le |f| \le W/2 \\ 0, & |f| > W/2 \end{cases} \quad (6.1)$$

  is a raised cosine frequency response with a rolloff factor $\alpha = B - 1$ that lies between 0 and 1.

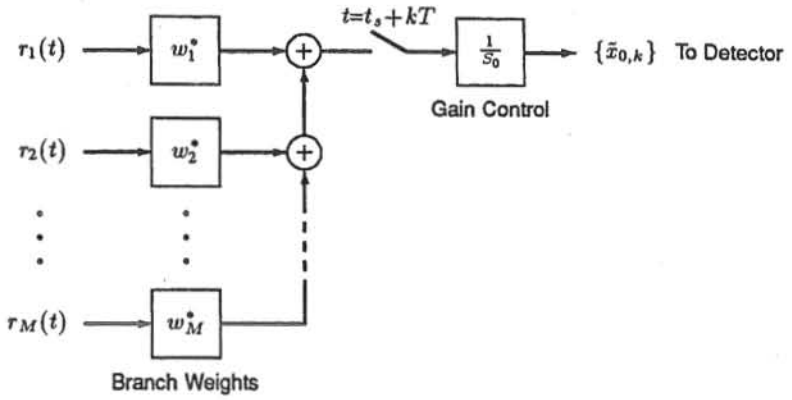

Figure 6.1 Receiver with stand-alone memoryless combining.

- **Timing Recovery:** The method for timing recovery described by Amitay and Greenstein [1984], where the timing loop bandwidth is assumed to be much greater than the fading rate, is adopted here. The timing epoch is derived as

$$t_s = \frac{T}{2\pi}\text{phase}\left[\sum_n S_n^2 \int_{-\infty}^{\infty} \mathbf{Q}_n^H(f)\mathbf{Q}_n(f-1/T)\,df\right] + k_s T \tag{6.2}$$

where $\mathbf{Q}_n(f)$ is defined in (2.23) and k_s is some integer (optimized numerically to minimize BER). This approach represents a practical timing recovery technique, although timing jitter and other perturbations associated with data randomness and noise-like CCI are ignored.

6.1.2 Analysis

Assume for the moment that the branch-weights $\{w_m^*\}$ have been set. The periodic frequency response between the nth source and the combiner output is

$$\tilde{G}_n(f) = \mathbf{w}^H \tilde{\mathbf{Q}}_n(f) \tag{6.3}$$

where

$$\mathbf{w} \triangleq \begin{bmatrix} w_1 \\ w_2 \\ \vdots \\ w_M \end{bmatrix} \tag{6.4}$$

and

$$\tilde{\mathbf{Q}}_n(f) \triangleq \frac{1}{T}\sum_i \mathbf{Q}_n(f - i/T)\exp\left(-\jmath 2\pi i t_s/T\right) \tag{6.5}$$

Specifically, $g_{0,0} = \mathbf{w}^H \mathbf{q}_0$ where

$$\mathbf{q}_0 \triangleq T\int_{-1/2T}^{1/2T} \tilde{\mathbf{Q}}_0(f)\exp\left(\jmath 2\pi f t_s\right) df \tag{6.6}$$

The mean-square value of the gaussian noise samples at the combiner output is

$$E\left[|\eta_k|^2\right] = \int_{-\infty}^{\infty} \mathcal{N}_L(f)\,df = K_\eta^2\,\mathbf{w}^H\mathbf{w} \tag{6.7}$$

where $K_\eta^2 \triangleq \int_{-\infty}^{\infty} \mathcal{N}_R(f)\,df$ (for noise-like CCI and cosine rolloff pulse shaping, $K_\eta^2 = S_0^2\sigma_x^2(1 - \alpha/4)/\mathrm{SIR}_w$).

Given the optimized $\mathbf{w}$ (e.g., one of those in Sections 6.1.3 and 6.1.4), $\{\tilde{G}_n(f)\}$ and $E\left[|\eta_k|^2\right]$ can be computed via (6.3) and (6.7). It is then straightforward, using the techniques described in Section 3.4, to compute the bit-error-rate.

6.1.3 Maximal Ratio Combining (Receiver I)

As already mentioned, maximal ratio combining is optimum in systems with no dominant CCI or ISI (i.e., designed for flat fading and additive gaussian noise) because it maximizes the signal-to-noise ratio at the combiner output [Jakes, 1974, ch. 5]. This optimization is achieved by choosing the branch-weight vector as

$$\mathbf{w} = \mathbf{q}_0 \tag{6.8}$$

which has the effect of co-phasing the desired signals from each branch (i.e., so that $g_{0,0} = |\mathbf{q}_0|^2$), and weighting more heavily those branches that have a high $|q_{m,0}(t_s)|^2$. Noise from each branch will add with random phase, thus suppressing it relative to the desired signal. Maximal ratio combining is also effective at combating ISI and dominant CCI because interference from each branch tends to add with random phase (as with noise), thus increasing the signal-to-ISI-plus-CCI ratio at the combiner output.

6.1.4 MMSE Combining (Receiver II)

MMSE combining is suitable in systems with both ISI and dominant CCI, to minimize the mean-square symbol error at the combiner output. The mean-square error is $\epsilon = \epsilon_{\mathrm{ISI}} + \epsilon_{\mathrm{CCI}} + \epsilon_{\mathrm{Noise}}$, where

$$\epsilon_{\mathrm{ISI}} = \sigma_x^2 T \int_{-1/2T}^{1/2T} |\mathbf{w}^H \tilde{\mathbf{Q}}_0(f) - \exp(-j2\pi f t_s)|^2\,df \tag{6.9}$$

$$\epsilon_{\mathrm{CCI}} = \sigma_x^2 \sum_{n=1}^{N} \left(\frac{S_n}{S_0}\right)^2 T \int_{-1/2T}^{1/2T} |\mathbf{w}^H \tilde{\mathbf{Q}}_n(f)|^2\,df \tag{6.10}$$

and

$$\epsilon_{\mathrm{Noise}} = \frac{K_\eta^2}{S_0^2}\mathbf{w}^H\mathbf{w} \tag{6.11}$$

The mean-square error can be rewritten as

$$\epsilon = \sigma_x^2(\mathbf{w}^H\mathbf{A}\mathbf{w} - \mathbf{w}^H\mathbf{q}_0 - \mathbf{q}_0^H\mathbf{w} + 1) \tag{6.12}$$

where

$$\mathbf{A} = \sum_{n=0}^{N} \left(\frac{S_n}{S_0}\right)^2 T \int_{-1/2T}^{1/2T} \tilde{\mathbf{Q}}_n(f)\,\tilde{\mathbf{Q}}_n^H(f)\,df + \mathcal{N}_0\,\mathbf{I} \tag{6.13}$$

$\mathbf{I}$ is an $M \times M$ identity matrix, and $\mathcal{N}_0 = K_\eta^2/(S_0^2\sigma_x^2)$ (for noise-like CCI and raised cosine pulse shaping, $\mathcal{N}_0 = (1 - \alpha/4)/\mathrm{SIR}_w$). We obtain the minimum mean-square error when

$$\frac{\partial\epsilon}{\partial\mathbf{w}} = \sigma_x^2(2\mathbf{A}\mathbf{w} - 2\mathbf{q}_0) = \mathbf{0} \tag{6.14}$$

That is, the MMSE solution for the branch-weight vector is

$$\mathbf{w} = \mathbf{A}^{-1}\mathbf{q}_0 \tag{6.15}$$

and the minimum mean-square error is $\epsilon_{\min} = \sigma_x^2(1 - \mathbf{q}_0^H\mathbf{A}^{-1}\mathbf{q}_0)$.

6.2 Post-Combiner Equalization

6.2.1 System Description

Figure 6.2 shows a receiver with memoryless combining and post-combiner equalization, where $\{w_m^*\}$ is a set of branch weights as described in Section 6.1.1.

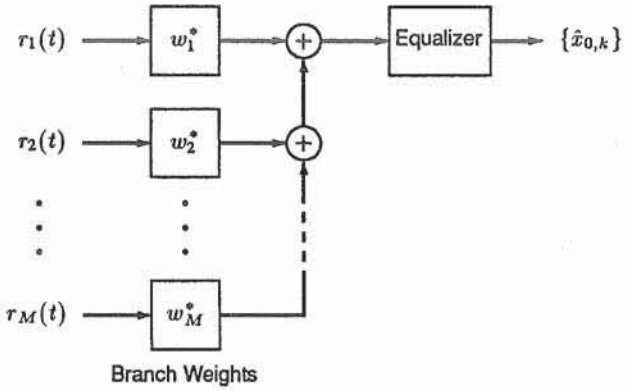

Figure 6.2 Receiver with memoryless combining and post-combiner equalization.

The *combined system* is illustrated in Figure 6.3, where $q_{cn}(t) = \sum_m w_m^* q_{m,n}(t)$ is the combined link impulse response for the nth source; $r_c(t) = s_c(t) + \eta_c(t)$ is the combined received signal; $s_c(t) = \sum_n S_n \sum_k x_{n,k}\, \theta_{n,k}\, q_{cn}(t - kT)$ is the combined sum of co-channel signals; and $\eta_c(t) = \sum_m w_m^* \eta_m(t)$ is the combined gaussian noise (which includes noise-like CCI). The

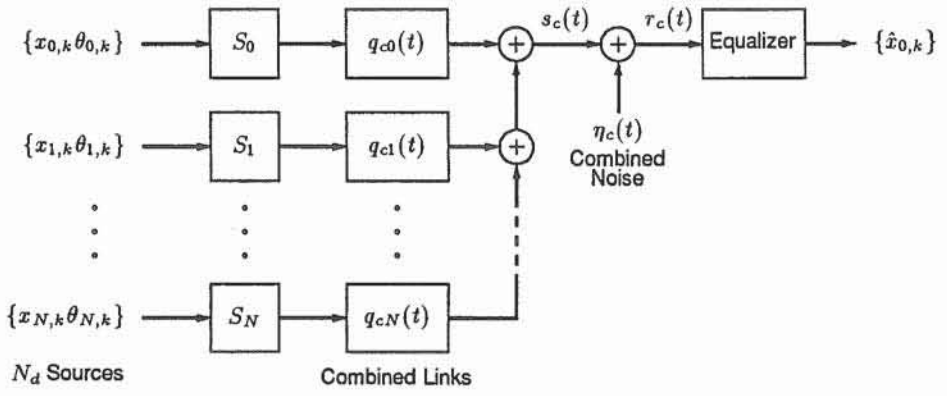

Figure 6.3 Combined system.

combined link frequency response for the nth source (excluding the signal gain factor S_n) is

$$Q_{cn}(f) = \mathcal{F}\left[q_{cn}(t)\right] = \mathbf{w}^H \mathbf{Q}_n(f) \tag{6.16}$$

where $\mathbf{w}$ is the branch-weight vector defined in (6.4) and $\mathbf{Q}_n(f)$ is the link response vector defined in (2.23). The power spectrum of the combined noise $\eta_c(t)$ is

$$\mathcal{N}_c(f) = \mathcal{N}_R(f)\, \mathbf{w}^H \mathbf{w} \tag{6.17}$$

where $\mathcal{N}_R(f)$ is the noise power spectrum in each diversity branch.

6.2.2 System Without Dominant CCI (Receivers III and IV)

6.2.2.1 Maximal Power Combining

In the case without dominant CCI, the combined noiseless signal is $s_c(t) = S_0 \sum_k x_{0,k}\, \theta_{0,k}\, q_{c0}(t - kT)$. Using standard techniques [Lucky *et al.*, 1968], it is easily shown that the average power of $s_c(t)$ is

$$\begin{aligned} P_s &= \frac{S_0^2\, \sigma_x^2}{T} \int_{-W/2+\Delta_0}^{W/2+\Delta_0} |Q_{c0}(f)|^2\, df \\ &= \frac{S_0^2\, \sigma_x^2}{T} \mathbf{w}^H \int_{-W/2+\Delta_0}^{W/2+\Delta_0} \mathbf{Q}_0(f)\, \mathbf{Q}_0^H(f)\, df\, \mathbf{w} \end{aligned} \tag{6.18}$$

where the average is taken over the random data from the desired source. Substituting (2.23) into (6.18), and using the orthonormality of the eigenvectors (in (2.22)), we get

$$P_s = \frac{S_0^2\, \sigma_x^2\, W}{T} \mathbf{w}^H\, \mathbf{c}_0\, \mathbf{\Lambda}_0\, \mathbf{c}_0^H\, \mathbf{w} \tag{6.19}$$

The average power of the combined noise $\eta_c(t)$ is

$$P_\eta = \mathbf{w}^H \mathbf{w} \int_{-\infty}^{\infty} \mathcal{N}_R(f)\, df \tag{6.20}$$

In maximal power combining, the power ratio P_s/P_η is maximized, which is equivalent to maximizing

$$z \triangleq \frac{\mathbf{w}^H\, \mathbf{c}_0\, \mathbf{\Lambda}_0\, \mathbf{c}_0^H\, \mathbf{w}}{\mathbf{w}^H\, \mathbf{w}} \tag{6.21}$$

From quadratic form theory [Noble and Daniel, 1988], the branch-weight vector that maximizes z, and hence maximizes the power ratio P_s/P_η at the combiner output, is

$$\mathbf{w} = \text{eigenvector associated with largest eigenvalue of } \mathbf{c}_0 \mathbf{\Lambda}_0 \mathbf{c}_0^H \tag{6.22}$$

6.2.2.2 Ideal Equalization — The Post-Combiner Matched Filter Bound (Receiver III)

The post-combiner matched filter bound specifies the performance of the ideal post-combiner equalizer (see Chapter 4 for a full discussion on the matched filter bound). It is computed assuming an isolated data symbol and ideal matched filter detection, as illustrated in Figure 6.4 where $p_c(t) = q_{c0}^*(t_d - t)$ is the impulse response of the post-combiner matched filter. The frequency response of this filter is

$$P_c(f) = Q_{c0}^*(f) \exp(-j2\pi f t_d) = \left[\mathbf{Q}_0^H(f)\, \mathbf{w}\right] \exp(-j2\pi f t_d) \tag{6.23}$$

Recall that in matched filter reception the fixed receive filter $c_R(t)$, which is included in $q_{c0}(t)$, is taken to be a whitening filter, such that the noise power spectrum in each branch is $\mathcal{N}_R(f)=\mathcal{N}_r$ (for noise-like CCI, $\mathcal{N}_r=\mathcal{N}_w$).

Following the same type of analysis as the one in Section 4.2, we have $\tilde{x}_{0,0} = g_{0,0} x_{0,0} + \eta_0/S_0$, where

$$\begin{aligned} g_{0,0} &= \int_{-W/2}^{W/2} Q_{c0}(f)\, P_c(f) \exp(j2\pi f t_d)\, df \\ &= \mathbf{w}^H \left[\int_{-W/2}^{W/2} \mathbf{Q}_0(f)\, \mathbf{Q}_0^H(f)\, df \right] \mathbf{w} \end{aligned} \tag{6.24}$$

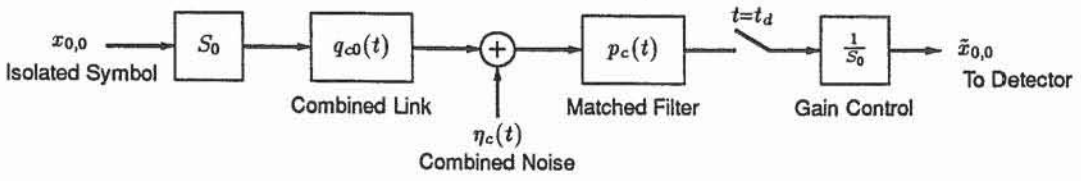

Figure 6.4 System for computing the matched filter bound on post-combiner equalizer performance.

and

$$E[|\eta_0|^2] = \int_{-W/2}^{W/2} \mathcal{N}_c(f)|P_c(f)|^2\, df = \mathcal{N}_r\, g_{0,0}\, \mathbf{w}^H\mathbf{w} \tag{6.25}$$

From (3.19) and (3.23), the bit-error-rate is given by

$$\text{BER} = \frac{L-1}{L}\text{erfc}\left[\sqrt{\mathcal{E}z}\right] \tag{6.26}$$

where $\mathcal{E} \triangleq S_0^2 W/\mathcal{N}_r$ (for noise-like CCI, $\mathcal{N}_r = \mathcal{N}_w \Rightarrow \mathcal{E} = B\,\text{SIR}/\sigma_x^2$) and, noting that $P_s{=}S_0^2\sigma_x^2 g_{0,0}/T$, z is the one defined in (6.21). Because maximizing z is equivalent to minimizing the BER in (6.26), maximal power combining is optimum if ideal post-combiner equalization is employed. The minimum BER is equal to $(L-1)/L\,\text{erfc}\left[\sqrt{\mathcal{E}z_{\max}}\right]$, where $z_{\max}$ is equal to the largest eigenvalue of $\mathbf{c}_0\mathbf{\Lambda}_0\mathbf{c}_0^H$.

6.2.2.3 Optimum Linear Equalization (Receiver IV)

Figure 6.5 shows the system with optimum linear post-combiner equalization, where $\tilde{v}_c(t)$ is the impulse response of an infinite-length transversal filter. (The structure is derived using the well known optimum receiver principles outlined in Chapters 4 and 5. Recall that the fixed receive filter $c_R(t)$ is taken to be a whitening filter, as in Section 6.2.2.2.) Following the same type of

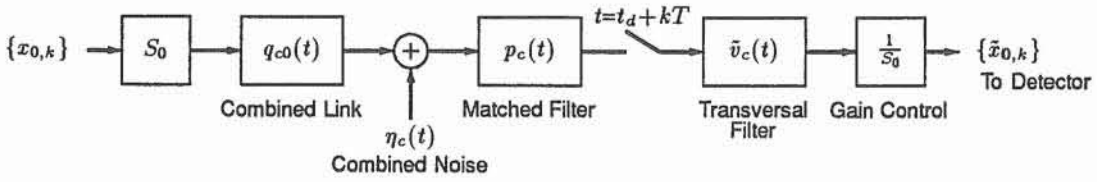

Figure 6.5 System with optimum linear post-combiner equalization.

analysis as the one in Section 5.2, the equivalent discrete system is characterized by

$$\tilde{G}_0(f) = \frac{1}{T}\tilde{V}_c^*(f)\,\mathbf{w}^H\,\mathbf{X}_0(f)\,\mathbf{w}\,\exp\left(-j2\pi f t_d\right) \tag{6.27}$$

and

$$\tilde{\mathcal{N}}_L(f) = \frac{\mathcal{N}_r\,\mathbf{w}^H\mathbf{w}}{T^2}\,|\tilde{V}_c^*(f)|^2\,\mathbf{w}^H\,\mathbf{X}_0(f)\mathbf{w} \tag{6.28}$$

where

$$\mathbf{X}_0(f) \triangleq \sum_i \mathbf{Q}_0(f - i/T)\,\mathbf{Q}_0^H(f - i/T) \tag{6.29}$$

and $\tilde{V}_c^*(f)$ is the periodic frequency response of the transversal filter (which, for simplicity, is taken to be non-causal).

Following the same type of optimization as the one in Section 5.3 (in the case of single-source transmission), the MMSE solution for the transversal filter response is

$$\frac{1}{T}\tilde{V}_c(f) = \frac{1}{\mathbf{w}^H(\mathbf{X}_0(f) + \mathcal{N}_0\mathbf{I})\,\mathbf{w}} \tag{6.30}$$

where $\mathbf{I}$ is an $M \times M$ identity matrix, and $\mathcal{N}_0 \triangleq \mathcal{N}_r T/(S_0^2\,\sigma_x^2)$ (for noise-like CCI, $\mathcal{N}_0 = 1/\mathrm{SIR}_w$). Thus, we get

$$\tilde{G}_0(f) = \frac{\mathbf{w}^H\mathbf{X}_0(f)\,\mathbf{w}}{\mathbf{w}^H(\mathbf{X}_0(f) + \mathcal{N}_0\mathbf{I})\,\mathbf{w}} \exp(-\jmath 2\pi f t_d) \tag{6.31}$$

and

$$\tilde{\mathcal{N}}_L(f) = \mathcal{N}_r\,\mathbf{w}^H\mathbf{w}\frac{\mathbf{w}^H\mathbf{X}_0(f)\,\mathbf{w}}{|\mathbf{w}^H(\mathbf{X}_0(f) + \mathcal{N}_0\mathbf{I})\,\mathbf{w}|^2} \tag{6.32}$$

It is now straightforward, using the techniques described in Section 3.4, to compute the bit-error-rate.

The minimum MSE is

$$\epsilon_{\min} = \sigma_x^2 T \int_{-1/2T}^{1/2T} \frac{\mathcal{N}_0\,\mathbf{w}^H\mathbf{w}}{\mathbf{w}^H(\mathbf{X}_0(f) + \mathcal{N}_0\mathbf{I})\,\mathbf{w}}\,df \tag{6.33}$$

It is not clear how to minimize $\epsilon_{\min}$ with respect to $\mathbf{w}$, i.e., how to jointly optimize the memoryless combiner and post-combiner equalizer in the MMSE sense. To obtain numerical results, therefore, maximal power combining is assumed. This combining scheme should be close to optimum because it produces a signal that is unlikely to be significantly faded at any frequency over the signal band. The post-combiner equalizer can thus combat ISI without significant noise enhancement.

6.2.3 System With Dominant CCI (Receiver V)

A memoryless combiner can improve receiver performance by exploiting the short-term branch-to-branch correlation (i.e., taken over the data, but not the fading) of dominant CCI. This means that if optimum combining and ideal post-combiner equalization (i.e., combining and post-combiner filtering jointly optimized in the minimum BER sense, and total post-combiner ISI cancellation) were employed in systems with dominant CCI (N>0), the receiver's performance would be *better* than the matched filter bound derived in Section 6.2.2.2 (which is for the N=0 case). Because it is the combiner, rather than the equalizer, that combats dominant CCI, similar dominant CCI gains would be observed in the case of linear post-combiner equalization. Exactly computing these potential performance gains, however, is not a straightforward task: in the dominant CCI case, it is unclear how to jointly optimize the combiner and the post-combiner filter. Fortunately, there is a simple method that can be used to tightly lower bound the dominant CCI gains.

Consider a receiver with the structure shown in Figure 6.1, but with all ISI somehow eliminated after the sampler so the combiner need deal with only dominant CCI and noise. This ideal ISI cancellation is equivalent to transmitting an isolated symbol $x_{0,0}$ from the desired source, as shown in the combined system illustrated in Figure 6.6. Note that the system is *not* optimum because the only filtering in the receiver, the receive filter $c_R(t)$, has a *fixed* response — the receiver's optimum filter is, of course, channel dependent. Nevertheless, combating dominant CCI is effected mainly by the memoryless diversity combiner, not the receiver filtering. If, therefore, the combiner is optimized to combat CCI and noise, the dominant CCI gain should tightly lower bound that of a receiver with jointly optimized combining and post-combiner filtering.

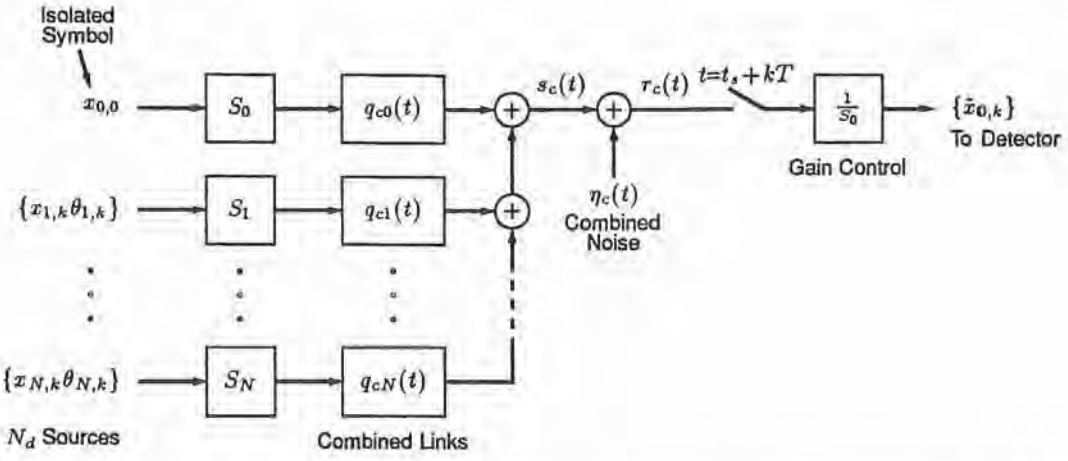

Figure 6.6 System for computing performance of memoryless combiner with ideal post-combiner ISI cancellation.

Assuming MMSE combining to perform the task of combating CCI and noise (and in the numerical results assuming root-cosine transmit and receive filtering), the BER performance of the system shown in Figure 6.6 is computed by simply replacing $\tilde{Q}_0(f)$ with $q_0 \exp(-j2\pi f t_s)$ in (6.9), (6.13), and (6.3). These substitutions have the desired effect of forcing all ISI to zero in the MMSE optimization (so the combiner deals with only dominant CCI and noise) and in the receiver's performance computation.

6.3 Numerical Results

6.3.1 General

Sections 6.1 and 6.2 describe methods with which one may analyse five memoryless combining receivers — listed at the beginning of this chapter (labelled I–V) — operating in a digital cellular radio environment with static multipath responses. Section 3.5 describes the simulation method for computing the BER performance over an ensemble of such multipath channels.

The following sections present numerical results showing the influence of various system and channel parameters on the performances of the five receivers. For receivers I, II, and V, results are shown in cases with and without dominant CCI; for receivers III and IV, results are shown for only the noise-like CCI case. The general approach to obtaining numerical results is, again, outlined in Section 3.6.

The following is a summary of the method for computing maximal ratio and MMSE combiner performance results (i.e., stand-alone combiners *without* post-combiner equalization; receivers I and II):

1. Specify parameters M, N, $P_h(\tau)$, and d (and number of Monte Carlo trials, N_T).
   Specify range of SIR values.
   Compute $\{S_n/S_0\}$, K_η^2, and $\mathcal{N}_0$ for each SIR value (Sections 6.1.1, 6.1.4, and 2.1.4).

2. Compute eigenvalues and eigenfunctions (Appendix 2A).
   Compute the matrix $\Lambda^{\frac{1}{2}}\phi(\beta)$ (Section 2.2).

3. Do the following steps N_T times:

   - Generate $\{c_n\}$ and $\{t_n/T\}$ (Section 2.2).

- Compute $\{\mathbf{Q}_n(f)\}$ via (2.23).
- Do the following steps for each SIR value[1]:
  - Compute t_s via (6.2).
  - Compute $\{\tilde{\mathbf{Q}}_n(f)\}$ via (6.5), and $\mathbf{q}_0$ via (6.6).
  - Compute maximal ratio branch-weight vector $\mathbf{w}$ via (6.8), and MMSE branch-weight vector $\mathbf{w}$ via (6.15).
  - For each combining scheme:
    * Compute $\{\tilde{G}_n(f)\}$ and $E\left[|\eta_k|^2\right]$ via (6.3) and (6.7).
    * Compute (and store) BER (Section 3.4).

4. For each combining scheme and each SIR value, compute P_{out} (for specified value or range of BER_o) and $\langle\text{BER}\rangle$ (Section 3.5).

To compute the performance of the MMSE combiner with ideal post-combiner ISI cancellation (receiver V), the above method is used and ISI is made zero by the condition outlined in Section 6.2.3. The key results obtained for this receiver are not so much the absolute performance figures, but the relative performance gains with reference to the noise-like CCI (N=0) case, i.e., the dominant CCI gains.

The following is a summary of the method for computing performance results of maximal power combining with ideal post-combiner equalization (post-combiner matched filter bound) and with optimum (MMSE) linear post-combiner equalization (i.e., receivers III and IV), in the noise-like CCI case (N=0):

1. Specify parameters M, $P_h(\tau)$, and d (and number of Monte Carlo trials, N_T).
   Specify range of SIR values.
   Compute $\mathcal{E}$, $\mathcal{N}_r$, and $\mathcal{N}_0$ for each SIR value (Sections 6.2.2 and 2.1.4).

2. Compute eigenvalues and eigenfunctions (Appendix 2A).
   Compute the matrices $\mathbf{\Lambda}_0$ and $\mathbf{\Lambda}^{\frac{1}{2}}\boldsymbol{\phi}(\beta)$ (Section 2.2).

3. Do the following steps N_T times:

   - Generate $\mathbf{c}_0$.
   - Compute $\mathbf{Q}_0(f)$ via (2.23), and $\mathbf{X}_0(f)$ via (6.29).
   - Compute maximal power branch-weight vector $\mathbf{w}$ via (6.22).
   - Do the following steps for each SIR value:
     - Compute $\tilde{G}_0(f)$ and $\tilde{\mathcal{N}}_L(f)$ via (6.31) and (6.32).
     - Compute (and store) post-combiner matched filter bound BER via (6.26).
     - Compute (and store) optimum linear equalizer BER (Section 6.2.2.3).

4. For each equalization scheme and each SIR value, compute P_{out} (for specified value or range of BER_o) and $\langle\text{BER}\rangle$ (Section 3.5).

[1] In fact, the steps are repeated a few times for each SIR value to search for a minimum BER over a range of k_s values.

6.3.2 Influence of BER Computation Scheme

It is of interest to compare the influence of the BER computation scheme on the performance results of memoryless combining receivers with that of the optimum linear receiver, particularly in the flat fading case (d=0) where it is expected that results of all receivers would be similar or identical. Figure 6.7 shows flat fading results for (i) a single-branch receiver without equalization (i.e., a memoryless attenuator and phase shifter) and one dominant co-channel interferer (M=N=1); and (ii) a two-branch stand-alone MMSE combiner and two dominant interferers (M=N=2). These results represent the most significant and interesting performance differences between the optimum linear receiver (see Figure 5.2) and all five memoryless combining receivers in the flat fading case. (Other flat fading results reveal an insignificant difference.)

The flat fading results computed using either Saltzberg's bound or the gaussian interference pdf approximation are better for the optimum linear receiver than those computed using the same method for the stand-alone memoryless combiner. The reason for this superior performance is quite simple. The optimum (MMSE) linear receiver always yields a mean-square error less than or equal to that of the stand-alone memoryless combiner: the optimum receiver can optimize its frequency response with complete freedom; the memoryless combiner can not. Because both the Saltzberg bound and the BER formula associated with the gaussian approximation are monotonically decreasing functions of the mean-square error, the optimum linear receiver always exhibits a superior performance (according to the two performance estimates). This is, however, not necessarily true when it comes to more accurate BER performance estimates, as shown by comparing Figures 5.2(a) and 6.7(a) for small values of BER_o. Nevertheless, in terms of both outage probability for $\mathrm{BER}_o=10^{-3}$ and average BER, the performance of the optimum linear receiver is approximately the same as or better than that of the stand-alone memoryless combiner over the important range of SIR values (compare Figures 5.2(b) and (c) with Figures 6.7(b) and (c)).

Although the gaussian approximation and Saltzberg bound are somewhat inaccurate, they make it easy to compute useful performance trends for the memoryless combining receivers in flat fading cases or in cases with gauss-like residual interference (for instance, in cases with post-combiner equalization and without dominant interference). They are not so useful in other cases. For example, Figure 6.8 shows results for four-branch diversity (M=4); stand-alone maximal ratio and MMSE combining (i.e., without post-combiner equalization); a double-spike delay spectrum with d=0.5; and purely noise-like CCI (N=0). It is clear from the results that after MMSE combining, the residual interference (ISI only, no dominant CCI) can be taken to be approximately gaussian distributed. But it is far from gaussian after maximal ratio combining. From a trial-by-trial examination in this simulation, it was found that the residual interference is generally composed of one or two dominant components, often making the interference pdf close to a double- or quadruple-spike. The gaussian approximation is thus very pessimistic, and the peak-limited gaussian approximation somewhat optimistic.

In the above example, and in other cases studied in the following sections, it would be very unfair to compare the performances of the MMSE and maximal ratio combiners by using Saltzberg's bound or the gaussian approximation — the results are heavily biased in favour of the MMSE combiner. For this reason and also for accuracy in the post-combiner equalization computations, *all* the following results are computed using Metzger's algorithm.

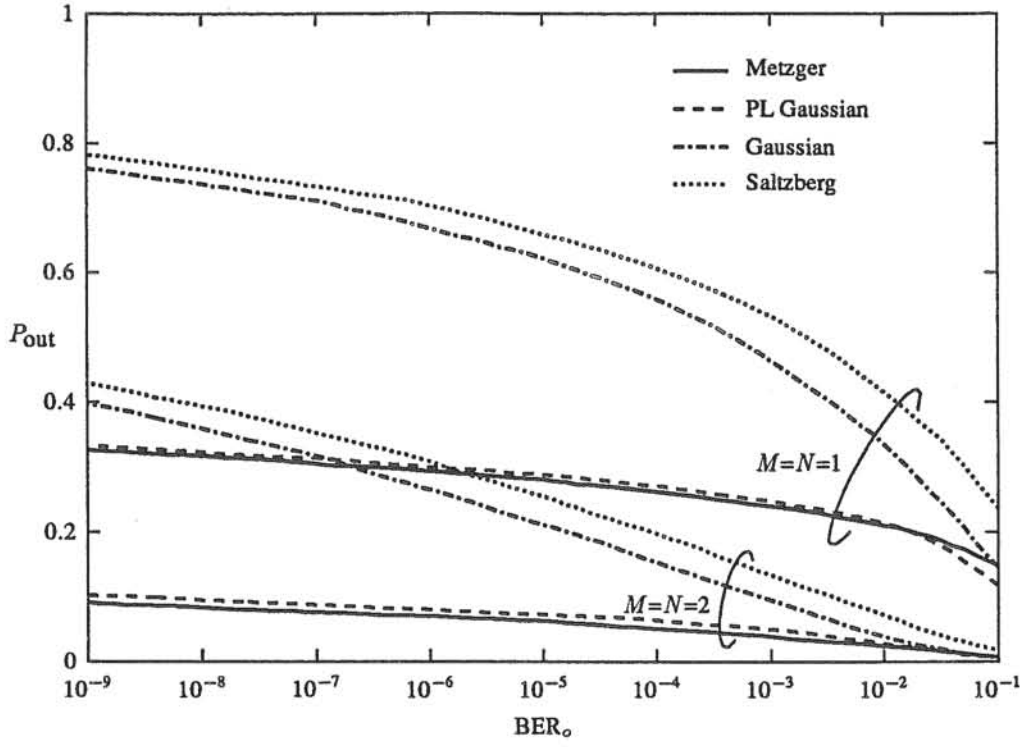

(a) BER distribution (SIR=10 dB).

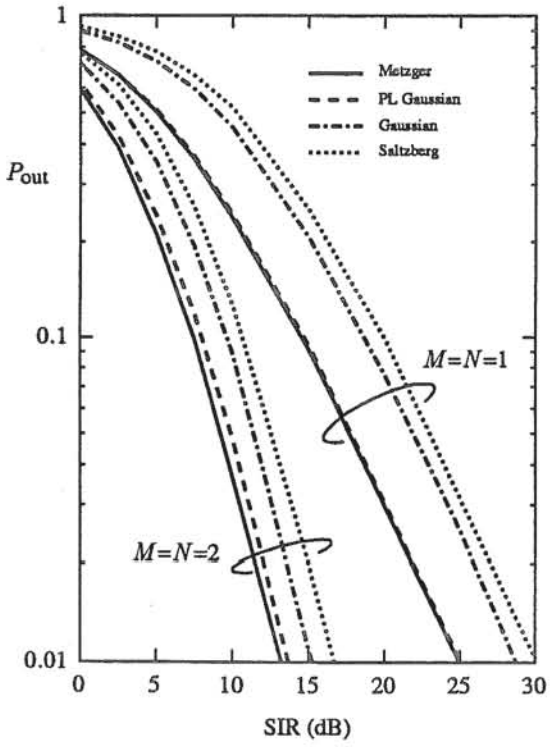

(b) Outage probability ($BER_o=10^{-3}$).

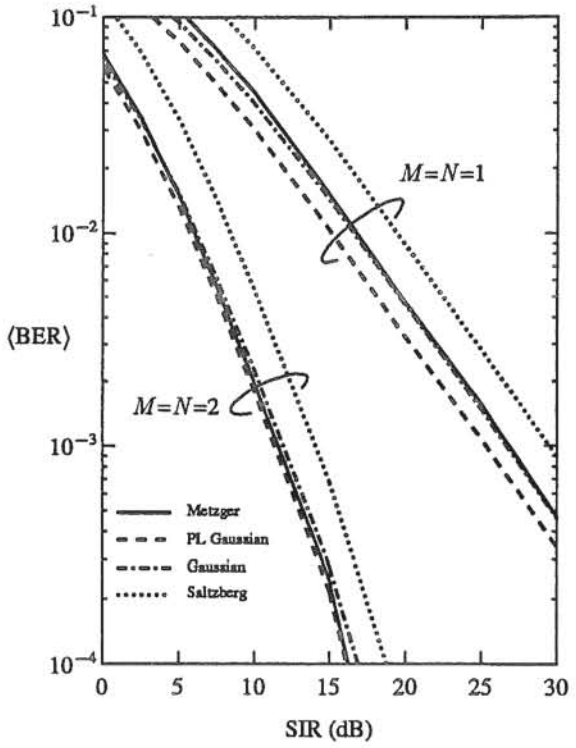

(c) Average BER.

Figure 6.7 Performance of stand-alone MMSE combining. Influence of BER computation method (PL ≡ Peak-Limited). Results for QPSK, B=1.5, d=0, and DWR=20 dB.

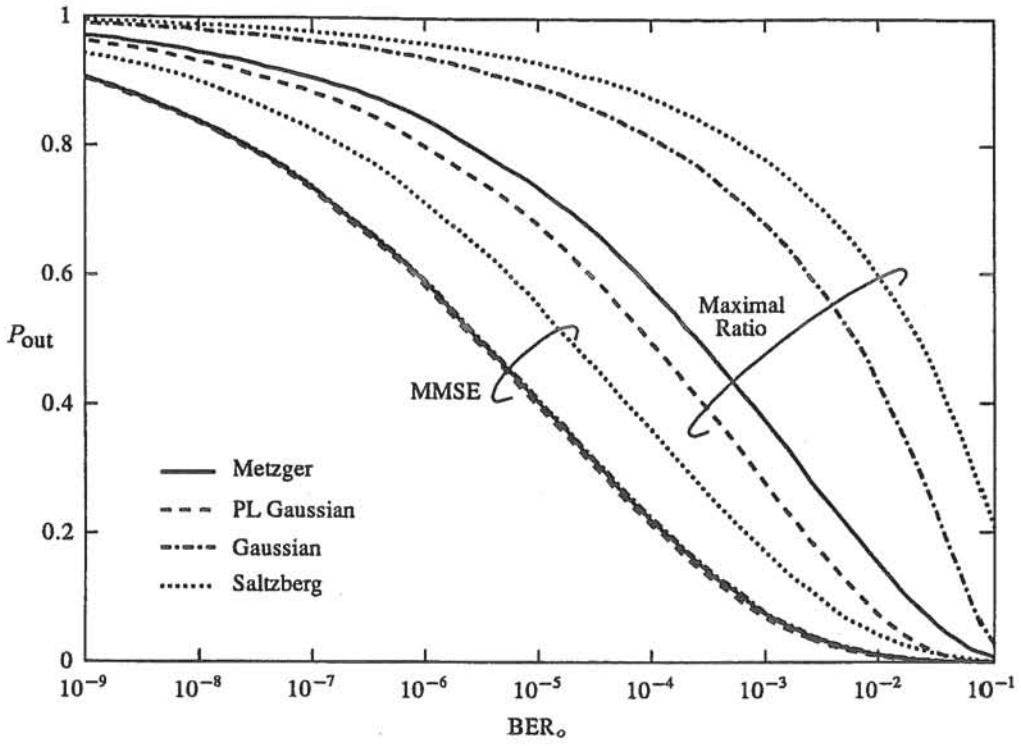

(a) BER distribution (SIR=10 dB).

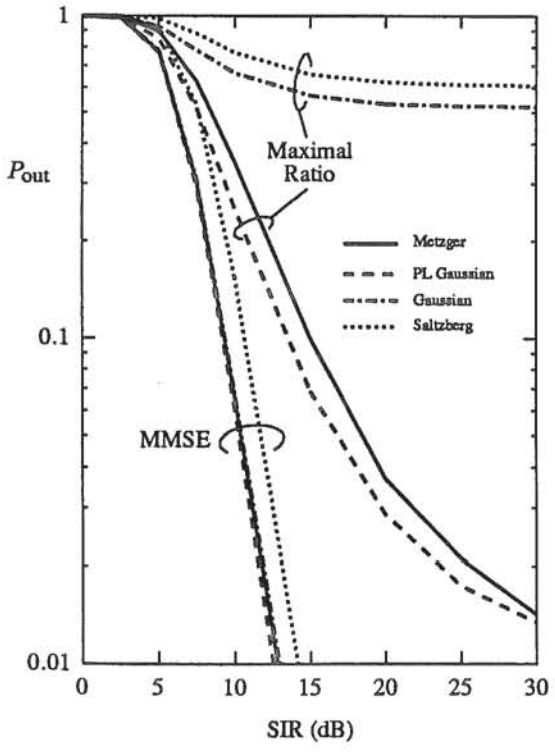

(b) Outage probability ($BER_o=10^{-3}$).

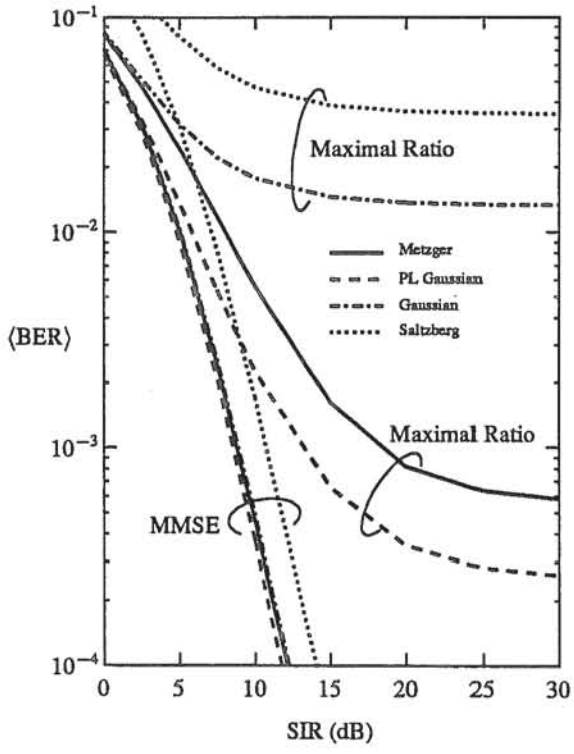

(c) Average BER.

Figure 6.8 Performance of stand-alone memoryless combining. Influence of BER computation method (PL ≡ Peak-Limited). Results for QPSK, B=1.5, M=4, N=0, $P_h(\tau)$=double-spike, and d=0.5.

6.3.3 Stand-Alone Combining (Receivers I and II)

6.3.3.1 Influence of Diversity Order, Dominant Interference, and Delay Spread

Figures 6.9 to 6.11 demonstrate how well M-branch MMSE combining works as an equalizer for frequency-selective fading channels with normalized delay spreads d=0.5 and d=1 (exponential delay spectrum). If space diversity is not used for these channels (M=1, not shown in the graphs although the simulations were performed), the BER is likely (greater than 50% probability) to be more than 10^{-1}, regardless of the signal-to-interference ratio. This high irreducible BER is due to the severe level of ISI caused by time dispersion. The flattening out of the performance curves in Figure 6.11 clearly illustrates the irreducible error rate phenomenon for the maximal ratio and MMSE diversity combiners.

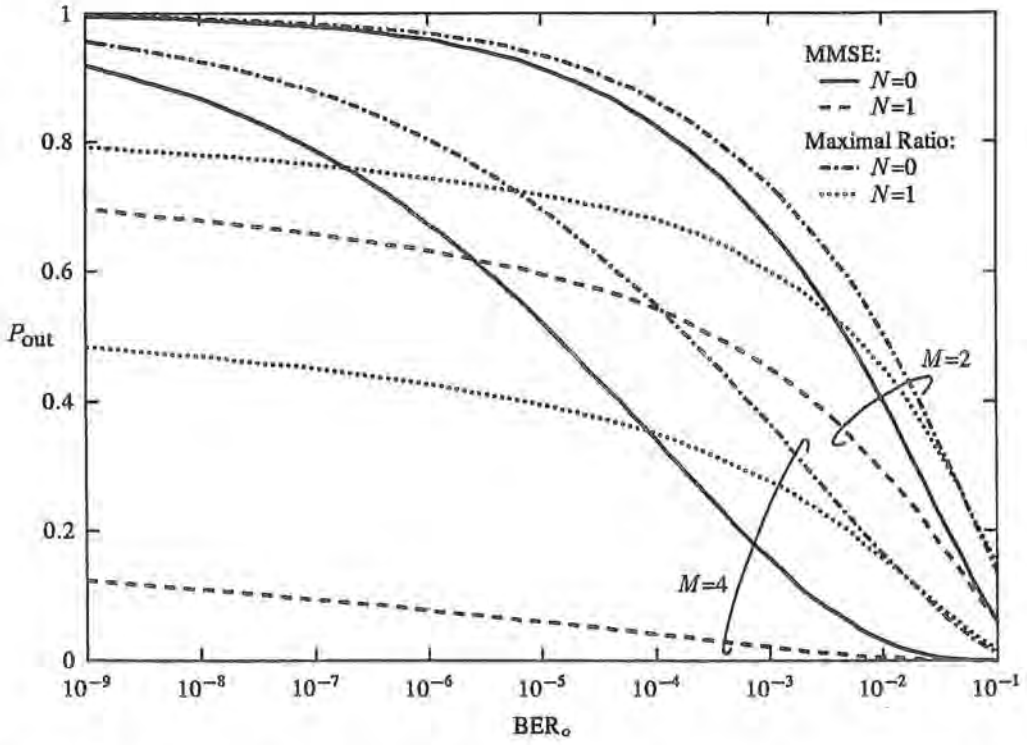

Figure 6.9 Performance of stand-alone memoryless combining. BER distribution (SIR=10 dB): Influence of diversity order and number of dominant interferers. Results for QPSK, B=1.5, $P_h(\tau)$=exponential, d=0.5, and DWR=20 dB.

The results show that four-branch MMSE combining is required in order to provide a good performance in these severely dispersive channels. Regarding an acceptable performance as $\langle \text{BER} \rangle = 10^{-3}$, the four-branch MMSE combiner can tolerate noise-like CCI with SIR$\approx$10 dB in the case d=0.5, and with SIR$\approx$16 dB in the case d=1.

In dispersive channels, stand-alone memoryless combiners show only a small advantage in dealing with dominant CCI as opposed to noise-like CCI (i.e., small dominant CCI gains). In the d=0.5 case, for example, even the four-branch MMSE combiner dealing with a single dominant interferer (N=1) offers only about 5 dB gain over the noise-like CCI case (N=0). Section 6.3.4.2 shows that this gain can be improved significantly if post-combiner equalization is employed.

(Note: flat fading results are not shown here because they are very similar to those of the

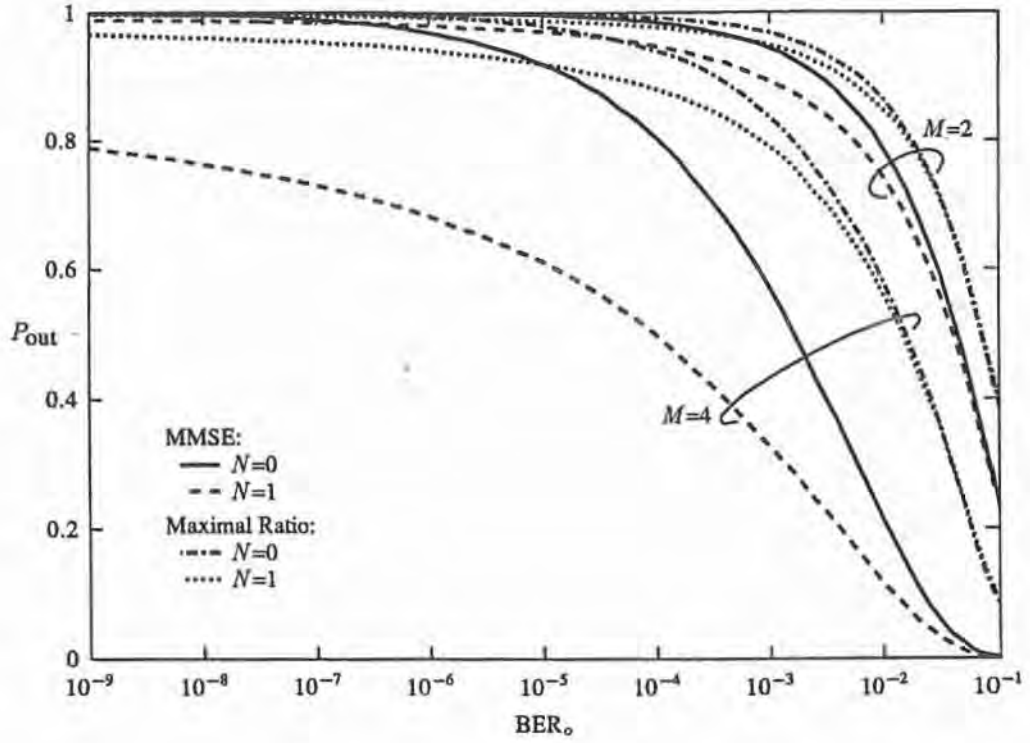

(a) SIR=10 dB.

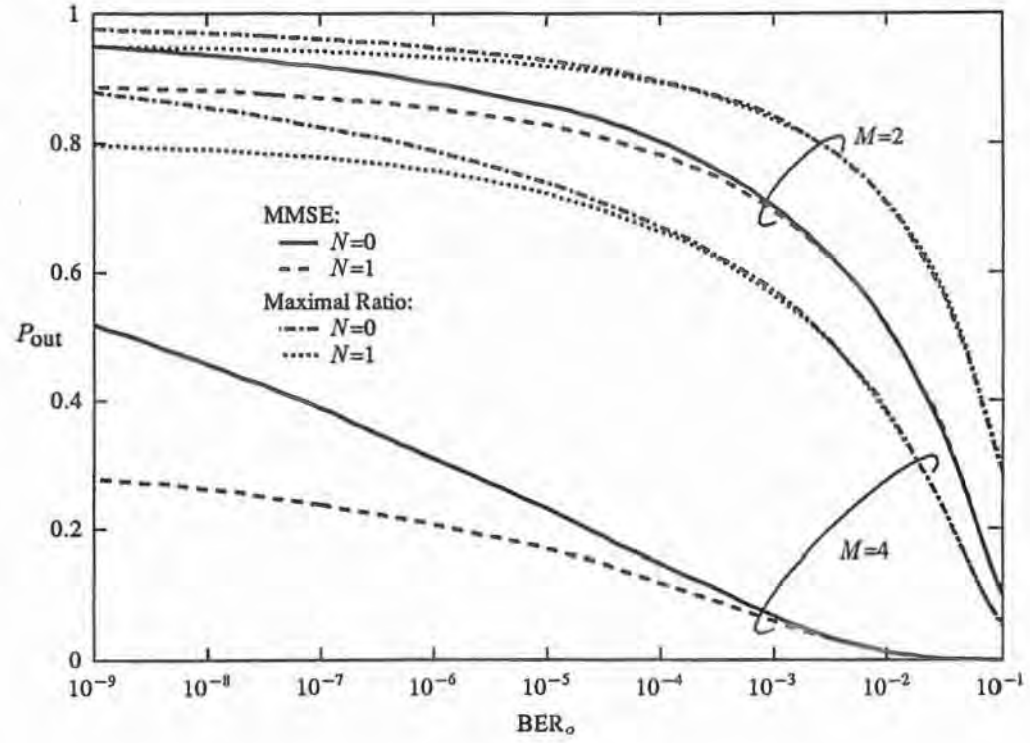

(b) SIR=20 dB.

Figure 6.10 Performance of stand-alone memoryless combining. BER distribution: Influence of diversity order and number of dominant interferers. Results for QPSK, B=1.5, $P_h(\tau)$=exponential, d=1, and DWR=20 dB.

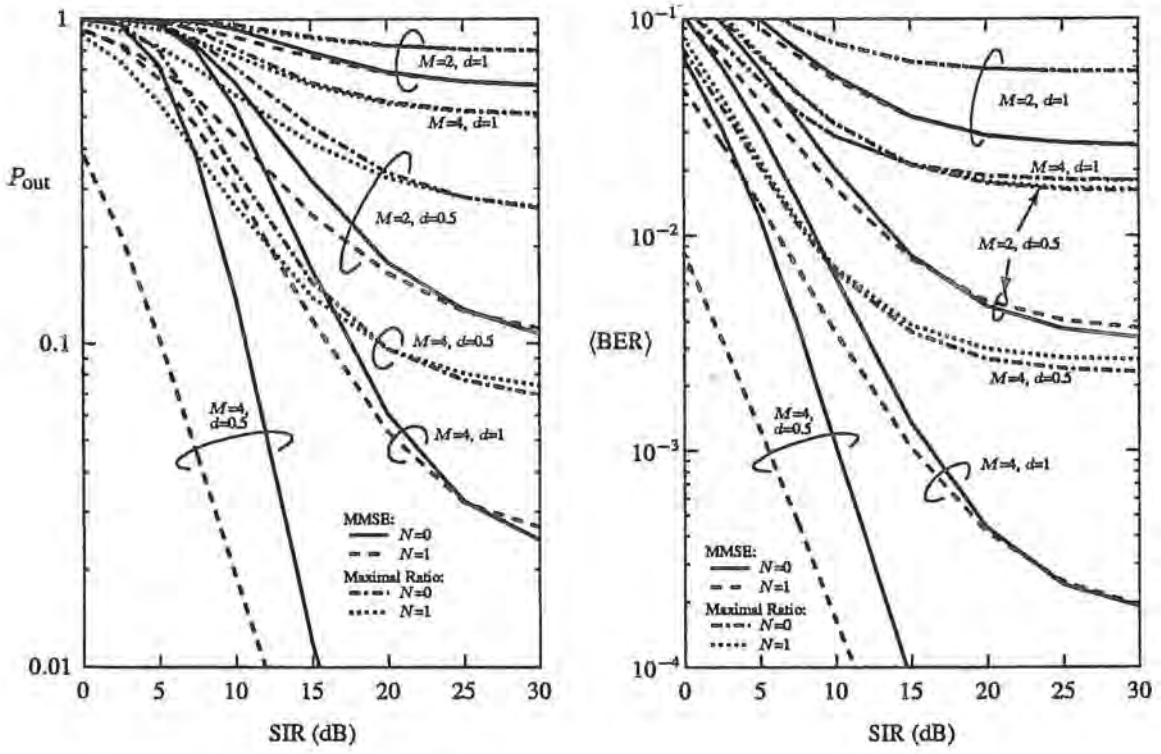

(a) Outage probability ($BER_o=10^{-3}$).

(b) Average BER.

Figure 6.11 Performance of stand-alone memoryless combining. Influence of diversity order, number of dominant interferers, and delay spread. Results for QPSK, B=1.5, $P_h(\tau)$=exponential, and DWR=20 dB.

optimum linear receiver. Furthermore, the flat fading case is treated extensively by Winters [1984].)

6.3.3.2 Influence of Continuous Delay Spectrum Shape

Figure 6.12 shows the influence of *continuous* delay spectrum shape (d=0.5 and 1) on four-branch combiner performance in the noise-like CCI case (from preliminary results, the trends are similar for M=2). As shown by Glance and Greenstein [1983], the performance of maximal ratio combining is significantly influenced by the delay spectrum shape for $d \geq 0.5$ (in fact, they showed it to be sensitive to the shape for values as low as 0.3) and is worse for the gaussian delay spectrum than it is for the exponential. For d=1, the delay spectrum shape has a similar influence on the MMSE combiner's performance. For d=0.5, however, the four-branch MMSE combiner provides a good equalization capability that is quite insensitive to the delay spectrum shape.

6.3.3.3 Double-Spike Delay Spectrum

Figure 6.13 illustrates that the MMSE combiner copes particularly well with a double-spike channel. Results are shown for d=0.5, but the MMSE combiner performs just as well with double-spike channels at higher delay spreads (unlike conventional equalizers which need longer time spans, i.e., more tap-weights).

This robustness to high delay spreads in the two-path channel case is due to the way the MMSE combiner effects equalization. Assume, for the sake of argument, that we have a two-

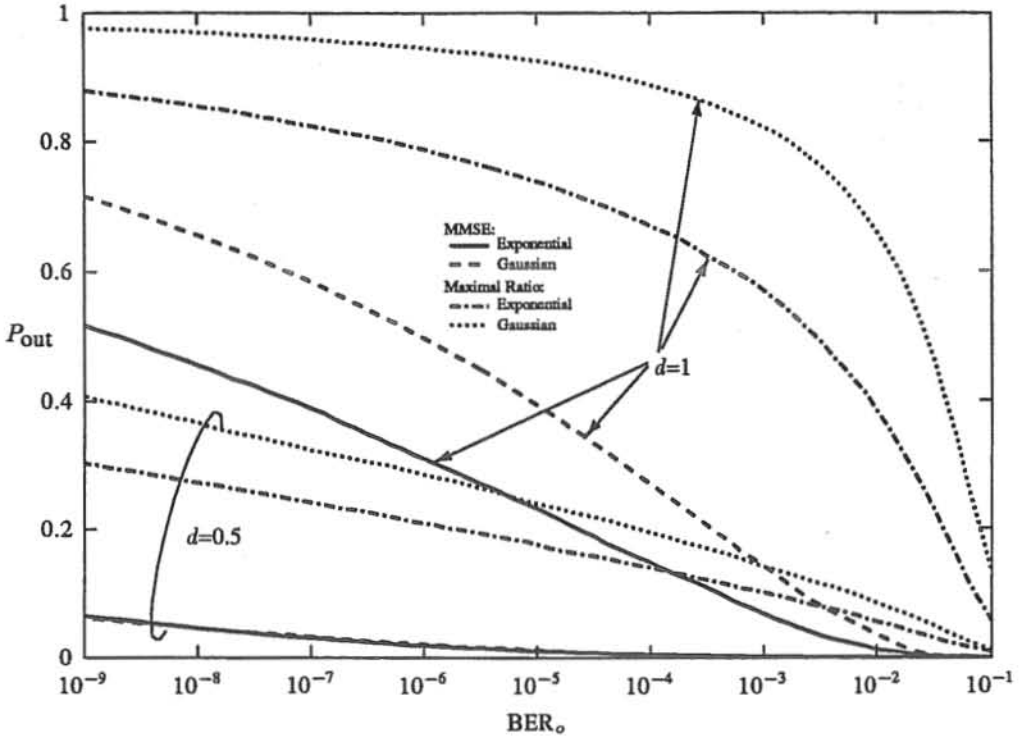

(a) BER distribution (SIR=20 dB).

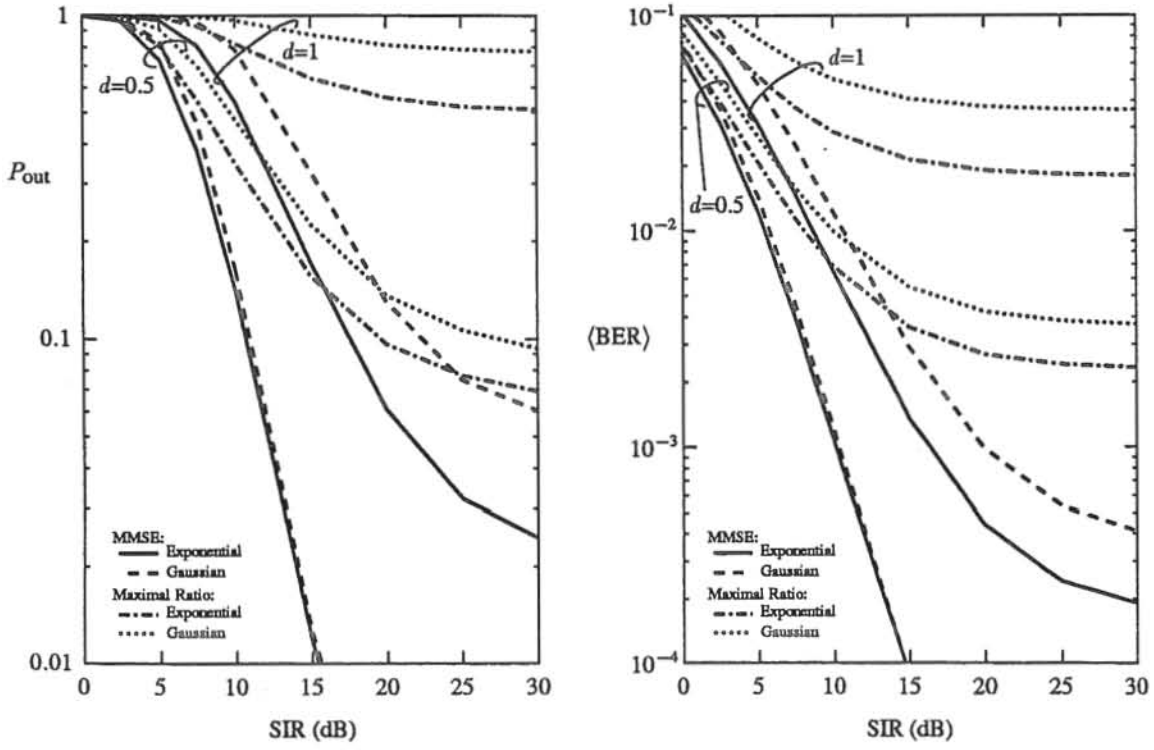

(b) Outage probability ($BER_o=10^{-3}$).

(c) Average BER.

Figure 6.12 Performance of stand-alone memoryless combining. Influence of delay spectrum shape. Results for QPSK, B=1.5, M=4, and N=0.

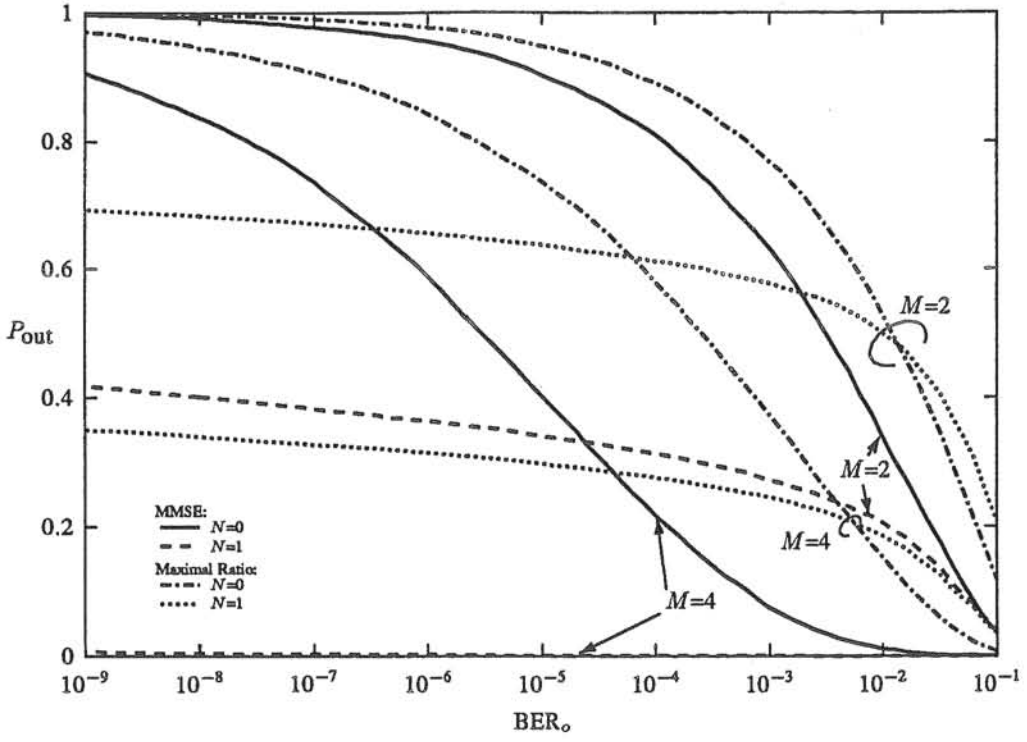

(a) BER distribution (SIR=10 dB).

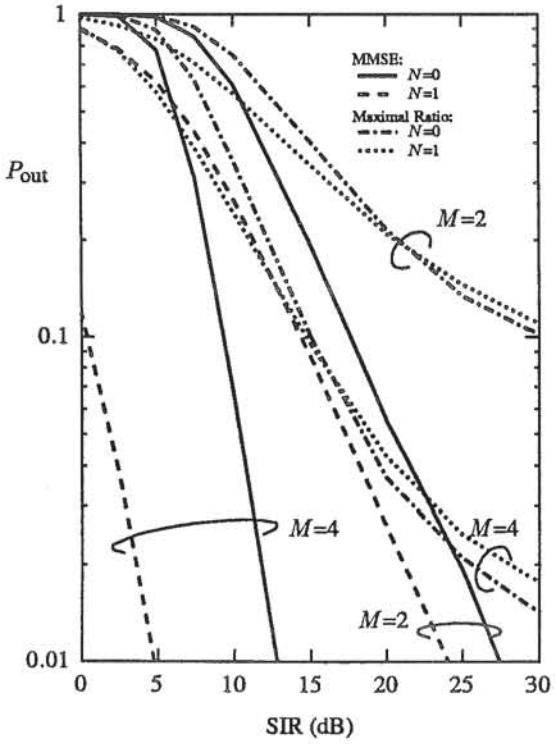

(b) Outage probability ($BER_o=10^{-3}$).

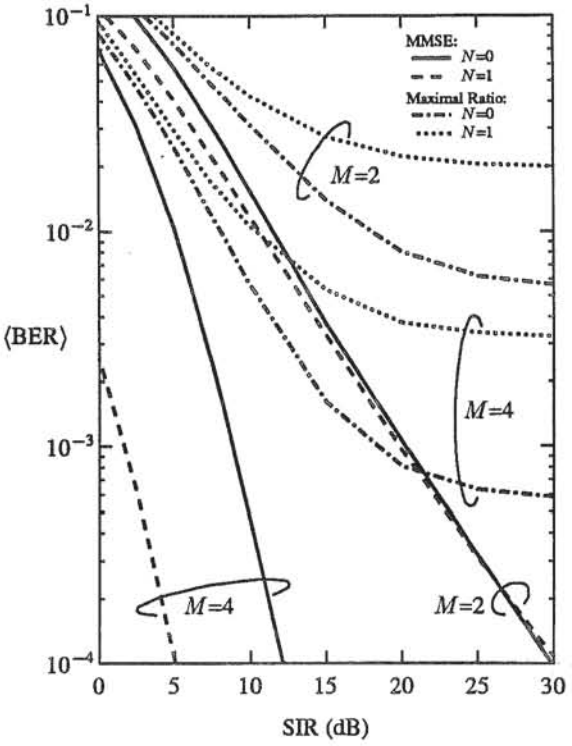

(c) Average BER.

Figure 6.13 Performance of stand-alone memoryless combining. Double-spike delay spectrum. Results for QPSK, B=1.5, d=0.5, and DWR=20 dB.

branch MMSE combiner and no CCI or noise. Imagine the received signal in each diversity branch: it is composed of two time-shifted copies of the same signal, each with its own delay, amplitude, and phase (because of independent fading in each *path*). The delays are the same in each branch, but the amplitudes and phases are probably not (because of independent fading in each *branch*). If the combiner could somehow eliminate one of the time-shifted copies, the signal at its output would be free of ISI. Say, for example, we want to eliminate the second copy. In the ideal noiseless case at hand, this elimination is possible with our two-branch MMSE combiner: it simply adjusts its complex weights so that (i) the amplitude of the second copy is the same in each branch; and (ii) the phase of the second copy in one branch differs by 180 degrees to that in the other branch. Thus, when the signals are combined, the second copy (and thus all ISI) is eliminated (so, in theory, the BER is zero in the noiseless case). This process is totally independent of the second copy's delay. In reality, the MMSE combiner has to effect this equalization process without enhancing noise, so all ISI can not be completely eliminated (the copy that the combiner chooses to supress is the one that yields the minimum MSE). Figure 6.13 shows the impact of noise on two-branch MMSE combiner performance. Note that, as expected, there is no irreducible error rate.

A two-branch MMSE combiner performs satisfactorily ($\langle \text{BER} \rangle = 10^{-3}$) at an SIR of about 20 dB, and a four-branch MMSE combiner at an SIR less than 10 dB. Moreover, the four-branch combiner provides up to 7 dB gain in combating dominant CCI.

Note also from Figure 6.13 the interesting effect of dominant interference (N=1) on the performance of maximal ratio combining. It causes a *worse* performance than the noise-like CCI case (N=0). The reason for this phenomenon relates to the interference pdf. At high BERs, the ISI pdf is often close to double-spike with the peak amplitudes greater than the decision threshold (this double-spike pdf relates to the delay spectrum itself being double-spike). Without noise, this makes possible, for some channels, the maximum BER of 50%. That is, in some events noise is actually desirable to bring the BER down, by making the ISI-plus-noise go below the decision threshold. If the SIR is fairly high, and the low power "noise" is peak-limited (e.g., in the N=1 case), it may not be possible to bring the ISI-plus-noise below the threshold. The N=0 case (not peak-limited) may, and evidently does, do better.

6.3.4 Post-Combiner Equalization (Receivers III, IV, and V)

6.3.4.1 Noise-Like CCI

Figures 6.14 and 6.15 show the performance of two- and four-branch maximal power combining with ideal post-combiner equalization (post-combiner matched filter bound, receiver III), and with optimum (MMSE) linear post-combiner equalization (receiver IV), in the purely noise-like CCI case (and for d=0.5 and 1). In Figure 6.15 (outage probability and average BER), results of stand-alone MMSE combining are shown for comparison. Table 6.1 shows the SIR that can be tolerated to achieve the $\langle \text{BER} \rangle = 10^{-3}$ performance criterion, for the three memoryless combining receivers listed above, the matched filter bound of Chapter 4, and the optimum (MMSE) linear receiver of Chapter 5. The results show that maximal power combining with ideal post-combiner equalization performs within about 1 or 2 dB of the matched filter bound (of Chapter 4). That is, if post-combiner ISI cancellation can be achieved, there is only a small advantage in employing adaptive filters in each diversity branch (in this noise-like CCI case). For maximal power combining with *linear* post-combiner equalization, the performance is not so impressive: it is within about 5–7 dB of the matched filter bound (of Chapter 4) and about 4 or 5 dB of the optimum linear receiver's performance. One might expect this performance to be closer to that of the optimum linear

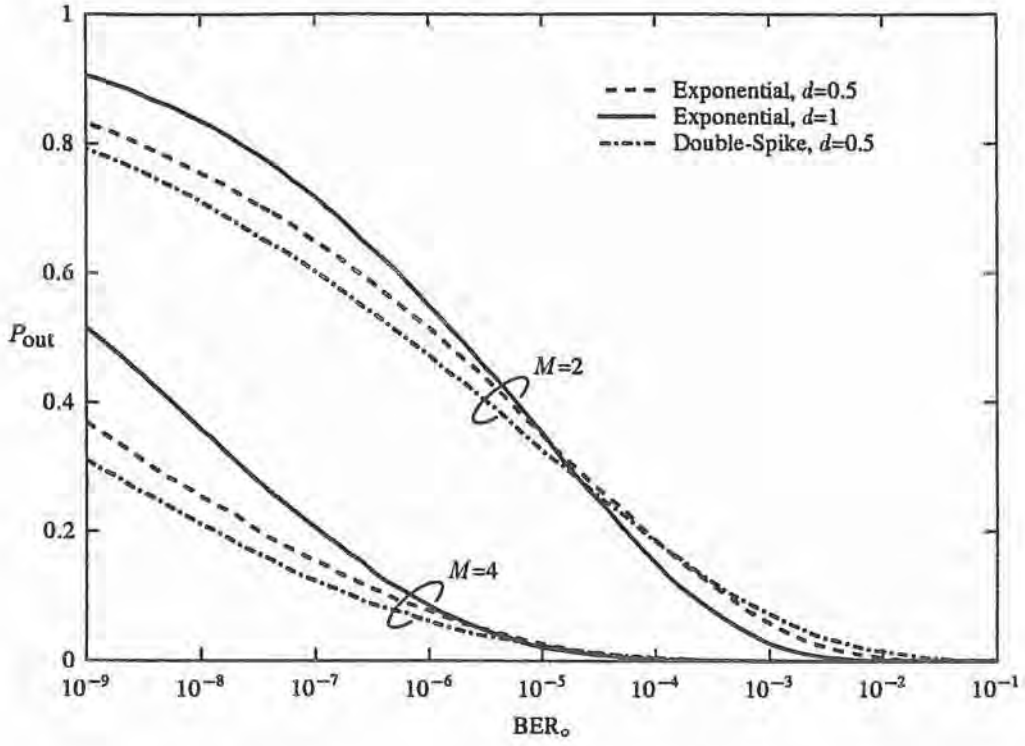

(a) Ideal post-combiner equalization (matched filter bound).

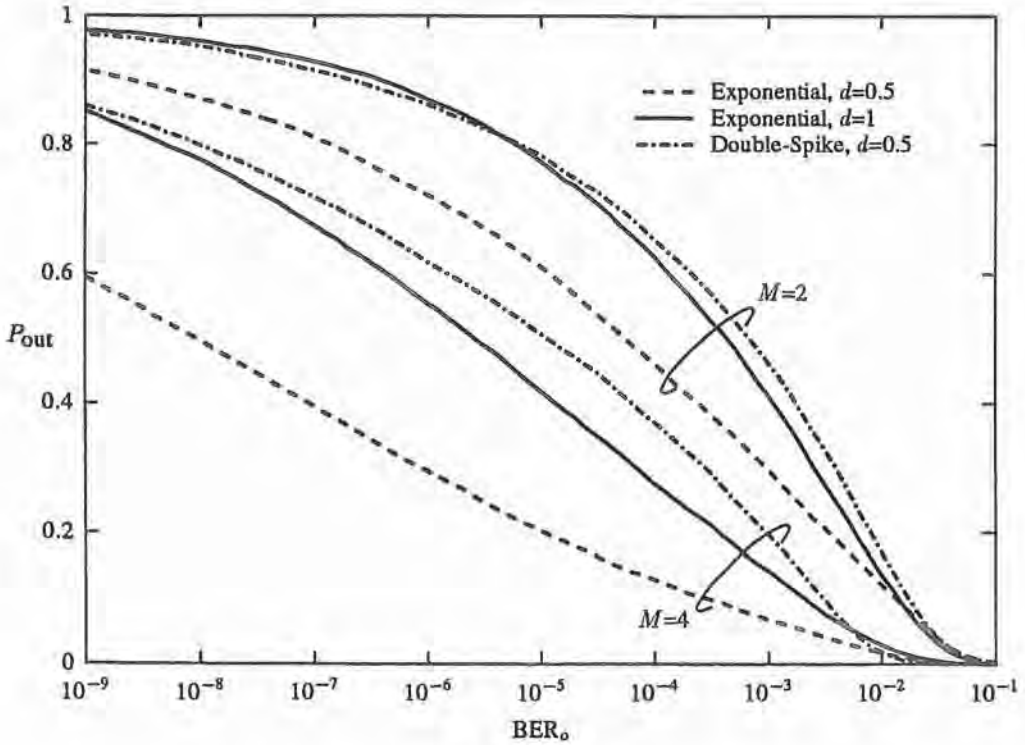

(b) Optimum linear (MMSE) post-combiner equalization.

Figure 6.14 Performance of maximal power combining with post-combiner equalization. BER distribution (SIR=10 dB): Influence of diversity order, delay spectrum shape, and delay spread. Results for QPSK, B=1.5, and N=0.

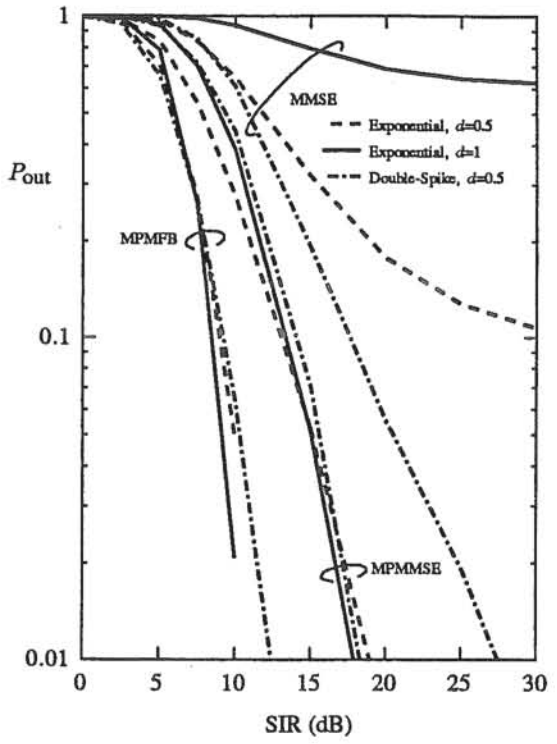

(a) Two-branch diversity: Outage probability ($BER_o=10^{-3}$).

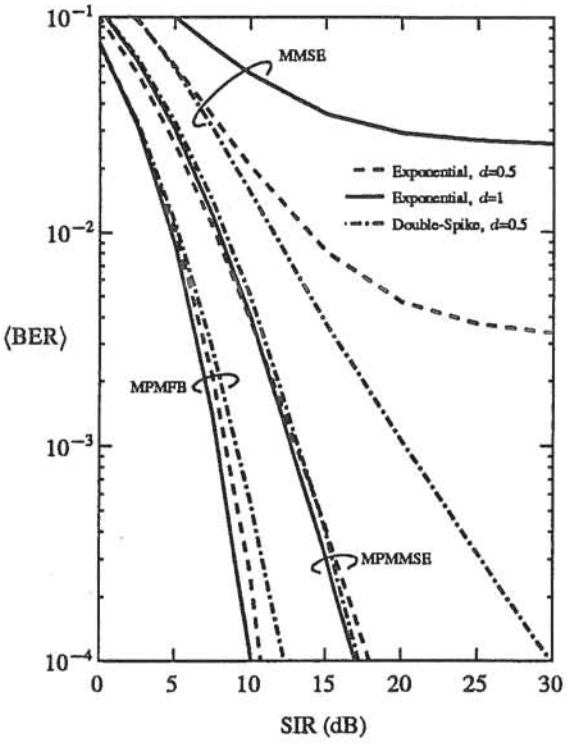

(b) Two-branch diversity: Average BER.

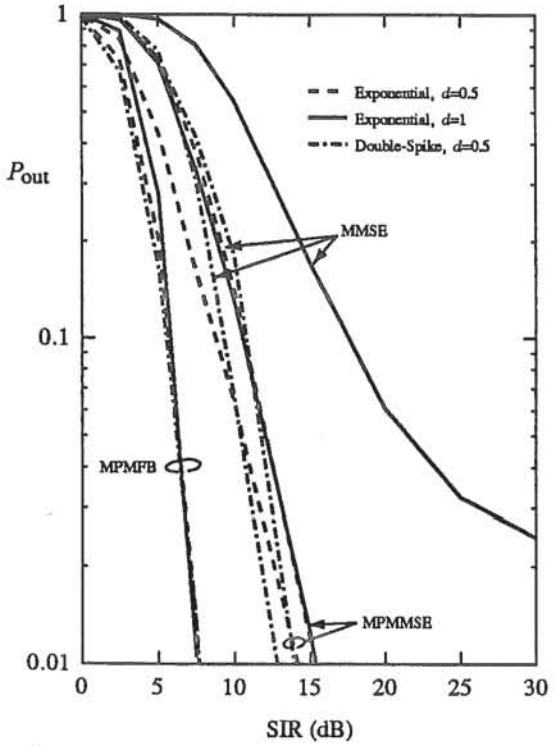

(c) Four-branch diversity: Outage probability ($BER_o=10^{-3}$).

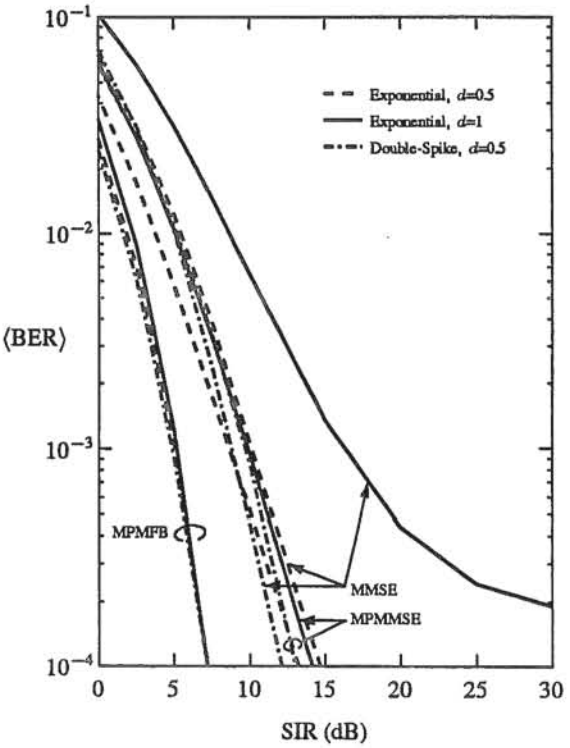

(d) Four-branch diversity: Average BER.

Figure 6.15 Performance of memoryless combining with and without post-combiner equalization (MMSE ≡ stand-alone MMSE combining; MPMFB ≡ maximal power combining with ideal equalization, i.e., post-combiner matched filter bound; MPMMSE ≡ maximal power combining with MMSE linear equalization). Influence of diversity order, delay spectrum shape, and delay spread. Results for QPSK, B=1.5, and N=0.

	M=2		M=4	
Receiver	d=0.5	d=1	d=0.5	d=1
MFB	7.4	6.4	3.3	2.7
OLR	9.7 (2.3)	8.9 (2.5)	4.5 (1.2)	4.0 (1.3)
MPMFB	8.4 (1.0)	7.9 (1.5)	4.9 (1.6)	5.2 (2.5)
MPMMSE	13.1 (5.7)	12.8 (6.4)	9.7 (6.4)	10.0 (7.3)
MMSE	–	–	10.2 (6.9)	16.1 (13.4)

Table 6.1 Performance of various diversity receivers (MFB ≡ matched filter bound; OLR ≡ optimum (MMSE) linear receiver; MPMFB ≡ maximal power combining with ideal equalization, i.e., post-combiner matched filter bound; MPMMSE ≡ maximal power combining with MMSE linear equalization; MMSE ≡ stand-alone MMSE combining). Tolerable SIR (±0.5 dB) for ⟨BER⟩=10^{-3}: Influence of diversity order and delay spread. (Figures in brackets show SIR degradation with reference to matched filter bound.) Results for QPSK, B=1.5, N=0, and $P_h(\tau)$=exponential.

receiver (say, within 1 or 2 dB, like the above post-combiner matched filter bound result). The poorer performance is partly due to maximal power combining not being optimum when linear post-combiner equalization is employed, i.e., the combiner is not *jointly* optimized. An optimum combiner would attempt to combat *some* of the ISI; the maximal power combiner makes no such attempt.

The maximal power combiner's sub-optimality is illustrated in the four-branch results (see Figure 6.15(d)) for a double-spike delay spectrum: the stand-alone MMSE combiner performs *better* (by about 1 dB) than maximal power combining with linear post-combiner equalization. This superior performance again shows how well the relatively low-complexity stand-alone MMSE combiner deals with ISI caused by two-path channels. Note, however, that it can not do as well as maximal power combining with ideal equalization because, unlike the idealized receiver, it needs to sacrifice path diversity to eliminate ISI.

6.3.4.2 Dominant CCI

Figure 6.16 shows the performance of MMSE combining with and without ideal post-combiner ISI cancellation (receiver V), in the case of M=4 and d=1. The dominant CCI gain is about 6 dB if ISI cancellation is employed, compared with about 1 dB if the MMSE combiner must deal with ISI. Table 6.2 shows such SIR gains for other system and channel parameters. The gains are reasonably high (the maximum possible gain is equal to the DWR, i.e., 20 dB) for flat fading, and diminish with increasing delay spread. These are the potential gains we could expect for a receiver with jointly optimized memoryless combining and post-combiner equalization. (Note, however, that absolute performance figures, such as those shown in Figure 6.16, will be somewhat less than the optimum, e.g., compare the N=0 case in Figure 6.16 with that of the matched filter bound in Figure 6.15 — a difference of about 3 dB).

The drop in performance with higher d is due to the increasing number of interfering components of each dominant CCI signal as dispersion increases. To approach ideal CCI cancellation, either the diversity order must be increased or the combiner must have memory — i.e., frequency-dependent processing — in each branch (as with the optimum linear receiver). Comparing the above gains with those exhibited by the optimum linear receiver (e.g., about 19 dB in the M=4, N=1 case), the advantage of memory in each branch is clear. Nevertheless, the results demonstrate that a simple memoryless MMSE combiner with sufficient diversity branches — or sufficient degrees of freedom — can combat dominant CCI in frequency-selective fading environments.

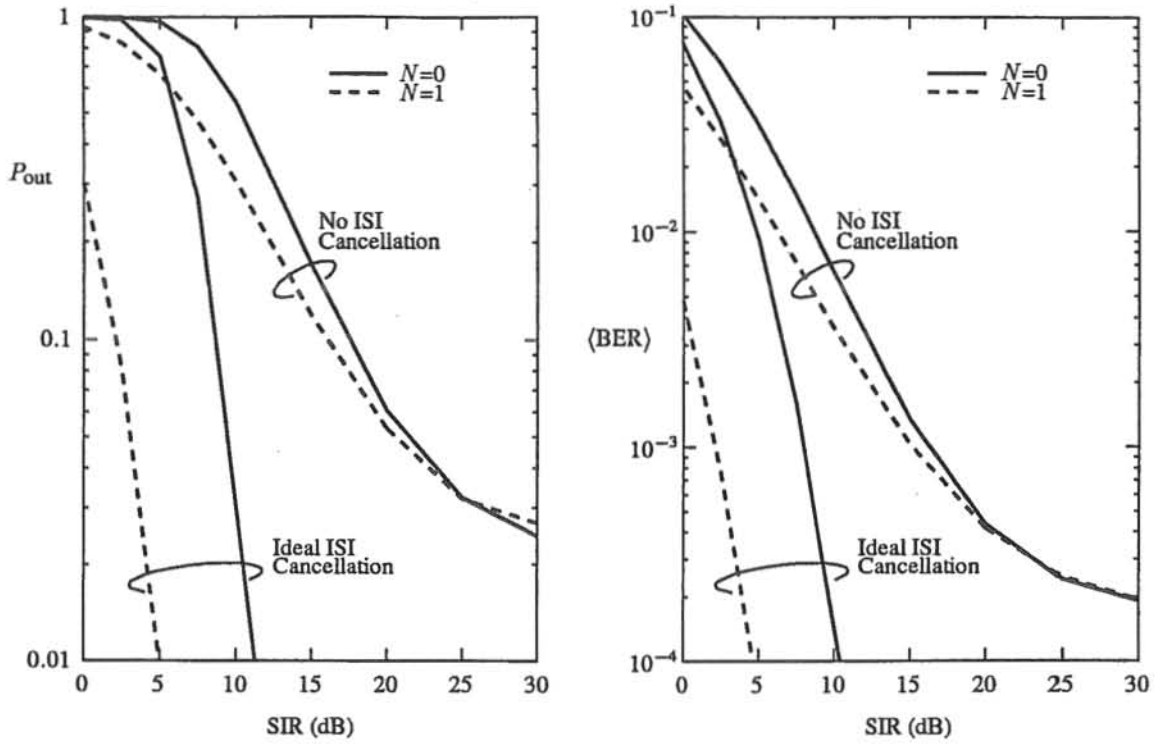

(a) Outage probability ($BER_o=10^{-3}$). (b) Average BER.

Figure 6.16 Performance of MMSE combining with and without ideal post-combiner ISI cancellation. Results for QPSK, B=1.5, M=4, $P_h(\tau)$=exponential, d=1, and DWR=20 dB.

		$P_h(\tau)$=exponential				$P_h(\tau)$=double-spike
M	N	d=0	d=0.5	d=1	d=2	d=0.5
2	1	9.2	3.0	1.9	1.3	2.3
4	1	15.6	9.5	5.9	3.5	14.3
4	2	11.7	4.5	2.8	1.7	4.7

Table 6.2 Performance of MMSE combining with ideal post-combiner ISI cancellation. SIR gain (±0.5 dB, for ⟨BER⟩=10^{-3}) with reference to N=0 case: Influence of diversity order, number of dominant interferers, delay spectrum shape, and delay spread. Results for QPSK, B=1.5, and DWR=20 dB.

6.4 Conclusion

This chapter has presented performance bounds for a range of memoryless combining diversity receivers, with and without post-combiner equalization, operating in a digital cellular radio environment with and without dominant co-channel interference.

The results show that memoryless combining with ideal post-combiner equalization performs almost as well as the best-possible (maximum likelihood) receiver, in combating fading. That is, there is only a small potential gain in having matched filters, as opposed to single weights, in the diversity branches. However, memory in each branch can offer substantial gains in combating dominant CCI in frequency-selective fading environments.

Chapter 7

CONCLUSION

Using many original techniques, this thesis has analysed and quantified the performance of various diversity receivers, ranging from a sophisticated maximum likelihood receiver to simple memoryless combining, operating in a digital cellular radio environment with frequency-selective multipath fading and co-channel interference. Because most of the relevant work in the literature focuses on systems with flat fading channels or no dominant CCI or both, the results in this thesis are quite novel.

Section 7.1 discusses the important tradeoffs, shown in the results of the thesis, between receiver performance and complexity. Section 7.2 identifies and addresses various practical issues relating to a class of promising receivers. Section 7.3 highlights some possible avenues for further work in this interesting and important research area.

7.1 Discussion of Results

For each receiver analysed in this thesis, and for various system and channel parameters, the following graphical results have been presented: (i) BER distribution (for a given value of SIR); (ii) outage probability (for $BER_o=10^{-3}$) against SIR; and (iii) average BER against SIR. The results yield useful insights into performance of receivers in both fast- and slow-moving mobile radio units, and into the "burstiness" of bit-errors (important in the design of error-correcting codes). In summarizing the relative performances of various receivers, tolerable SIR values are compared for the $\langle BER\rangle=10^{-3}$ performance criterion. (The relative gains are usually somewhat smaller for less stringent criteria.)

The emphasis in the results is on significant time dispersion (d=0.5–2), where multipath channels are statistically characterized by a delay spectrum. The results apply to high data-rate systems, e.g., wideband time-division multiple access (TDMA) systems [Balston, 1989].

Transmission over frequency-selective fading channels offers intrinsic frequency diversity at the cost of introducing ISI. If ISI is somehow equalized in the receiver, however, intrinsic frequency diversity can offer up to a substantial 17 dB gain against multipath fading (single-branch matched filter bound with reference to flat fading case, shown in Chapter 4). Space diversity provides an even better defence against fading. But in receivers employing space diversity, the potential gain due to intrinsic frequency diversity diminishes with an increasing number of antennas. For example, a four-branch receiver can achieve a potential 20 dB gain without any intrinsic frequency diversity (i.e., with flat fading), but an additional gain of up to only 3 dB is possible with intrinsic frequency diversity.

Space diversity offers a means of combating not only fading, but also CCI and ISI: the optimum linear receiver study (Chapter 5) shows that dominant CCI can be almost completely eliminated with a sufficient number of space diversity branches; and both the optimum linear receiver and

memoryless combiner studies showed that space diversity can offer a powerful equalization effect that can almost completely eliminate ISI under certain conditions (particularly in channels with a few dominant paths).

A practical receiver can not eliminate all ISI and CCI, and can not obtain the full potential benefit against multipath fading. To achieve an adequate performance in the presence of all these impairments, i.e., fading, ISI, and CCI, the diversity receiver's complexity generally increases with delay spread because the receiver may need a greater number of adaptable tap-weights. (*Complexity* is defined here to include the computational load of digital signal processing and adaptive algorithms.) This fact raises the following question: Assuming space diversity with a few branches (say, 2 to 4) and frequency-selective fading channels (with, say, d=0.5–2), i.e., channels with intrinsic frequency diversity, what is the performance penalty of a reduced receiver complexity? We can begin to answer this important question with the following key results from this thesis:

- In combating fading and ISI, an optimum (MMSE) linear diversity receiver performs almost as well as the relatively high complexity maximum likelihood receiver with the same number of diversity branches (falling short by only about 1 or 2 dB). That is, if space diversity is employed, increased receiver complexity, e.g., employing decision-feedback equalization at the combiner output, buys only a small performance gain. An optimum linear diversity receiver also offers a good defence against dominant CCI in frequency-selective fading environments. With four branches, for example, it can almost completely eliminate a dominant interferer (about 1 dB short of total cancellation if the background noise power is 1% of the average interference power).

- A memoryless combiner has the least complexity of all possible diversity combining structures. In the case without dominant CCI, maximal power combining with ideal post-combiner equalization (matched filter and total ISI cancellation) performs approximately as well as the optimum linear receiver and, thus, almost as well as the maximum likelihood receiver. The same combining scheme with optimum (MMSE) linear post-combiner equalization suffers a 4–5 dB performance degradation, which suggests that non-linear post-combiner equalization schemes, such as decision feedback equalization, would significantly improve the performance of memoryless combining receivers.

  Unfortunately, a diversity receiver with jointly optimized memoryless combining and post-combiner equalization (even ideal equalization) does not cope particularly well with dominant CCI in frequency-selective fading environments (typically 1–6 dB dominant CCI gain, compared with 19 dB achieved by the optimum linear receiver), except in special cases (e.g., double-spike channels — about 14 dB gain).

- The low complexity memoryless MMSE combiner *without* post-combiner equalization yields a surprisingly good performance if four diversity branches are employed, particularly in cases of low dispersion (d=0.5) or with double-spike channels (any delay spread). In these cases, it falls short of the optimum linear receiver's performance (with the same number of diversity branches) by only about 4 or 5 dB in combating noise-like CCI, and offers a dominant CCI gain of 4–7 dB.

7.2 Practical Issues

One of the most important practical issues is the feasibility and cost of employing space diversity. Radios with multiple antennas are bulky and require circuitry in each diversity branch (thus increasing cost and consuming more power). Thus, high-order space diversity in handheld radios may be impractical because of the desire to make such portable units small, even pocket size. Nevertheless, recent efforts make two-branch diversity in handheld units possible [Tsunekawa, 1989], and higher order diversity may be feasible in future cellular systems because higher frequencies (hence smaller antennas and antenna separation) might be employed[1].

Space diversity at base stations is not so impractical, is cost-effective, and, given that future radio designs may be able to better use it, is probably a good investment. Using adaptive retransmission schemes, moreover, it is possible to exploit the diversity at the base station to avoid that at mobile units [Henry and Glance, 1981]. The disadvantage of such retransmission schemes is that only linear transceivers can be employed effectively.

The size, cost, and power consumption of a cellular radio transceiver depends not only on the number of space diversity branches, but also on the complexity of the adaptive signal processing in the receiver. In the following discussion, a broad and important class of receivers is considered: receivers which are implemented using adaptive linear filters and memoryless threshold detection. This class includes all linear receivers (such as those analysed in this thesis) and receivers with decision-feedback equalization (which, in the noise-like CCI case at least, brings performance closer to the matched filter bound, i.e., to maximum-likelihood receiver performance) [Monsen, 1971; Salz, 1973].

It is likely that adaptive linear filters would be implemented using finite-length fractionally-spaced tapped delay lines (TDLs). A TDL constitutes a finite number of adaptable complex quantities and, with a sufficient number of tap-weights and a sufficiently small tap-spacing, can effectively sythesize the desired filter response. Moreover, the adaptive TDL can be implemented using baseband digital signal processing techniques. For instance, the optimum linear diversity receiver could be synthesized using the following stages in each diversity branch: (i) fixed front-end filtering; (ii) down-conversion and demodulation (producing in-phase and quadrature baseband signals); (iii) automatic gain control; (iv) 2/T-rate sampling (assuming $B < 2$) in the in-phase and quadrature rails; (v) analog-to-digital conversion in the in-phase and quadrature rails; and (vi) finite impulse response complex digital filtering (i.e., a digital TDL). The outputs of the TDLs would then be combined (digital summing) for subsequent detection. A memoryless combiner with linear post-combiner equalization could use the same hardware except that stage (vi) would simply consist of a single complex weight (single-tap TDL), and a digital filter would be employed at the combiner output prior to detection. In both receivers, performance could be improved by employing decision feedback equalization (in the post-combiner stage), which uses a symbol-spaced digital filter.

In receivers consisting of an arrangement of TDLs, such as the receivers described above, there is some total number of adaptable complex weights in the diversity branches and the post-combiner stage. Ideally, the weights should be optimized according to a performance criterion such as the minimum mean-square error. There are three important practical issues relating to these weights: (i) how many weights are required to effectively synthesize the adaptive filters, and how does decreasing the number of weights degrade performance? (ii) how are the weights set, and how are they automatically adjusted to track changing channel responses? (iii) how sensitive

[1]However, higher frequencies have poorer propagation properties. They also mean that channel responses change over smaller distances, placing more stringent requirements on channel tracking algorithms.

is performance to the values of the weights, i.e., to the sub-optimality of their values? These issues should not be addressed independently. For instance, the sensitivity to weight errors may depend on the number of weights; the typical weight errors will depend on the method of setting the weights; and the number of weights influences the complexity of the weight-setting method.

Much work has been done in the area of adaptive filters: there are many algorithms for optimizing a set of weights according to symbol-error criteria (usually the least-square or least-mean-square error criteria) [Lucky, 1965; Haykin, 1986; Qureshi, 1985; Godard, 1974; Falconer and Ljung, 1978; Ungerboeck, 1972]. Most of these algorithms work best with some type of training sequence (e.g., 26 symbols in the GSM system [Balston, 1989]), i.e., a transmitted data sequence about which the receiver knows. Because such a sequence is an overhead that lowers spectrum efficiency (particularly if used, say, in every time-slot in a TDMA system), it should be made as short as possible in cellular radio applications. Sophisticated fast-converging algorithms, such as the recursive least-squares (or Kalman) algorithm, may thus be required for quick training. However, less complex algorithms, such as the least-mean-square algorithm, running in decision-directed mode may be adequate to track slow changes in the channel. (Within short data bursts, it may even be adequate to avoid such tracking.) An important practical issue, in relation to all adaptive strategies, is the vehicle speeds that can be tolerated to maintain good performance.

The complexity of adaptive algorithms increases with the number of adjustable weights. There is, therefore, a practical motivation (because of limitations on circuit speed, and of the desire to reduce circuit size and power consumption) to minimize the number of weights or, possibly, to control subsets of the weights by separate algorithms, e.g., by separately optimizing the memoryless combiner and post-combiner equalizer. The second option should be avoided[2], however, because it would usually lead to a costly tradeoff between performance and complexity, especially in the example cited.

Given some practical total number of weights to be adapted by a single algorithm, an important issue is how the weights should be allocated, i.e., the relative number of weights in the diversity branches, in the post-combiner forward filter, and in the decision-feedback filter. This thesis has shown the potential performance of two extreme allocations of a great many weights: (i) the optimum linear receiver has all the weights in the diversity branches; and (ii) the memoryless combiner with post-combiner equalization has the minimum number of weights in the diversity branches and the remaining weights in the post-combiner stage. The results suggest that (i) in the dominant CCI case, the weights may be better allocated in the diversity branches; and (ii) in the noise-like CCI case, the weights may be better allocated in the post-combiner stage, where they operate mainly on the ISI. That is, the best allocation of weights is dependent on the CCI composition. Maybe, then, a possibility worth considering is a multi-mode receiver, or a receiver with weight allocation that is itself adaptive (i.e., an adaptive *structure*). If this is not practical (it would increase receiver complexity), a fixed allocation of weights that is optimal over all possible CCI compositions should be somehow determined.

There are many other important practical issues that are probably best addressed via simulation or experimental means: How sensitive is receiver performance to imperfect gain control, imperfect carrier recovery, and timing errors? How does the timing loop bandwidth, relative to the fading rate, affect performance? How does TDL tap-spacing and TDL length affect the sensitivity to timing errors? Is it adequate to have a single timing recovery loop for all diversity branches, or should timing recovery be done independently in each branch? How do slightly different carrier frequencies, data rates, and bandwidths amongst co-channel signals affect receiver performance?

[2]Unless there are convergence or stability problems with joint optimization.

How do quantization noise and finite word-length affect receiver performance and algorithm stability?

7.3 Suggestions for Future Work

There are many avenues for further work in this research area. Section 7.2 has already highlighted some possibilities. The following list proposes some research projects of particular interest and importance:

- **Optimum Receivers:**
  - Investigate accurate approximations (or bounds) of the maximum likelihood receiver's performance, particularly in the case of dominant CCI. As a check in particular static channel cases, perform Monte Carlo simulations (random symbol-by-symbol transmission) of the maximum likelihood receiver with Viterbi detection. How effective is the M-branch maximum likelihood receiver at combating N dominant interferers?
  - Quantify the potential performance of a diversity receiver with both optimum (say, MMSE) filters in each branch and ideal post-combiner ISI cancellation, in the case of dominant CCI. (For the minimum BER criterion and the *noise-like CCI* case, this performance is equal to the matched filter bound.) How close does this performance get to that of the maximum likelihood receiver? How does it compare with the performance of the optimum (MMSE) *linear* receiver?
- **Jointly Optimized Pre-Combiner and Post-Combiner Filters:**
  - Develop analytical or numerical techniques for jointly optimizing finite-length branch-TDLs and post-combiner filtering (say, in the MMSE sense), in cases of dominant and noise-like CCI. Consider infinite-length post-combiner filtering, ideal post-combiner ISI cancellation, finite-length post-combiner TDLs, and decision-feedback equalization (infinite- and finite-length).
  - Analyse and quantify the potential performance of the above structures. What is the best allocation of a given number of weights, for various CCI scenarios, in receivers with finite-length TDLs in both pre-combiner and post-combiner stages? What is the impact of tap-spacing and timing epoch errors?
- **Adaptive Algorithms and Practical Impairments:**
  For a set of promising finite-length TDL receivers —
  - Analyse the sensitivity in performance to sub-optimal tap-weights.
  - Evaluate adaptive algorithms. Consider training, tracking, and, possibly, blind equalization. Study impact of channel dynamics (via second-order channel statistics, e.g., Doppler spectra). What vehicle speeds can the algorithms tolerate?
  - Evaluate the possibility of decision-feedback from receivers that estimate data from other co-channel sources, thus effecting CCI cancellation without noise enhancement. Is such a scheme stable?
  - Study the impact of miscellaneous practical impairments (listed in Section 7.2).
- **Performance Evaluation and Impact on System Capacity:**

- Assess other performance statistics, such as the short-term average BERs and the outage probability that relates to this average. Relate these statistics to vehicle speed. How useful are P_{out} and $\langle BER \rangle$, as defined in this thesis, as performance statistics over a range of vehicle speeds?
- Develop techniques for determining the potential impact of receiver performance on the all-important *system capacity* of cellular radio systems. Such an evaluation could be achieved by evaluating the distribution of a given receiver's $\langle BER \rangle$, taken over an ensemble of CCI scenarios, i.e., over an ensemble of $\{S_n\}$ (characterized by the statistics of shadow fading and time-varying propagation distances). Because the statistics of mobile distances are related to the cellular layout and frequency reuse plan, the distribution of $\langle BER \rangle$ can thus be related to a known system capacity (or, at least, a capacity relative to that of other cellular plans). If the outage probability Prob $[\langle BER \rangle > \langle BER \rangle_o]$ (where $\langle BER \rangle_o$ is some specified acceptable performance threshold) is less than, say, 1%, the receiver is said to perform satisfactorily: receiver performance is thus related to system capacity.

  If a receiver shows no special ability at combating dominant CCI, the $\langle BER \rangle$ distribution is easy to approximate: the pdf of $\langle BER \rangle$ is computed using standard methods from the $\langle BER \rangle$ as a function of SIR, and the pdf of SIR. But if the receiver deals particularly well with dominant CCI, the approach is not so simple. The exhaustive approach involves a Monte Carlo simulation of $\{S_n\}$, with $\langle BER \rangle$ being computed every trial [Glance and Greenstein, 1983]. Because the computation of $\langle BER \rangle$ is intensive for most receivers, this procedure may be very time consuming. An alternative is to somehow use the short-term average BER instead. Or one could compute $\langle BER \rangle$ in several special CCI scenarios, and then estimate the $\langle BER \rangle$ distribution from statistics on these scenarios. For instance, the $\langle BER \rangle$ as a function of SIR in the cases N=0, N=1, and N=2 (with equal-power dominant interferers), along with a set of associated statistics, may be sufficient to make a good approximation of the impact of receiver performance on system capacity.

In addition, researchers may want to consider different modulation schemes (e.g., high-order linear modulations, or continuous-phase modulations), coded-modulations and decoder performance, correlation of fading amongst diversity branches, other fading statistics (e.g., Rician), other delay spectra, and other interference and noise models.

REFERENCES

Aaron, M.R. and Tufts, D.W. (1966), "Intersymbol interference and error probability," *IEEE Trans. Inform. Theory*, Vol. IT-12, January, pp. 26–34.

Abramowitz, M. and Stegun, I.A. (1972), *Handbook of Mathematical Functions*, Dover, ch. 7.

Amitay, N. and Greenstein, L.J. (1984), "Multipath outage performance of digital radio receivers using finite-tap adaptive equalizers," *IEEE Trans. Commun.*, Vol. COM-32, May, pp. 597–608.

Balaban, P. and Salz, J. (1991), "Dual diversity combining and equalization in digital cellular mobile radio," *IEEE Trans. Vehicul. Tech.*, Vol. VT-40, May, pp. 342–354.

Balston, D.M. (1989), "Pan-European cellular radio: or 1991 and all that," *Electronics and Communications Engineering Journal*, January, pp. 7–13.

Bello, P.A. (1964), "Time-frequency duality," *IEEE Trans. Inform. Theory*, January, pp. 18–33.

Bogachev, V.M. and Kisalev, I.G. (1980), "Optimum combining of signals in space-diversity reception," *Telecommun. Radio Eng.*, Vol. 34/35, October, pp. 83–85.

Brennan, D.G. (1959), "Linear diversity combining techniques," *Proc. IRE*, Vol. 47, June, pp. 1075–1102.

Calhoun, G. (1988), *Digital Cellular Radio*, Massachusetts:Artech House.

Chuang, J.C. (1987), "The effects of time delay spread on portable communications channels with digital modulation," *IEEE J. Select. Areas Commun.*, Vol. SAC-5, June, pp. 879–889.

Cooper, G.R. and Nettleton, R.W. (1983), "Cellular mobile technology: The great multiplier," *IEEE Spectrum*, June, pp. 30–37.

Cox, D.C. (1975), "Distributions of multipath delay spread and average excess delay for 910-MHz urban mobile radio paths," *IEEE Trans. Antennas Propagat.*, Vol. 23, July, pp. 206–213.

Cox, D.C. (1987), "Universal digital portable radio communications," *Proc. IEEE*, Vol. 75, April, pp. 436–477.

Cox, D.C. (1989), "Portable digital radio communications: An approach to tetherless access," *IEEE Commun. Mag.*, July, pp. 30–40.

D'Avella, R., Moreno, L. and Sant'Agostiro, M. (1989), "An adaptive MLSE receiver for TDMA digital mobile radio," *IEEE J. Select. Areas Commun.*, Vol. SAC-7, January, pp. 122–129.

Davenport, W.B. and Root, W.L. (1958), *An Introduction to the Theory of Random Signals and Noise*, McGraw-Hill, 1st ed., pp. 96–101.

Despins, C.L., Falconer, D.D. and Mahmoud, S.A. (1991), "Coding and optimum baseband combining for wide-band TDMA indoor wireless channels," *Can. J. Elect. & Comp. Eng.*, Vol. 16, No. 2, pp. 53–62.

Falconer, D.D. and Ljung, L. (1978), "Application of fast Kalman estimation to adaptive equalization," *IEEE Trans. Commun.*, Vol. COM-26, October, pp. 1439–1446.

Forney, G.D., Jr. (1972), "Maximum-likelihood sequence estimation of digital sequences in the presence of intersymbol interference," *IEEE Trans. Inform. Theory*, Vol. IT-18, May, pp. 363–378.

Forney, G.D., Jr. (1973), "The Viterbi algorithm," *Proc. IEEE*, Vol. 61, March, pp. 268–278.

Foschini, G.J. and Salz, J. (1983), "Digital communications over fading radio channels," *Bell Syst. Tech. J.*, Vol. 62, February, pp. 429–456.

George, D.A. (1965), "Matched filters for interfering signals," *IEEE Trans. Inform. Theory*, Vol. IT-11, January, pp. 153–154.

Glance, B. and Greenstein, L.J. (1983), "Frequency selective fading effects in digital mobile radio with diversity combining," *IEEE Trans. Commun.*, Vol. COM-31, September, pp. 1085–1094.

Godard, D. (1974), "Channel equalization using Kalman filter for fast data transmission," *IBM J. Res. Dev.*, May, pp. 267–273.

Goodman, D.J. (1991), "Trends in cellular and cordless communications," *IEEE Commun. Mag.*, Vol. 29, June, pp. 31–40.

Greenstein, L.J. and Yeh, Y.S. (1985), "A simulation study of space diversity and adaptive equalization in microwave digital radio," *AT&T Tech. J.*, Vol. 64, April, pp. 907–935.

Groves, I.S. (1990), "Personal mobile communications — a vision of the future," *Br. Telecom. Technol. J.*, Vol. 8, January, pp. 7–11.

Haykin, S. (1983), *Communication Systems*, Wiley, 2nd ed.

Haykin, S. (1986), *Adaptive Filter Theory*, Information and System Sciences, Englewood Cliffs:Prentice Hall.

Henry, P.S. and Glance, B.S. (1981), "A new approach to high-capacity digital mobile radio," *Bell Syst. Tech. J.*, Vol. 60, October, pp. 1891–1904.

Jakes, W.C., Jr. (1974), *Microwave Mobile Communications*, New York:Wiley.

Kaye, A.R. and George, D.A. (1970), "Transmission of multiplexed PAM signals over multiple channel diversity systems," *IEEE Trans. Commun. Technol.*, Vol. COM-18, October, pp. 520–526.

Lee, E.A. and Messerschmitt, D.G. (1988), *Digital Communication*, Boston:Kluwer Academic.

Lo, N.W.K., Falconer, D.D. and Sheikh, A.U.H. (1990), "Adaptive equalization and diversity combining for a mobile radio channel," In *GLOBECOM '90 Conf. Proc.*, IEEE Communications Society, San Diego, CA, December, pp. 507A.2.1–507A.2.5.

Lucky, R.W. (1965), "Automatic equalization for digital communications," *Bell Syst. Tech. J.*, Vol. 44, April, pp. 547–588.

Lucky, R.W., Salz, J. and Weldon, E.J. (1968), *Principles of Data Communications*, New York:McGraw-Hill, ch. 4 and 5.

MacDonald, V.H. (1979), "Advanced mobile phone service: The cellular concept," *Bell Syst. Tech. J.*, Vol. 58, January, pp. 15–41.

Magee, F.R., Jr. and Proakis, J.G. (1973), "Adaptive maximum-likelihood sequence estimation for digital signalling in the presence of intersymbol interference," *IEEE Trans. Inform. Theory*, Vol. IT-19, January, pp. 120–124.

Mazo, J.E. (1991), "Exact matched filter bound for two-beam Rayleigh fading," *IEEE Trans. Commun.*, Vol. COM-39, July, pp. 1027–1030.

Metzger, K. (1987), "On the probability density of intersymbol interference," *IEEE Trans. Commun.*, Vol. COM-35, April, pp. 396–402.

Moler, C. (1990), *PRO-MATLAB User's Guide for Sun Workstations*, Massachusetts:The Mathworks.

Monsen, P. (1971), "Feedback equalization for fading dispersive channels," *IEEE Trans. Inform. Theory*, Vol. IT-17, January, pp. 56–64.

Monsen, P. (1984), "MMSE equalization of interference on fading diversity channels," *IEEE Trans. Commun.*, Vol. 32, January, pp. 5–12.

Nagrath, I.J. and Gopal, M. (1982), *Control Systems Engineering*, Wiley, pp. 681–685.

Noble, B. and Daniel, J.W. (1988), *Applied Linear Algebra*, Englewood Cliffs:Prentice-Hall, 3rd ed.

Papoulis, A. (1965), *Probability, Random Variables, and Stochastic Processes*, McGraw-Hill, 1st ed., pp. 153–155.

Press, W.H., Flannery, B.P., Teukolsky, S.A. and Vettering, W.T. (1986), *Numerical Recipes: The Art of Scientific Computing*, Cambridge University Press.

Price, R. and Green, P.E., Jr. (1958), "A communication technique for multipath channels," *Proc. IRE*, Vol. 46, March, pp. 555–570.

Proakis, J.G. (1989), *Digital Communications*, McGraw-Hill, 2nd ed.

Proakis, J.G. (1991), "Adaptive equalization for TDMA mobile radio," *IEEE Trans. Vehicul. Tech.*, Vol. VT-40, May, pp. 333–341.

Qureshi, S.U.H. (1985), "Adaptive equalization," *Proc. IEEE*, Vol. 73, September, pp. 1349–1387.

Ross, I.M. (1991), "Wireless network directions," *IEEE Commun. Mag.*, Vol. 29, February, pp. 40–42.

Saltzberg, B.R. (1968), "Intersymbol interference error bounds with application to ideal bandlimited signaling," *IEEE Trans. Inform. Theory*, Vol. IT-14, July, pp. 563–568.

Salz, J. (1973), "Optimum mean-square decision feedback equalization," *Bell Syst. Tech. J.*, Vol. 52, October, pp. 1341–1373.

Salz, J. (1985), "Digital transmission over cross-coupled linear channels," *AT&T Tech. J.*, Vol. 64, July, pp. 1147–1159.

Schwartz, S.C. and Yeh, Y.S. (1982), "On the distribution function and moments of power sums with log-normal components," *Bell Syst. Tech. J.*, Vol. 61, September, pp. 1441–1462.

Schwartz, M., Bennett, W.R. and Stein, S. (1966), *Communication Systems and Techniques*, New York:McGraw-Hill.

Smith, J.W. (1965), "The joint optimization of transmitted signal and receiving filter for data transmission systems," *Bell Syst. Tech. J.*, December, pp. 2263–2392.

Tsunekawa, K. (1989), "Diversity antennas for portable telephones," In *39th Vehicular Technology Conference*, IEEE, San Fransisco, CA, May, pp. 50–56.

Ungerboeck, G. (1972), "Theory of speed of convergence in adaptive equalizers for digital communication," *IBM J. Res. Dev.*, Vol. 16, November, pp. 546–555.

Ungerboeck, G. (1974), "Adaptive maximum-likelihood receiver for carrier-modulated data-transmission systems," *IEEE Trans. Commun.*, Vol. COM-22, May, pp. 624–636.

Valenzuela, R.A. (1989), "Performance of adaptive equalization for indoor radio communications," *IEEE Trans. Commun.*, Vol. COM-37, March, pp. 291–293.

Van Etten, W. (1975), "An optimum linear receiver for multiple channel digital transmission systems," *IEEE Trans. Commun.*, Vol. COM-23, August, pp. 828–834.

Van Etten, W. (1976), "Maximum likelihood receiver for multiple channel transmission systems," *IEEE Trans. Commun.*, Vol. COM-24, February, pp. 276–283.

Vary, P. (1988), "Speech codec for the European mobile radio system," *Telecommunications*, September, pp. 51–54.

Winters, J.H. (1984), "Optimum combining in digital mobile radio with cochannel interference," *IEEE J. Select. Areas Commun.*, Vol. SAC-2, July, pp. 528–539.

Wong, W.C. and Greenstein, L.J. (1984), "Multipath fading models and adaptive equalizers in microwave digital radio," *IEEE Trans. Commun.*, Vol. COM-32, August, pp. 928–934.

Wozencraft, J.M. and Jacobs, I.M. (1965), *Principles of Communication Engineering*, New York:Wiley.